Uncertainty Quantification for Annual Energy Production Uplift due to Wake Steering

Yaren Cürgül

TU Delft

Uncertainty Quantification for Annual Energy Production Uplift due to Wake Steering

A case study on NoordzeeWind using FLORIS software

Master of Science Thesis Report

by

Yaren Cürgül

University Supervisors:	Dr. Marilena Pavel
Company Supervisors:	Dr. Bart Doekemeijer (daily supervisor)
	Dr. Jasper Kreeft (line manager)
Place:	Faculty of Aerospace Engineering, Delft
Student number:	4563026
Cover image credit:	Vestas

Faculty of Aerospace Engineering, Delft University of Technology · Shell Global Solutions International B.V.

Preface

Over the past year, I had the opportunity to learn more about wind energy and uncertainty quantification. The fact that my academic journey that started with building airplanes ended in contributing to sustainable energy was a fun and unexpected surprise. Similarly, the thesis research process had many twists and turns. Throughout this journey, I not only learned how to conduct academic research but also showed personal growth by being responsible for my own research project. While at first the responsibility could be heavy, with time I rejoiced in the opportunity to show my creativity and initiative by conducting my own investigation into the wind energy world. With this, I would like to thank the people I worked with for their support and commitment to this research project.

I want to thank Jan-Willem van Wingerden from the Faculty of Mechanical Engineering for his support on the first half of the project and for sharing his knowledge on wake steering with me. In addition to him, I would like to thank his researchers Robin de Jong for helping me understand FLORIS better and Marcus Becker for helping me understand the integration of FLORIS with uncertainty quantification methods.

From the Faculty of Aerospace Engineering, I would like to thank Marilena Pavel for supervising me in this research project and providing me guidance on the topics of uncertainty quantification and control systems.

Moreover, I am grateful to Shell for giving me the opportunity to work on this project in collaboration with Delft University of Technology. Many thanks to the wind energy team for welcoming me and providing me information on the offshore wind energy industry; to Bart Doekemeijer for providing me with the research topic and for his daily supervision, guidance and insights into wake steering; to Jasper Kreeft for his management and for his explanations on wind farm physics; and to PJ Stanley for his availability for brainstorming sessions.

Finally, I want to thank my family and friends for giving me support and motivation from the first day of the bachelor studies to the last day of the master.

Contents

Nomenclature

List of Abbreviations

ADM	Actuator Disk Model
AEP	Annual Energy Production
CC	Cumulative Curl
CFD	Computational Fluid Dynamics
FLORIS	FLOw Redirection and Induction in Steady-state
GCH	Gaussian Curl Hybrid
HAWT	Horizontal-axis Wind Turbine
IEA	International Energy Agency
IPC	Individual Blade Pitch Control
LCoE	Levelized Cost of Energy
LES	Large Eddy Simulation
LUT	Lookup Table
MC	Monte Carlo
NOWRDC	National Offshore Wind Research and Development Consortium
OEM	Original Equipment Manufacturer
PDF	Probability Distribution Function
RANS	Reynolds-averaged Navier-Stokes
SOWFA	Simulator fOr Wind Farm Applications
TRL	Technology Readiness Level
WF	Wind Farm
WFFM	Wind Farm Flow Model
WT	Wind Turbine

List of Symbols

γ	Yaw angle [$^\circ$]
ρ	Air density [$\frac{kg}{m^3}$]
τ_g	Generator torque [$N \cdot m$]
θ	Blade pitch angle [$^\circ$]
A	Rotor swept area [m^2]
C_p	Power coefficient [-]
C_T	Thrust coefficient [-]
D	Rotor diameters [m]
$P\rho$	Empirical parameter in yaw-power curve [-]
U_i	Effective wind speed at the wind turbine [m/s]

List of Figures

List of Tables

1

Introduction

1.1. Context

In 2022 the increasing oil price, driven by embargoes and inflation, showed the importance of reducing the reliance on fossil fuels for Europe's energy security and the population's prosperity [92]. Together with an increasing number of climate-related natural disasters over the past 50 years [95], this highlighted the significance of investing in clean and abundant renewable energy sources. In 2023 alone, the worldwide renewable power capacity was increased by 473 GW, with wind power accounting for 24% of the expansion [46]. The expansion in wind power generation is projected to continue. For instance, nine European countries have pledged to boost the offshore wind farm capacity in the North Sea [40]. To generate more and more energy, wind turbines are getting bigger and more powerful. While the average rotor diameter was 60 m in 1999, this number has grown to 130 m in 2022 [39]. Larger wind turbines produce more power but also create more significant wake effects. Wake effects are responsible for reducing energy production in downstream wind turbines [10]. Moreover, wind farm size is increasing [88]. As more wind turbines are placed closer together, wake-induced power losses increase. Wake losses are one of the major challenges in making wind farms profitable [96]. Therefore, the mitigation and quantification of wake losses is important for maximizing power in wind farms. A wake loss mitigation method that has been gaining increased attention is wind farm flow control [41].

Axial induction control was the first wind farm flow control technique proposed for power maximization in wind farms [62]. However, the results of numerous field experiments with this wind farm flow control method showed inconclusive power gain benefits [1, 11, 57, 100]. Dynamic wind farm flow control methods such as dynamic induction control [66] and the helix [32] were proposed. However, to this date no field experiments took place to test the benefit of these wind farm control methods. Yaw-based wake steering is the only wind farm control method to date that has been implemented commercially [106]. This is as a result of successful wake steering field experiments that showed significant AEP gains [20, 41]. Therefore, the focus of this study is on the practical application of wake steering for power maximization in wind farms.

1.2. Problem Statement

Wake steering has shown promising results in increasing power production in wind farms in various field experiments in literature. In one particular field experiment, AEP gains ranging from 7-13% at average wind speeds and up to 28-47% at low wind speeds were achieved. However, these gains were highly dependent on wind direction and speed and the modelling of the power curve, and overall annual energy production (AEP) gains remain insignificant [44]. In [28], uncertainties arise from the controller's inability to adapt to changing wind directions and unstable atmospheric conditions, resulting in under-performance. Considering the power losses in the upstream WTs led to the net AEP uplift of 4% over the same wind direction and wind speed range for the five WT test case. At the time of the field experiment, the FLORIS model used for yaw optimization was not able to model terrain effects or near-wake effects accurately. Incorporating an improved FLORIS model and some wind direction uncertainty in the yaw optimization phase predicted wake steering-induced wake loss reduction values that approached field experiment results [29]. [21] demonstrated wake steering in a 43-turbine wind farm, achieving up to 16% power gains for specific wind directions, but noted significant uncertainties due to terrain modeling limitations and mismatches between real and modeled yaw-power curves in FLORIS. To conclude, uncertain conditions cannot be fully captured by the yaw controller.

In the current market, offshore wind farm developers compete for sea bed leases that are auctioned by country governments years prior to the actual construction of the wind farm [82]. The winning party will receive a permit for constructing and operating a wind farm, typically for a period of 25 years. The auction winner is often decided as the bidding party that offers the most financially interesting offer to the government, for example, by paying a large sum for the sea bed lease and/or offering a very low power purchase agreement (PPA) price. This pushes strong financial burdens on developers, and puts developers in a race to design the most profitable farms. Most profitable in this scenario boils down to wind farms with the highest electricity production at minimal construction, operation and decommissioning costs. To maximize electricity production, technological innovations such as wind farm control are often included in the early-phase design of wind farms. In order to come up with a bankable bid, developers use extensive economic and technical models to estimate the costs and energy yield of a future wind farm, which allows them to determine the financial feasibility of their offer, and allows them to decide whether it's worth investing in. In this thesis, we focus on the estimation of the benefit of the wake steering technology on a future farm's energy yield. This technology affects the predicted annual energy yield in the order of 1%, and thereby has substantial impact on the financial feasibility of an early-phase wind farm design. Accurate energy yield estimation is important for managing risks and for performing financial analysis of wind farm projects. With increasing financial pressure on wind energy viability, both improvement in wind energy innovation and how the innovations are assessed are of vital importance. The AEP uplift estimated due to wake steering during yield estimations is inherently uncertain due to stochastic atmospheric conditions and a lack of knowledge in certain parameters. This could raise doubts on the benefit of wake steering estimated for future wind farm projects. For example, a recent field experiment has shown that the uncertainty in wind direction could lead to estimating a wide range of AEP uplift values which do not lead to a concrete conclusion on the benefit of wake steering [42]. Hence, the question of how much benefit can be obtained from wake steering in real-life applications that are inherently uncertain remain unanswered. By understanding the uncertainties in AEP gain predictions for wake steering, the estimations of AEP gains during the early phases of wind farm project development become more reliable. As a result, the knowledge obtained from such an uncertainty quantification study can contribute to increasing confidence in wake steering as a potential wake mitigation technique in future wind farms.

There were several uncertainty quantification studies dealing with the optimization under uncertainty problem [42, 51, 75, 78, 83, 97]. In all cases, this involved obtaining new yaw offsets following the inclusion of uncertainties in, amongst others, model parameters [42, 97], wind direction [42, 51, 76, 78, 83, 97], yaw position [42, 51, 75, 76, 83, 97], wind speed [42, 51, 76], wind shear [42, 76] and/or turbulence intensity [42, 51, 76]. Understanding the change in optimized yaw offset angles with uncertainties and the effect of the new yaw angles on the AEP uplift is valuable. However, wake steering controllers used in industry remain deterministic, as the wake steering controllers that perform optimization under uncertainty have not been tested in field experiments yet. Therefore, the accuracy of AEP uplift obtained with deterministic wake steering controllers, specifically FLORIS, remains unknown. Moreover, there are uncertainties associated with the early-design phase due to time gap between the bidding period and the operating period of the wind farm. Assumptions are made regarding wind farm properties, such as the wind turbine specifications and wind rose, due to the inability to predict the state of these properties in the future. Understanding the accuracy of AEP uplift involves propagating forward the uncertainties arising during a typical wake steering assessment using FLORIS. [51] tackled this problem in the first part of his study by propagating forward a number of uncertain input parameters and quantifying their effect on the power gain. However, this was done for the dynamic FarmFlow wake model and it was limited to the test case of five wind turbines. The importance of different input parameters on the AEP uplift of a wind farm [97] and on WT output [19] was determined. However, both cases this was limited to model parameters since the goal was to calibrate the FLORIS model for the wake steering application [97] or the FLORIDyn model - FLORIS considering the time-dependent influence of wake model parameters - without considering the wake steering application. Therefore, there is no study focused on understanding the significance and effect of uncertain input parameters on the AEP uplift of a wind farm using deterministic yaw optimization with FLORIS.

1.3. Research Formulation

This thesis addresses this scientific gap by performing an uncertainty quantification of wake steering with the goal of determining the statistical uncertainty of the AEP uplift estimated in wake steering assessments.

The **research objective** of the thesis can be formalized as:

Research Objective

Understanding uncertainties in annual energy production gain predictions for wake steering in wind farms through uncertainty propagation.

This leads to the following **research question**:

Research Question 1

How do uncertainties affect the predicted annual energy production gains for wake steering?

With this research question, the goal is to understand both the global impact of uncertainties on the AEP uplift and the significance of each uncertainty on the AEP uplift. Next, it is important to rank the significance of the uncertainties considered on the estimated AEP uplift and to understand how they may correlate to each other. This is addressed by formalizing the following **research question**:

Research Question 2

How significant is the impact of input uncertainties on the predicted AEP gain from wake steering?

By addressing these goals, the thesis aims to quantify the statistical uncertainty in AEP uplift due to wake steering for the early design phase of wind farms.

The purpose of this report is to understand the effect of uncertainties on AEP uplift predictions for wake steering in wind farms. The focus is on energy yield - and more particularly on wake steering uplift - assessments. This is achieved by (1) creating a framework for uncertainty propagation while keeping the wake steering assessment tool as a black box and (2) performing a sensitivity analysis on the AEP uplift obtained. Therefore, the main contribution of the thesis is the framework to assess the accuracy of the AEP uplift obtained following deterministic wake steering uplift assessments. In addition to this, the interactions between the uncertain atmospheric parameters is observed and the significance of the parameters on the AEP uplift of a wind farm is evaluated for the first time. Finally, this uncertainty quantification is performed for two wind farm flow models, allowing for a deeper understanding of each model's limitations.

1.4. Structure of the Report

The structure of the report is as follows. First, Chapter 2 presents a summary of this thesis in the form of a scientific article, in Part I. Second, Part II presents a literature study on wind farms, wind farm flow modeling and wind farm control. This starts with a general introduction of wind farm technology including controller architecture and wind farm flow control strategies in Chapter 3. Next, this is followed by an overview of wind farm flow modelling in Chapter 4 and a review of the state-of-the-art wake steering technology in Chapter 5. The literature study ends with the thesis contribution in Chapter 6. It should be noted that the thesis contribution has in fact changed as research has progressed. Therefore, this research is in fact conducted for the thesis contribution - including the research gap and research questions - presented in Chapter 1. Having noted this, Part III contains the main body of the thesis. This starts with performing the deterministic wake steering analysis in Chapter 7. Then, the uncertainty quantification framework and the input data for the uncertain parameters are described in Chapter 8. Next, the uncertainty quantification framework is applied to the OWEZ wind farm using the uncertain input parameters previously defined. The results are shown in Chapter 9. This is followed by the verification and validation of the framework and the results in Chapter 10. The report is finalized in Chapter 11 with the conclusions and recommendations, in Part IV.

Part I

Scientific Article

MDPI

Article

Uncertainty Quantification for Annual Energy Production Uplift due to Wake Steering

Yaren Cürgül [1], Bart Doekemeijer [2] and Marilena Pavel [1]

[1] Delft University of Technology
[2] Shell Global Solutions International B.V.

Abstract: Accurate yield estimations are necessary to prove the financial viability of wind farms in early-phase design. Due to the long time period between sea bed lease auctions and the decommissioning of wind farms, uncertainties in wind farm properties and atmospheric conditions arise. Wake steering is a wind farm flow control technology that was shown to have a substantial impact on annual energy production (AEP) in many field experiments;however, the accuracy of the AEP uplift estimated during the uncertain, early design phase is unknown. The present article addresses this concern by propagating uncertainties in atmospheric conditions, - namely turbulence intensity, wind shear and air density - wind rose and thrust curve forward to quantify the statistical uncertainty in AEP uplift estimations and by performing a sensitivity analysis to rank the significance of these uncertainties. For the Offshore Windpark Egmond aan Zee (OWEZ), the 95% confidence interval for the GCH is between 0.88% and 0.93%, while for the CC model this is between 1.08% and 1.14%. When compared with the deterministic AEP uplift of 0.97% for the GCH and 1.16% for the CC respectively, it is concluded that there is benefit from wake steering under input uncertainty for the OWEZ wind farm. Finally, for this case study the main driver of the variation in AEP uplift is the wind rose, with the other parameters having negligible effects.

Keywords: wake steering; uncertainty quantification; FLORIS; annual energy production; sensitivity analysis; early-phase assessments

Received:
Revised:
Accepted:
Published:

Citation: . Uncertainty Quantification for Annual Energy Production Uplift due to Wake Steering. *Journal Not Specified* **2025**, *1*, 0. https://doi.org/

1. Introduction

In the past five years, the increasing oil price, driven by embargoes and inflation, [1] and the surge in climate-related natural disasters highlighted the importance of investing in clean and abundant renewable energy sources. From these, wind power generation is projected to continue with nine European countries having pledged in 2023 to boost the offshore wind farm capacity in the North Sea [2]. To generate more and more energy, wind farm size is increasing [3]. As more wind turbines are placed closer together, wake-induced power losses increase. Wake losses are one of the major challenges in making wind farms profitable [4]. Therefore, the mitigation and quantification of wake losses is important for maximizing power in wind farms. A wake loss mitigation method that has been gaining increased attention is wind farm flow control [5]. The only wind farm control method to date that has been implemented commercially [6] - as a result of successful field experiments that showed significant annual energy production (AEP) gains [5,7] - is yaw-based wake steering.

In the current market, offshore wind farm developers compete for seabed leases that are auctioned by country governments years prior to the actual construction of the wind

farm [8]. The winning tender is often the one that makes the most financially interesting offer to the government and receives a permit for constructing and operating a wind farm, typically for a period of 25 years. This pushes strong financial burdens on developers and puts developers in a race to design wind farms that maximize electricity production while minimizing construction, operation and decommissioning costs. Technological innovations, such as wake steering, may play an important role in the early-phase design of wind farms by improving the financial feasibility of an auctioned future wind farm. With increasing pressure on wind energy viability, accurate yield estimation is important to prove the investment viability of the wind farm project. One example of a wind farm yield estimation tool used in wake steering applications is FLOw Redirection and Induction in Steady-state (FLORIS) [9]. FLORIS has been widely used in field experiments for wake steering controller design, more specifically for finding the optimal yaw angles of wind turbines (eg. [10–12]). In this thesis, we focus on the estimation of the benefit of the wake steering technology on a future wind farm's energy yield using FLORIS. This technology affects the predicted annual energy production in the order of 1%, and thereby has substantial impact on the financial feasibility of an early-phase wind farm design.

There is extensive literature on (yaw) optimization under uncertainty, for example in wind direction, wind speed and turbulence intensity (eg. [13–17]). However, because this concept has not been validated through field experiments, yaw optimizations for early-phase wake steering assessments in industry remain deterministic. Instead the accuracy of AEP uplift estimations are improved by quantifying the uncertainties through uncertainty propagation. During the early design phase, assumptions about the future wind turbine specifications, atmospheric conditions and wind rose are made. These include - amongst others - assumptions on the characteristics of the thrust curves, the value of the turbulence intensity and the frequency of occurence of certain wind directions and wind speeds.

[17] performed a sensitivity analysis of the input parameters on the yaw optimization and on the power gain due to yaw optimization under uncertainty using the dynamic FarmFlow wake model; however, the test case was limited to five wind turbines and the significance of the input parameters in terms of power gain with deterministic yaw optimization was not analyzed. The importance of different input parameters on the AEP uplift of a wind farm [18] and on WT output [19] was determined. However, in both cases this was limited to model uncertainty since the goal of the studies was to calibrate the FLORIS model for the wake steering application [18] or the FLORIDyn model - an adaptation of FLORIS considering the time-dependent influence of wake model parameters - without considering the wake steering application. Therefore, there is no study focused on understanding the significance and effect of uncertainties in input parameters on the AEP uplift for a wind farm using deterministic yaw optimization with FLORIS.

This paper addresses this scientific gap by propagating the uncertainties in atmospheric conditions and wind farm properties forward to determine the statistical uncertainty of the AEP uplift estimated in wake steering assessments. This is done by (1) quantifying the effect of the uncertainties in the input parameters with a Monte Carlo simulation and (2) ranking the significance of the same input parameters on the estimated AEP uplift due to wake steering through a sensitivity analysis. The by-product of the sensitivity analysis is quantifying the correlations between the significant input parameters. The scientific article describes the data set of the case study, the quantification of the uncertainty sources, FLORIS and the uncertainty quantification (UQ) framework in Section 2; discusses the results of the deterministic assessment, the convergence study on the smaller test case, the Monte Carlo (MC) simulation and the Sobol' method in Section 3; and, finally, presents the conclusions in Section 4.

2. Materials and Methods

2.1. Data Set

The case study is conducted on Offshore Windpark Egmond aan Zee (OWEZ) which is located in the North Sea at approximately 10 km off the Dutch shore. This WF has 36 Vestas V90 WTs with a nameplate capacity of 3 MW each. To its south-west, it is neighbored by the Prinses Amalia (PA) Wind Farm. This WF consists of 60 Vestas V80 WTs with a nameplate capacity of 2 MW each. The neighboring PA wind farm is considered in order to quantify the effect of the wakes of this neighboring wind farm on the AEP uplift of the OWEZ WF. The wind rose input for the case study is based on wind direction and wind speed data from the North Sea collected for the time interval between December 2006 and December 2010. The turbulence intensity for this time interval is kept constant at 0.06 for the deterministic wake steering assessment. The characteristics of the two wind turbine (WT) types, the wind rose and the exact locations of the WTs are shown in Table 1 and in Figure 1 respectively.

Table 1. Characteristics of wind turbines in OWEZ and PA.

Feature	Vestas V90	Vestas V80
Nameplate capacity [MW]	3	2
Hub height [m]	70.0	60.0
Rotor diameter [m]	90.0	80.0

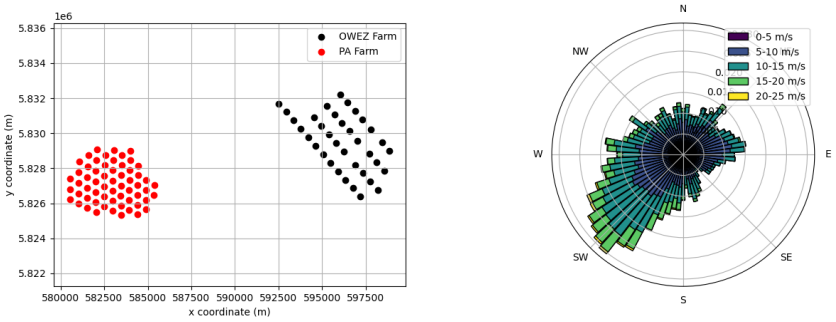

(**a**) (**b**)

Figure 1. Description of case study: (**a**) Layout of wind farms in NoordZeeWind. (**b**) Wind rose.

The uncertainty quantification framework is developed by initially introducing uncertainties in (1) *air density*, (2) *turbulence intensity* and (3) *wind shear*. These parameters are chosen for the development of the framework due to their ease of implementation and due to AEP output results found in existing uncertainty quantification literature (eg. [15,17]). The data set used to model the uncertainties in the atmospheric conditions is taken from the measurements at the meteorological mast between July 2005 and December 2010 and is fitted into PDFs using the Kolmogorov-Smirnov distance criterion, resulting in the marginal PDFs depicted in Figure 2.

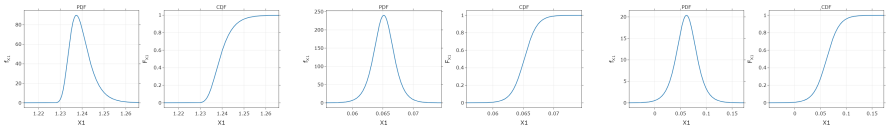

(**a**) (**b**) (**c**)

Figure 2. Probability distribution functions of input variables: (**a**) Air density. (**b**) Turbulence intensity. (**c**) Wind shear.

These marginal PDFs are assembled into a random input vector with joint PDF denoted as $\boldsymbol{X} \sim f_{\boldsymbol{X}}(\mathbf{x})$ [20]. The input vector represents the quantification of the sources of uncertainty (step B in Figure 5). Once the uncertainty quantification framework is verified with this input vector, a new input vector is created using the significant atmospheric variables, eleven wind roses available for Noordzeewind (shown in Figure 3) and thrust curves from nine wind turbines. Uncertainty in the wind rose is introduced because wind direction and wind speed were shown to be significant parameters [15–17,21]. Uncertainty in the thrust curve is introduced because developers often assume the characteristics of the thrust curve due to the lack of access to this information in the early stage design phase. Since the wind roses and thrust curves are discrete, these variables are modeled as uniform distributions with the ranges of [0,10] and [1,9] respectively.

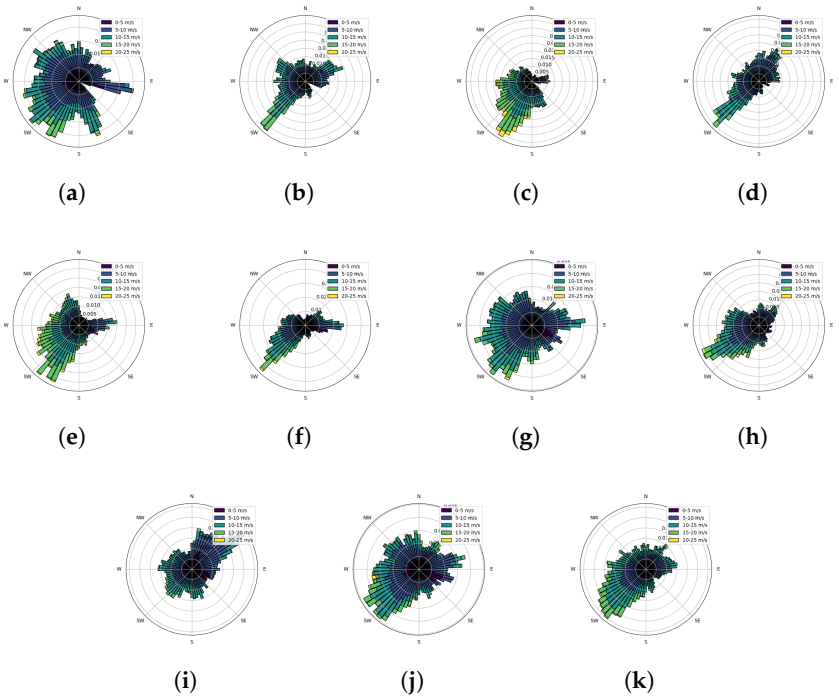

(**a**) (**b**) (**c**) (**d**)

(**e**) (**f**) (**g**) (**h**)

(**i**) (**j**) (**k**)

Figure 3. Possible wind rose selections: (**a**) Fig.0 (**b**) Fig.1 (**c**) Fig.2 (**d**) Fig.3 (**e**) Fig.4 (**f**) Fig.5 (**g**) Fig.6 (**h**) Fig.7 (**i**) Fig.8 (**j**) Fig.9 (**k**) Fig.10

2.2. FLORIS

FLORIS is a low fidelity steady-state model-based open-loop simulation software [9]. It is computationally efficient since, being low fidelity, the time-averaged flow field characteristics of wind farms for a given wind direction are estimated [22] using simplified analytical equations [14,23]. Open-loop controllers are the current practice in industry for wake steering because their use has been demonstrated in many field experiments (eg. [11,14,24,25]). However, open-loop control also means that all uncertainties are propagated

forward (eg. [26,27]). Confidence in yield assessments increases with more accurate models [11].

The results of the FLORIS model are highly dependent on the accuracy of the wind farm flow model used. This is because the wind farm flow model's calculation of the wake losses in the wind farm influences the AEP output. It is interesting to compare how differences in the wind farm flow model affect the input uncertainty since this can also reveal possible limitations of the wind farm flow models. In this research, two wind farm flow models are compared to understand their impact on the model response: (1) *Gaussian-Curl Hybrid (GCH)* and (2) *Cumulative Curl (CC)*.

GCH is the model that is the most frequently used in field experiments for wake steering (eg. [12]). This model maintains the relatively lower computational cost of the Gaussian wind farm flow model, while including ground effects, secondary steering effects and an enhanced wake deflection model with vortex-induced effects [28]. More recent studies show that deep array effects are underestimated with GCH, more specifically losses are under-predicted in the rear part of large wind farms and turbine pairs at distances larger than 25D [29,30]. The Cumulative Curl (CC) model [30] accounts for these effects. Since deep array effects are considered, more accurate near-wake predictions are made. Therefore, the power and wake estimations are more accurate while the same performance is obtained for smaller wind farms. In contrast to GCH, CC has still not been validated in field experiments with larger wind farms, having been used primarily in simulation studies [30]. By performing the uncertainty quantification on the two models,

2.3. Wake Steering Yield Assessment with FLORIS

Within FLORIS, the wake steering assessment can be separated into two portions: the yaw optimization and the annual energy production (AEP) output [31]. The two calculations are performed separately and independently for the entirety of the uncertainty quantification framework, as shown in Figure 4. The input variables - such as the wind rose, turbulence intensity and wind farm layout - are shown by arrows pointing towards the schematic, while the output variables - namely the deterministic AEP with no wake steering and the deterministic AEP with wake steering - are emphasized with the red font and arrows pointing out of the schematic.

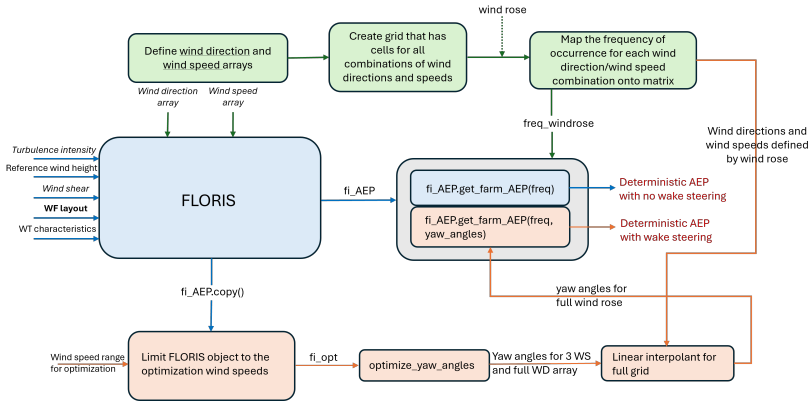

Figure 4. Methodology for deterministic wake steering yield assessment in FLORIS.

Within FLORIS, the wake steering assessment can be separated into two parts: yaw optimization and annual energy production (AEP) output [31]. The yaw optimization process is depicted in Figure 4 with pink boxes, while the flow chart to calculate the annual energy production is depicted with blue boxes. The two calculations are performed separately and independently for the entire uncertainty quantification framework.

The optimum yaw angles over the defined wind direction and wind speed combi-

nations are obtained for a given wind turbine type and wind farm layout. In this case, the Serial-Refine method is used to find the optimal yaw angles that minimize the wake losses of the wind farm. This optimization method reduces computational cost compared to other methods [32] and was used in recent field experiments to identify the optimal yaw angles for wake steering [33]. The wake losses of the wind farm are quantified differently according to the wind farm flow model selected. Therefore, the yaw angle optimization is repeated for different wind farm flow models. Table 2 summarizes the specifications of the yaw optimization used in the case study.

Table 2. Yaw optimization specifications

Feature	Selection
Optimization method [-]	Serial-Refine [32]
Wind direction array [°]	[0,360] with step size of 3°
Wind speed array $[m/s]$	[1,25] with step size of 1 $[m/s]$

In order to further reduce computational cost, the wind speed array is restricted to three wind speeds. This can be done because optimal yaw angles have been shown to barely change for different ambient wind speeds [17]. Then, the resulting yaw offset angles for the three wind speeds and full wind direction array are linearly interpolated over the full wind speed array. Thus, the optimal yaw offsets for all combinations of wind direction/wind speed are determined.

The wind direction and wind speed arrays in Table 2 are used to create a grid representing all possible combinations of wind direction/wind speed for the defined arrays. Then, SCADA wind direction and wind speed time series data is used to create the wind rose. The wind rose is a representation of the frequency of occurrence of each combination of wind direction/wind speed. This process is illustrated with the green boxes in Figure 4. Therefore, the probability of occurrence of each combination of wind direction/wind speed is obtained along with its associated optimal yaw angle.

The deterministic annual energy production output without wake steering is computed by taking the weighted sum of the power for a specific combination of wind direction and speed and the probability of occurrence of that combination of wind direction and wind speed. This weighted sum is multiplied by the number of hours in a year. To calculate the deterministic AEP for wake steering, the power under the yaw offset angle is used for the specific combination of wind direction and speed. For uncertainty quantification, the input variables that were identified as sources of uncertainty are replaced by the random input vector defined in **??**. Next, the yaw offset angles are introduced, resulting in the annual energy production with wake steering (optimized AEP). In this way, the effect of the uncertainties in the input variables on the AEP is quantified. This is compared with the AEP without the optimized yaw angles (baseline AEP) to evaluate the AEP uplift due to wake steering.

2.4. Uncertainty Quantification Framework

The uncertainty in wake steering yield estimation, more specifically the AEP uplift estimation, during the early-phase wind farm design is defined as an uncertainty propagation problem. The uncertainty propagation problem means analyzing the effect of input uncertainties on the system's output [34]; or, in mathematical terms:

$$P(x|k) \xrightarrow{f} P(y|k) \tag{1}$$

The uncertainty quantification framework that propagates uncertainties and performs the sensitivity analysis for ranking the importance of the sources of uncertainty is depicted in Figure 5.

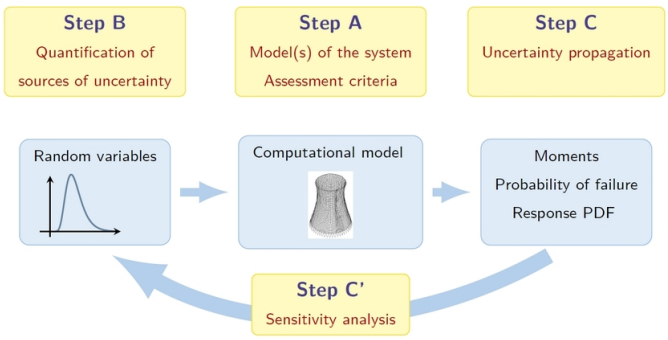

Figure 5. Uncertainty quantification framework [35]

The steps shown in the uncertainty propagation framework are briefly described below [35].

- *Step A* relates to defining the model of the physical system and the criteria to assess the physical system. The uncertainties are propagated from the input to the output through the computational model, preferably without introducing additional biases. In this case, the complex wake interactions of the wind farm are modeled with FLORIS software which is a black-box model.
- *Step B*: the sources of uncertainty are quantified by identifying and modeling the uncertain input parameters. In this way, a random vector of input parameters is obtained.
- *Step C*: the uncertainty defined by the random input vector is propagated through the computational model. In this analysis, a response probability distribution function is obtained following the uncertainty propagation.
- *Step C'*: using the relationship between the output and input, the importance of the uncertain input variables are ranked. This is the sensitivity analysis.

To perform the uncertainty propagation (step C in Figure 5), Monte Carlo method is used. This is because this is a non-intrusive method that assumes the computational model is a 'black box' [36]. Therefore, unlike surrogate models such as polynomial chaos expansion and Kriging, the computational model is not approximated [34] and, thus, an approximation error is not introduced [(34,37)]. Moreover, with the Monte Carlo method, it is possible to use the same framework even when input parameters are changed [37]. In addition, MC simulations do not suffer from the curse of dimensionality. The curse of dimensionality means that the number of samples necessary increases exponentially with the number of random variables [34]. The main drawback of the MC is that experiments with many input parameters or requiring many iterations may be computationally expensive [36]. This disadvantage may be dealt with by proving the convergence of output values as demonstrated in subsection 3.2.

The final step of the uncertainty quantification framework (step C' in Figure 5) is performing a global sensitivity analysis using Sobol' indices [35]. The goal is to understand the importance of each input parameter in terms of its effect on the variation in AEP uplift. Sobol' indices decompose the total variance of the model response into the sum of the variances of its summands. The variance decomposition assumes that the input variables are independent [38], which fits this study since there is no data on the correlations between the input variables. With Sobol' indices, the significance of the input parameters and the interaction effects of groups of input parameters can be identified [39]. The advantage of

Sobol' indices is that the model is not assumed to be monotonic or linear. In addition, with Sobol' indices the combined influence of the parameters on the uncertainty in the output can be discovered [35].

2.4.1. Monte Carlo Simulation

The Monte Carlo method involves generating random samples from the input vector defined in subsection 2.1. With Monte Carlo sampling, the samples $\mathcal{U} = \left\{\boldsymbol{u}^{(1)}, \ldots, \boldsymbol{u}^{(N)}\right\}$ are produced in the standard uniform space $\boldsymbol{Z} \sim \mathcal{U}([0,1]^M)$. Then, these samples are transformed back into the samples $\mathcal{X} = \left\{\boldsymbol{x}^{(1)}, \ldots, \boldsymbol{x}^{(N)}\right\} \sim F_{\boldsymbol{X}}$ for any multivariate distribution $F_{\boldsymbol{X}}$ with independent marginals F_{X_i} using the inverse probability integral transform (PIT):

$$x_j^{(i)} = F_{X_j}^{-1}\left(u_j^{(i)}\right) \tag{2}$$

for all $i = 1, ..., N$ and all $j = 1, ..., M$ [20]. The vector of generated random samples $\boldsymbol{X}$ is inserted into the black-box computational model, in this case FLORIS:

$$\boldsymbol{Y} = \mathcal{M}(\boldsymbol{X}) \tag{3}$$

to obtain the vector of model responses $\boldsymbol{Y}$ [40]. This is used to compute the expectation, standard deviation and the confidence intervals [41] using the estimators in Equation 5.

2.4.2. Sobol Method

The variance of the model response is defined by the sensitivity measure, or Sobol' index, as [42]:

$$S_{i_1,\ldots,i_s} = \frac{Var(Y(X_{i_1,\ldots,i_s}))}{Var(Y)} \tag{4}$$

for a group of variables $X_{i_1,\ldots,i_s}$, where $Var(Y(X_{i_1,\ldots,i_s}))$ denotes the partial variances of the summands and $Var(Y)$ denotes the total variance of the model response Y.

The first-order Sobol' index is the relative contribution of only one input variable X_i on the total variance. The first-order Sobol' indices must be positive. There are also indices with multiple term called higher-order Sobol' indices that account for the effects of the interactions between the input variables that cannot be divided into separate variances. The sum of all Sobol' indices for an input variable X_i is denoted as the total Sobol index S_i^T. The variances described in Equation 4 are computed using the mean, variance and partial variance estimators respectively that were derived from the Monte Carlo simulation [42]:

$$\begin{aligned}
\widehat{f_0} &= \frac{1}{N}\sum_{n=1}^{N} f\left(\boldsymbol{x}^{(n)}\right) \\
\widehat{Var(Y)} &= \frac{1}{N}\sum_{n=1}^{N} f^2\left(\boldsymbol{x}^{(n)}\right) - \widehat{f_0}^2 \\
\widehat{Var(Y(x_i))} &= \frac{1}{N}\sum_{n=1}^{N} f\left(x_i^{(n)}, \boldsymbol{x}_{\sim i}^{(n)}\right) f\left(x_i^{(n)}, \boldsymbol{x}_{\sim i}^{\prime(n)}\right) - \widehat{f_0}^2
\end{aligned} \tag{5}$$

where $\boldsymbol{x}'$ denotes a realization of $\boldsymbol{X}$ independent of $\boldsymbol{x} = \left\{x_i^{(n)}, \boldsymbol{x}_{\sim i}^{(n)}\right\}^\top$, and the subscript $\boldsymbol{x}_{j,\sim i}$ indicates the j-th realization of $\boldsymbol{x}$ which does not contain the input variable i.

The total computational cost of computing MC-based Sobol' indices is $(M+2) \times N$, where M is the input dimension and N is the sample size [42]. To improve the computational efficiency of uncertainty quantification, a convergence study must be performed.

3. Results and Discussion

3.1. Deterministic Wake Steering Assessment

For deterministic wake steering assessment, the yaw optimization is conducted for OWEZ. With these yaw offset angles, two cases are evaluated: the one including the wake effects of the neighboring wind farm and the one ignoring these wake effects. Including the wake effects of the neighboring wind farm provides a more realistic assessment of the AEP but increases the computational cost. The cases are evaluated for the GCH and CC models. The results are given in Table 3.

Table 3. Results of deterministic wake steering yield assessment.

WFFM	Baseline AEP [GWh]	Optimized AEP [GWh]	AEP uplift
GCH (with neighbor)	448.428	452.778	+0.97%
GCH (no neighbor)	448.635	452.998	+0.97%
CC (with neighbor)	441.434	446.547	+1.16%
CC (no neighbor)	443.204	448.345	+1.16%

The neighboring WF's wake is shown to have no significant effect on the AEP uplift of OWEZ. This can be explained by the fact that the WTs are placed 7.5 km apart, which is a distance greater than $80D$. At this distance from the WT, wake mixing has occurred to a great extent. While there are some changes in the baseline and optimized AEP, it is interesting to note that this does not change the AEP uplift. With this conclusion, the uncertainty quantification is performed ignoring the neighboring wind farm in order to reduce computational time. It is also observed that the AEP uplift increases when a more accurate WFFM is selected in FLORIS. This shows that typical wake steering yield assessments that are conducted using the GCH model under-estimate the AEP uplift in OWEZ.

3.2. Convergence Study

The convergence study for the AEP uplift is conducted on a smaller test case of five equally distanced Vestas V90-3 MW WTs using the GCH model to reduce the computational cost. The convergence of the total Sobol' index for one of the input parameters, namely the turbulence intensity, is also evaluated under the same conditions. It is assumed that the total Sobol' indices for the other parameters converge similarly because the total Sobol' indices form fractions of a whole. Figure 6 depicts the results of the convergence studies.

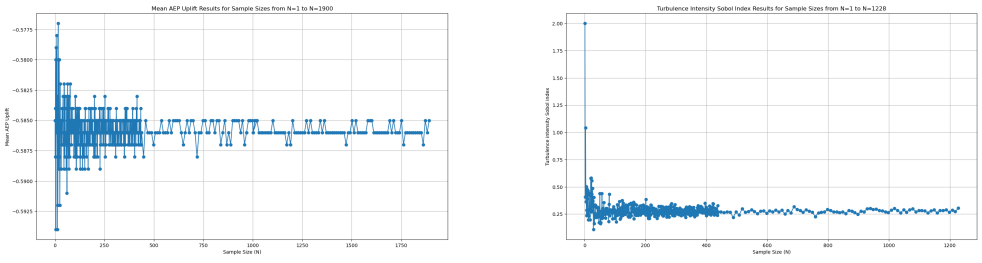

(**a**) (**b**)

Figure 6. Convergence study for five wind turbines using GCH as a function of sample size: (**a**) Convergence of mean AEP uplift. (**b**) Convergence of the total Sobol' index of turbulence intensity.

Starting from N = 100, the maximum and minimum mean AEP uplift fluctuate within a relatively small range of 0.65%. As the sample size increases, the range of fluctuation in

mean AEP uplift decreases further, indicating convergence. Therefore, N = 100 is chosen as the minimum sample size required to estimate the mean AEP uplift. The computational cost of this sample size is small enough to not necessitate the use of surrogate models.

Starting from N = 225, the total Sobol' index for turbulence intensity fluctuates by 25%. At N = 1228, the rate of fluctuation in the total Sobol' index decreases to 12% which implies that at higher sample sizes convergence occurs. Thus, the Sobol' index has a moderate level of sensitivity to sample size. Despite this, the fluctuation rate is not significant enough to change conclusions regarding the importance of input parameters on the AEP uplift. Since computing Sobol' indices is more resource-intensive than MC-sampling for uncertainty propagation, there is further motivation to select the lowest sample size that leads to the appropriate conclusions instead of the sample size that has the same fluctuation rate as the convergence study for the mean AEP uplift. Repeating the calculation of the total Sobol' index for N = 10000 - which is a significantly higher sample size - shows that the ranking of the Sobol' indices remain the same as the N = 225 but the computational cost is significantly higher. This justifies the selection of N = 225 as the minimum sample size required. Since uncertainty propagation and sensitivity analysis is inherently connected, the same sample size is chosen for both. The most conservative estimate (N = 225) is selected.

In order to verify that the sample size selected for the smaller test case can be used for the full OWEZ wind farm, the convergence rate of first order Sobol' indices are evaluated as as a function of the number of wind turbines for N = 225 and N = 400 in Figure 7.

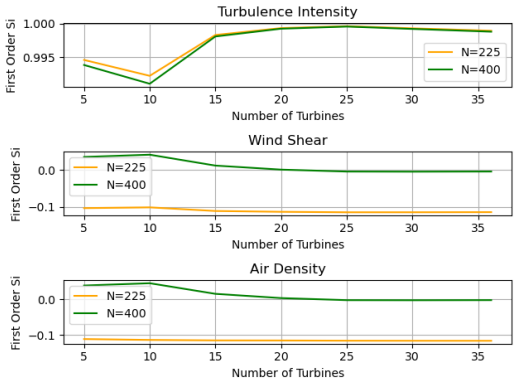

Figure 7. Convergence study for first order Sobol' indices using GCH as a function of the number of wind turbines: (**a**) Turbulence intensity. (**b**) Wind shear. (**b**) Air density.

The convergence rate for the first order Sobol' index of turbulence intensity is almost the same for both sample sizes, while the ones for the air density and wind shear are constant for both sample sizes due to the AEP uplift being almost entirely driven by the turbulence intensity. Hence, it is shown that while there are small differences in the first order Sobol' indices as the number of samples increases, the difference is negligible enough to not change the conclusions obtained from the study. Additionally, the first order Sobol' indices converge at 20 wind turbines. It is theorized that this is due to the aerodynamic flow becoming fully developed as one goes deeper into the wind farm; therefore, once a specific limit is reached, no variation in the estimated AEP uplift as a function of the variations in input variables would take place [43]. This brings forth the possibility of reducing the computational cost further in future research by running the wake steering assessment on fewer wind turbines from the OWEZ wind farm.

3.3. Sobol' Method

The sensitivity analysis is performed on the full OWEZ wind farm at N = 225 for both GCH and CC using Sobol' indices in order to rank the importance of each input variable on the

estimated mean AEP uplift. The total Sobol' indices for the input vector with the air density, wind shear and turbulence intensity are shown in Figure 8.

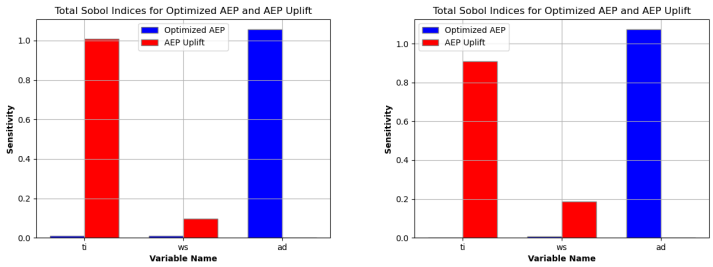

(**a**) (**b**)

Figure 8. Sobol' indices resulting from sensitivity analysis on OWEZ at N = 225: (**a**) Total Sobol' indices for GCH. (**b**) Total Sobol' indices for CC.

The most significant parameters are not the same for the optimized AEP and the AEP uplift. While air density is the only driving parameter for the optimized AEP, it has no influence on the estimation of the AEP uplift. Instead, for both wind farm flow models, the AEP uplift is estimated with the turbulence intensity and wind shear. The contribution of turbulence intensity is significant, while the contribution of wind shear is relatively insignificant at 0.1 for GCH and 0.2 for CC. This is consistent with findings in literature demonstrating that significant changes in yaw misalignment angles occur for turbulence intensity, but not for wind shear and air density, following an uncertainty quantification study [17]. The difference in the Sobol' indices between the two models is insignificant. Therefore, the UQ framework's efficacy is demonstrated, and turbulence intensity is the only variable added to the new input vector. Because the new input vector has the same number of variables as the initial input vector, the convergence study is not repeated. This results in Figure 9.

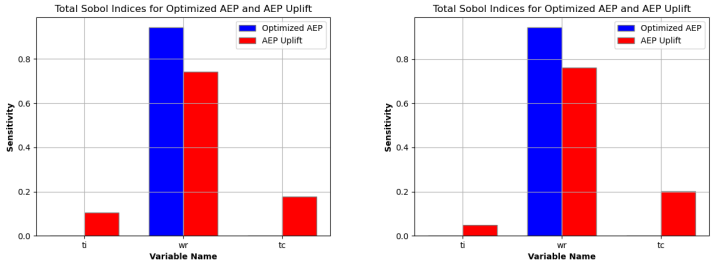

(**a**) (**b**)

Figure 9. Sobol' indices resulting from sensitivity analysis on OWEZ at N = 225: (**a**) Total Sobol' indices for GCH. (**b**) Total Sobol' indices for CC.

The difference in total Sobol' indices between the two models is insignificant. However, in this case, the ranking of the input variables is the same for the optimized AEP and for the AEP uplift. While the optimized AEP is fully determined by the wind rose, the AEP uplift is also influenced by smaller, relatively insignificant turbulence intensity and thrust curve contributions. The large contribution of the wind rose to the total variance of the AEP uplift is attributed to the significant variations in the wind directions of the input wind roses. This is a limitation of the input data available and shows the sensitivity of the output to the selected input range. With the Monte Carlo method, a more in-depth analysis of the influence of these variables on the estimated AEP uplift is performed.

3.4. Monte Carlo Simulation

The Monte Carlo simulation is performed for the full OWEZ wind farm with the input vector that includes the turbulence intensity, the thrust curves and the wind roses. Figure 10 shows the AEP uplift distributions for the two WFFMs.

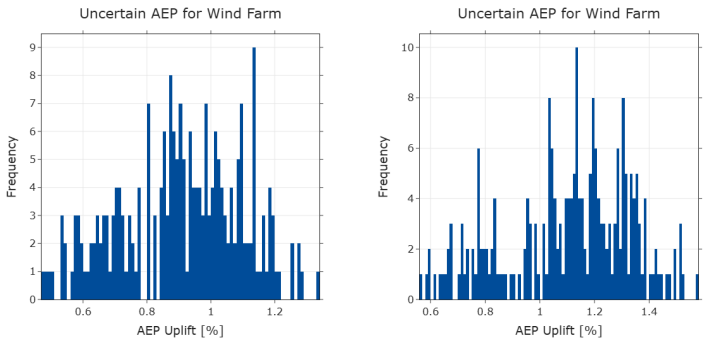

(**a**) (**b**)

Figure 10. AEP Uplift Distributions for OWEZ at N = 225 for: (**a**) GCH. (**b**) CC.

The mean AEP uplift for the GCH model is 0.91% with a standard deviation of 0.19, while the mean AEP uplift for the CC model is 1.11% with a standard deviation of 0.23. In both cases, there is benefit from wake steering within one standard deviation of the mean. The 95% C.I. for the GCH model is between 0.88% and 0.93% with a range of 0.050, while the 95% C.I. for the CC model is between 1.08% and 1.14% with a range of 0.060. This means that there is a wider spread in the distribution and a more pronounced difference between the two WFFMs.

In the GCH model, the smallest AEP uplift is between 0.45% and 0.64%. Fig. 2 and Fig. 4 are the most frequently occurring wind roses with the dominant wind direction coming from the south and south-west and a heavy skew towards the western direction, and wind speeds of 15-20 m/s concentrated on the dominant wind directions. The turbulence intensities are between 6.6% and 7.0%, and - while this AEP uplift range has a mix of different thrust curves - thrust curve 6 appears the most frequently. On the other end of the spectrum, the largest AEP uplift values are between 1.16% and 1.33%. Fig. 8 is the most frequently occurring wind rose with the dominant wind direction coming from the north-east direction. Fig.0 - that has a wider spread across different wind directions - and Fig.3 - whose wind directions are concentrated in the south-west direction - are also frequently observed at this AEP uplift range. Wind speeds in the range 5-10 m/s and 15-20 m/s and turbulence intensities between 6.2% and 6.45% occur the most. Thrust curve 1 is the most frequently used. From this analysis, it is concluded that the thrust curve has a more modest influence on the estimated AEP uplift than the wind speed and wind direction combination. At the 95% C.I., there is no dominant thrust curve, which confirms the previous conclusion. The dominant wind direction is from the south-west direction and the dominant wind speed is between 10-15 m/s with significant 15-20 m/s wind speed components in the same direction. The turbulence intensity varies between 6.4% and 6.8%. This shows the importance of the wind speed contribution and, to a lesser extent of the wind direction, in determining the estimated AEP uplift.

The CC model has slightly smaller turbulence intensities than the GCH, but the range of turbulence intensities is the same for the different AEP uplift levels. Therefore, the influence of the turbulence intensity on the estimated AEP uplift does not show a significant change. At the largest AEP uplift values, which are between 1.16% and 1.33%,

fig. 5 replaces fig. 0 as one of the most frequently occurring wind roses. Therefore, the wind roses that result in the highest AEP uplift either have the combination of the dominant wind direction in the north-east and wind speed of 5-10 m/s or the combination of the dominant wind direction in the south-west and the higher wind speeds of 10-15 m/s or 15-20 m/s. At the 95% C.I., the GCH model had one dominant wind rose. The 95% C.I. for the CC model has more than one dominant wind rose. Besides the wind direction/wind speed combination that occurs in the GCH, wind roses with the dominant south-west wind direction and a heavier skew towards the western direction combined with wind speeds of 10-15 m/s and some 5-10 m/s components.

4. Conclusions

The uncertainty quantification framework developed effectively determined the statistical uncertainty in the AEP uplift estimated in wake steering assessments. The 95% confidence interval for both GCH and CC consistently showed positive AEP uplift estimates. For the GCH model, this was between 0.88% and 0.93%, while for the CC model this was between 1.08% and 1.14%. The mean AEP uplift for GCH was 0.91% with a standard deviation of 0.19, while the mean AEP uplift for CC was 1.11% with a standard deviation of 0.23. Based on these findings, it was concluded that wake steering had significant benefit for the OWEZ wind farm for the defined input variables. For future research, it would be interesting to compare the statistical uncertainties for the two wind farm flow models given a larger wind farm size, as it is known that, unlike GCH, CC models deep array effects which are more relevant for larger wind farms [30].

The framework was verified by performing uncertainty quantification on the input vector consisting of wind shear, air density, and turbulence intensity. With this, the turbulence intensity was identified as the most significant driver for estimating the AEP uplift. This was consistent with findings related to the effect of the input parameters on the yaw offset angles [17], leading to the recommendation that in further wake steering assessments that are significantly limited by computational cost air density and wind shear uncertainty should not be considered. Afterwards, the main uncertainty quantification study was performed on the input vector consisting of turbulence intensity, wind rose and thrust curve. The wind rose was shown to have the most significant influence on the estimated AEP uplift which was anticipated by previous studies on the estimation of the yaw angle effect and optimized AEP (eg. [17,18]). Moreover, the wind roses that resulted in the highest AEP uplift either had the combination of the dominant wind direction in the north-east and wind speed of 5-10 m/s or the combination of the dominant wind direction in the south-west and the higher wind speeds of 10-15 m/s or 15-20 m/s. It was concluded that with these wind roses the greatest benefit from wake steering was obtained.

Overall, future researchers must expand the input variables considered and validate the uncertainty quantification framework further on (1) different input data and (2) different wind farms. When different input variables are considered and the study is repeated on different wind farms, the convergence study that determines the maximum WT number and the minimum sample size required must be repeated. This is because for different wind farm layouts and wind turbine configurations different conclusions regarding convergence may be obtained. Repetition of the study on different input data sets yields more reliable estimates of statistical uncertainties. Once a larger database of AEP uplift estimations and input variable rankings is obtained for a wider variety of wind farms and input data, the database can be grouped and classified into different categories. In this way, behavioral patterns are obtained that can be used to create rules of thumb for AEP uplift estimations and even to train algorithms that estimate AEP uplift.

Author Contributions: Conceptualization, Y.C., B.D. and M.P.; methodology, Y.C.; software, Y.C.; validation, Y.C..; formal analysis, Y.C.; investigation, Y.C.; resources, B.D. and Y.C.; data curation, B.D.; writing—original draft preparation, Y.C.; writing—review and editing, Y.C., B.D. and M.P.; visualization, Y.C.; supervision, B.D. and M.P.; project administration, M.P.; funding acquisition, B.D. All authors have read and agreed to the published version of the manuscript.

Funding: This research was funded by Shell Global Solutions International B.V.

Acknowledgments: Thanks to Dr. Jasper Kreeft for his technical and administrative support and to Prof. Dr. Jan-Willem van Wingerden, Marcus Becke, PJ Stanley and Robin de Jong for their technical support.

References

1. The Economist. Why the oil price is spiking again. https://www.economist.com/finance-and-economics/2022/05/31/why-the-oil-price-is-spiking-again, 2022. Accessed: 01/05/2024.
2. Henley, J. European countries pledge huge expansion of North Sea wind farms. https://www.theguardian.com/environment/2023/apr/24/european-countries-pledge-huge-expansion-of-north-sea-wind-farms, 2023. Accessed: 01/05/2024.
3. SSE. Construction begins on the world's largest offshore wind farm. https://www.sse.com/news-and-views/2022/04/construction-begins-on-the-world-s-largest-offshore-wind-farm/, 2022. Accessed: 02/05/2024.
4. University of Bergen. The wake effect: Offshore wind farms can 'steal' wind from one another. https://techxplore.com/news/2023-10-effect-offshore-farms.html, 2023. Accessed: 01/05/2024.
5. Houck, D.R. Review of wake management techniques for wind turbines. *Wind Energy* **2022**, *25*, 195–220. https://doi.org/10.1002/we.2668.
6. Wind Systems. WindESCo installs industry-first wake steering. https://www.windsystemsmag.com/windesco-installs-industry-first-wake-steering/, 2023. Accessed: 13/03/2024.
7. Doekemeijer, B.M. Closing the loop in model-based wind farm control. PhD thesis, Delft University of Technology, 2020. https://doi.org/10.4233/uuid:35022242-b3ba-48d9-b3f6-c6ab20b8cc19.
8. Sijtsma, L. Financial Auctions for Offshore Wind. https://guidehouse.com/insights/energy/2023/financial-auctions-for-offshore-wind, 2023. Accessed: 13/01/2025.
9. Gebraad, P.M.O.; Teeuwisse, F.W.; van Wingerden, J.W.; Fleming, P.A.; Ruben, S.D.; Marden, J.R.; Pao, L.Y. Wind plant power optimization through yaw control using a parametric model for wake effects—a CFD simulation study. *Wind Energy* **2016**, *19*, 95–114, [https://onlinelibrary.wiley.com/doi/pdf/10.1002/we.1822]. https://doi.org/https://doi.org/10.1002/we.1822.
10. Simley, E.; Fleming, P.; King, J.; Sinner, M. Wake Steering Wind Farm Control With Preview Wind Direction Information. In Proceedings of the 2021 American Control Conference (ACC), May 2021, pp. 1783–1789. https://doi.org/10.23919/ACC50511.2021.9483008.
11. Doekemeijer, B.M.; Kern, S.; Maturu, S.; Kanev, S.; Salbert, B.; Schreiber, J.; Campagnolo, F.; Bottasso, C.L.; Schuler, S.; Wilts, F.; et al. Field experiment for open-loop yaw-based wake steering at a commercial onshore wind farm in Italy. *Wind Energy Science* **2021**, *6*, 159–176. https://doi.org/10.5194/wes-6-159-2021.
12. Fleming, P.; King, J.; Simley, E.; Roadman, J.; Scholbrock, A.; Murphy, P.; Lundquist, J.K.; Moriarty, P.; Fleming, K.; Dam, J.V.; et al. Continued results from a field campaign of wake steering applied at a commercial wind farm - Part 2. *Wind Energy Science* **2020**, *5*, 945–958. https://doi.org/10.5194/wes-5-945-2020.
13. Rott, A.; Doekemeijer, B.; Seifert, J.K.; Wingerden, J.W.V.; Kühn, M. Robust active wake control in consideration of wind direction variability and uncertainty. *Wind Energy Science* **2018**, *3*, 869–882. https://doi.org/10.5194/wes-3-869-2018.
14. Simley, E.; Fleming, P.; King, J. Design and analysis of a wake steering controller with wind direction variability. *Wind Energy Science* **2020**, *5*, 451–468. https://doi.org/10.5194/wes-5-451-2020.
15. Quick, J.; King, J.; King, R.N.; Hamlington, P.E.; Dykes, K. Wake steering optimization under uncertainty. *Wind Energy Science* **2020**, *5*, 413–426. https://doi.org/10.5194/wes-5-413-2020.
16. Howland, M.F. Wind farm yaw control set-point optimization under model parameter uncertainty. *Journal of Renewable and Sustainable Energy* **2021**, *13*. https://doi.org/10.1063/5.0051071.
17. Kanev, S.; Bot, E. Dynamic robust active wake control. *Wind Energy Science* **2021**. https://doi.org/10.5194/wes-2021-71.
18. van Beek, M.; Viré, A.; Andersen, S. Sensitivity and Uncertainty of the FLORIS Model Applied on the Lillgrund Wind Farm. *Energies* **2021**, *14*, 1293. https://doi.org/10.3390/en14051293.
19. Dighe, V.V.; Becker, M.; Göçmen, T.; Sanderse, B.; van Wingerden, J.W. Sensitivity analysis and Bayesian calibration of a dynamic wind farm control model: FLORIDyn. *Journal of Physics: Conference Series* **2022**, *2265*, 022062. https://doi.org/10.1088/1742-6596/2265/2/022062.

20. Lataniotis, C.; Torre, E.; Marelli, S.; Sudret, B. UQLab user manual – The Input module. Technical report, Chair of Risk, Safety and Uncertainty Quantification, ETH Zurich, Switzerland, 2024. Report UQLab-V2.1-102.
21. Quick, J.; Annoni, J.; King, R.; Dykes, K.; Fleming, P.; Ning, A. Optimization under Uncertainty for Wake Steering Strategies. In Proceedings of the Journal of Physics: Conference Series. Institute of Physics Publishing, 6 2017, Vol. 854. https://doi.org/10.1088/1742-6596/854/1/012036.
22. Dong, H.; Xie, J.; Zhao, X. Wind farm control technologies: From classical control to reinforcement learning. *Progress in Energy* **2022**, *4*. https://doi.org/10.1088/2516-1083/ac6cc1.
23. Fleming, P.; King, J.; Dykes, K.; Simley, E.; Roadman, J.; Scholbrock, A.; Murphy, P.; Lundquist, J.K.; Moriarty, P.; Fleming, K.; et al. Initial results from a field campaign of wake steering applied at a commercial wind farm – Part 1. *Wind Energy Science* **2019**, *4*, 273–285. https://doi.org/10.5194/wes-4-273-2019.
24. Fleming, P.; Annoni, J.; Shah, J.J.; Wang, L.; Ananthan, S.; Zhang, Z.; Hutchings, K.; Wang, P.; Chen, W.; Chen, L. Field test of wake steering at an offshore wind farm. *Wind Energy Science* **2017**, *2*, 229–239. static LUT, https://doi.org/10.5194/wes-2-229-2017.
25. Bossanyi, E.; Ruisi, R. Axial induction controller field test at Sedini wind farm. *Wind Energy Science* **2021**, *6*, 389–408. https://doi.org/10.5194/wes-6-389-2021.
26. Howland, M.F.; Ghate, A.S.; Lele, S.K.; Dabiri, J.O. Optimal closed-loop wake steering – Part 1: Conventionally neutral atmospheric
boundary layer conditions. *Wind Energy Science* **2020**, *5*, 1315–1338. https://doi.org/10.5194/wes-5-1315-2020.
27. Liew, J.; Göçmen, T.; Lio, W.H.; Larsen, G.C. Model-free closed-loop wind farm control using reinforcement learning with recursive least squares. *Wind Energy* **2023**. https://doi.org/10.1002/we.2852.
28. Martínez-Tossas, L.A.; Annoni, J.; Fleming, P.A.; Churchfield, M.J. The aerodynamics of the curled wake: A simplified model in view of flow control. *Wind Energy Science* **2019**, *4*, 127–138. https://doi.org/10.5194/wes-4-127-2019.
29. Nygaard, N.G.; Steen, S.T.; Poulsen, L.; Pedersen, J.G. Modelling cluster wakes and wind farm blockage. In Proceedings of the Journal of Physics: Conference Series. IOP Publishing Ltd, 9 2020, Vol. 1618. https://doi.org/10.1088/1742-6596/1618/6/062072.
30. Bay, C.J.; Fleming, P.; Doekemeijer, B.; King, J.; Churchfield, M.; Mudafort, R. Addressing deep array effects and impacts to wake steering with the cumulative-curl wake model. *Wind Energy Science* **2023**, *8*, 401–419. https://doi.org/10.5194/wes-8-401-2023.
31. NREL. FLORIS Wake Modeling and Wind Farm Controls Software v4.0.1. https://github.com/NREL/floris, 2024. Accessed: 30/04/2024.
32. Fleming, P.A.; Stanley, A.P.; Bay, C.J.; King, J.; Simley, E.; Doekemeijer, B.M.; Mudafort, R. Serial-Refine Method for Fast Wake-Steering Yaw Optimization. In Proceedings of the Journal of Physics: Conference Series. Institute of Physics, 6 2022, Vol. 2265. https://doi.org/10.1088/1742-6596/2265/3/032109.
33. Moriarty, P.; Bodini, N.; Cheung, L.; Hamilton, N.; Herges, T.; Kaul, C.; Letizia, S.; Pekour, M.; Simley, E. Overview of recent observations and simulations from the American WAKE experimeNt (AWAKEN) field campaign. In Proceedings of the Journal of Physics: Conference Series. Institute of Physics, 2023, Vol. 2505. https://doi.org/10.1088/1742-6596/2505/1/012049.
34. van den Bos, L.; Sanderse, B. Uncertainty quantification for wind energy applications - Literature review. Technical Report SC-1701, Centrum Wiskunde Informatica, 2017.
35. Sudret, B. Uncertainty propagation and sensitivity analysis in mechanical models - Contributions to structural reliability and stochastic spectral methods. PhD thesis, Université Blaise Pascal - Clermont II, 2007.
36. Benke, K.K.; Norng, S.; Robinson, N.J.; Benke, L.R.; Peterson, T.J. Error propagation in computer models: analytic approaches, advantages, disadvantages and constraints. *Stochastic Environmental Research and Risk Assessment* **2018**, *32*, 2971–2985. https://doi.org/10.1007/s00477-018-1555-8.
37. Tyson, S.; Donovan, D.; Thompson, B.; Lynch, S.; Tas, M. Uncertainty modelling with polynomial chaos expansion: Stage 1 – Final Report. Technical Report 149297, University of Queensland, 2015.
38. Sobol, I.M. Sensitivity Estimates for Nonlinear Mathematical Models. *Mathematical Modelling and Computational Experiments* **1993**, *1*, 407–414.
39. Zhang, J.; Yin, J.; Wang, R. Basic Framework and Main Methods of Uncertainty Quantification. *Mathematical Problems in Engineering* **2020**, *2020*, 6068203, [https://onlinelibrary.wiley.com/doi/pdf/10.1155/2020/6068203]. https://doi.org/https://doi.org/10.1155/2020/6068203.
40. Lataniotis, C.; Zhu, X.; Marelli, S.; Sudret, B. UQLab user manual – The Model module. Technical report, Chair of Risk, Safety and Uncertainty Quantification, ETH Zurich, Switzerland, 2024. Report UQLab-V2.1-103.
41. Zhang, J. Modern Monte Carlo methods for efficient uncertainty quantification and propagation: A survey. *Wiley Interdisciplinary Reviews: Computational Statistics* **2021**, *13*. https://doi.org/10.1002/wics.1539.
42. Marelli, S.; Lamas, C.; Konakli, K.; Mylonas, C.; Wiederkehr, P.; Sudret, B. UQLab user manual – Sensitivity analysis . Technical report, Chair of Risk, Safety and Uncertainty Quantification, ETH Zurich,Switzerland, 2024. Report UQ[py]Lab - V1.0-106.
43. Wu, K.L.; Porté-Agel, F. Flow adjustment inside and around large finite-size wind farms. *Energies* **2017**, *10*. https://doi.org/10.3390/en10122164.

Part II

Literature Study*

*This part has been assessed for the course AE4020 Literature Study; therefore, no modifications were made to this part.

3

Wind Farm Technology

In Chapter 1, wake-induced energy losses were posed as a significant challenge in making wind farms viable. To better understand how wind farms function, Chapter 3 introduces the reader to wind farm technology and the concept of wind farm flow control. This chapter focuses solely on the physical mechanism used in wind farms and on wind farm flow physics. Section 3.1 explains the main working principle of a wind turbine, of wind farms and the effect of turbine interactions in wind farms. Section 3.2 describes the concept of wind farm control, the different existing wind farm control strategies and the main working principle of wake steering.

3.1. Wind turbines, wind farms and wakes

In order to comprehend energy generation using wind technology, it is crucial to understand the working principle of wind farms and physical effects affecting energy production. This section starts by introducing the working mechanism of wind turbines in Section 3.1.1. This is then followed by introducing the concept of wind farms in Section 3.1.2. The wake interactions that arise when wind turbines are arranged together are explained in Section 3.1.3. Finally, methods to reduce the negative effect of wake interactions are presented in Section 3.1.4.

3.1.1. Main working principle of a wind turbine

With increasing demand for wind energy, new wind turbine installations are getting bigger and more powerful. Vestas is planning to install an offshore wind turbine of 15 MW by 2024, while Siemens Gamesa launched a wind turbine with an energy production capacity of 14 MW [3]. Wind turbines produce energy by saving kinetic energy from the mass of air passing through the area swept by the rotors [13]. In horizontal-axis wind turbines (HAWTs) - which are the most commonly used wind turbine type [50] and thus the focus of this study - the rotor blades are used to convert the flow of the incoming wind into an aerodynamic torque. This is transferred from the rotors to the generator which converts the rotational kinetic energy into electrical power. Hence, the wind turbine generator uses the work done by both the tangential and axial velocity components to produce energy. The power production and the forces on the turbines can be influenced using three control variables: generator torque τ_g, rotor blade pitch angle θ and WT yaw angle γ. The blade pitch angle is the angle between the chord of the blade and the WT's rotational plane (commonly referred to as the disk plane), while the yaw angle is the angle between the incoming wind and the rotor shaft of the WT [10, 13]. The wind turbine's mechanism and degrees of freedom are depicted in Figure 3.1.

3.1.2. Wind farms

Many areas around the world with sufficient wind resource lack the necessary infrastructure, such as road accessibility and electricity grid availability, for wind turbine installations. Other areas have a high density of settlements or are protected natural areas. These factors limit the available wind turbine installation area, motivating governments and businesses to group large numbers of wind turbines together and form wind farms [49]. In the Netherlands, the government aims for an offshore wind capacity of 21 GW by 2030/2031. When both average supply of energy and average natural gas consumption are considered, this has the potential to meet the energy needs of 1.4 million Dutch households [14]. This is a significant number since in the Netherlands the use of renewable sources in the residential sector is more than three

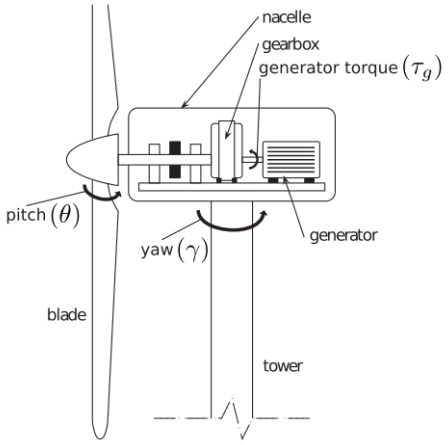

Figure 3.1: Horizontal-axis wind turbine [10]

times less than the EU average, with natural gas being the dominant energy source in the residential sector at 71.2% [24]. One of the measures taken for increasing energy production capacity is building wind farms in the North Sea [64]. Clustering wind turbines in farms has unintended consequences on individual turbine performance. The aerodynamic interactions between WTs in wind farms affect individual turbines by decreasing their possible power capture and by shortening their lifetime as a result of fatigue loads and increased structural degradation. These aerodynamic interactions are the *wake effects* [10].

3.1.3. Wake interactions

Wake effects can lead to losses in wind farm power output. In large offshore wind farms average power losses due to wake effects can reach 10% to 20% of the total output [4]. Wakes in wind farms are shown in Figure 3.2. Wind turbine wakes are complex, stochastic aerodynamic phenomena. The most rudimentary

Figure 3.2: Photograph of the Horns Rev 2 offshore wind farm - courtesy of Vatenfall

definition of a wake is a region of reduced mean wind velocity and increased turbulence downstream of the turbine [10]. As the wind turbine extracts kinetic energy from the incoming wind, the static pressure of the downstream flow decreases and the mean wind velocity is reduced. Turbine blade rotation creates blade tip vortices and disrupts the flow at the blades contributing to an increase in turbulence [10]. Due to

the incompressibility of the flow and the principle of conservation of mass, the velocity deficit in the flow translates to an increase in the surface area of the wake. This is the concept of *wake expansion*, and it impacts the wind speed at wind turbines downstream. Moreover, as turbine blades rotate, they exert an equal and opposite reaction torque on the downstream air causing the air to rotate. This tangential velocity component results in *wake rotation* [13]. For more information on the aerodynamics of HAWTs including the forces acting on the blades and elements of blade design, see Chapter 3 of [13] and [91]. Wake is a time-dependent phenomenon. *Wake meandering* which describes large-scale wake fluctuations in the lateral and vertical directions occurs. This effect increases the turbulence of the wake [12]. The downstream turbines experience the wake of the upstream turbines with a time delay rather than instantaneously [35]. Further downstream, turbulent mixing of the flow occurs and the wake deficit dissipates. At a certain distance downstream of the turbine - depending on the surface area of the wake - the flow eventually returns to its undisturbed state. The return to the undisturbed flow's atmospheric pressure levels and the mean wind velocity is called *wake recovery* [101].

On the wind farm level, wakes from different WTs interact as multiple turbines are placed together. Therefore, the downstream turbine's performance is affected by every upstream turbine whose wake crosses with the area swept by the downstream turbine [35]. The number and intensity of wake interactions increases as the aggregated wakes expand downstream. Higher wake-induced power losses occur at the back of wind farms than at the front. This is the *deep array effect*, and it is the most prevalent in large wind farms [71]. When an upstream turbine is misaligned with the wind direction, its wake is deflected. Counter-rotating vortices are generated in the upstream turbine's wake. These propagate throughout multiple rows of downstream turbines and deflect the wake of a downstream turbine that is aligned with the wind. This is called the *secondary steering* effect [25]. On the wind farm scale, large numbers of accumulated wakes alter the atmosphere, creating additional aerodynamic effects. A comprehensive overview of these effects is beyond the scope of this thesis. An introduction to the topic may be found in [107].

3.1.4. Mitigation of wake losses

Through the mitigation of wake effects, the total power production and lifetime of wind farms is increased [10]. The current industry standard for addressing wake-induced power losses in wind farms is placing wind turbines at sufficiently large distances from each other ($7D$ to $10D$). Although large inter-turbine distances allow for wake recovery, annual revenue losses of up to 20% to 30% are still observed [53]. There is growing interest by researchers and developers in other wake loss mitigation strategies that further decrease revenue losses, namely *wind farm layout optimization* and *wind farm flow control* [2, 41]. *Wind farm layout optimization* involves using optimization algorithms to determine the ideal wind turbine positions that maximize power production and minimize costs while adhering to project-specific boundary constraints [16]. *Wind farm flow control* or *active wake control* refers to achieving a wind farm level objective such as power maximization or load reduction through the use of a wind farm controller that influences the control variables of individual wind turbines. Wind farm layout optimization is used during the design phase to position wind turbines such that there are minimal wake losses. On the other hand, wind farm flow control is implemented on existing wind farms in order to minimize the remaining wake losses [53]. This means that wind farm flow control can be used to mitigate wake losses in atmospheric conditions that are less likely to occur and thus the wind farm layout was not optimized for [41]. In this study, only the mitigation of wake losses with wind farm flow control are included.

The main objective of wind farm flow control is minimizing the levelized cost of energy (LCoE). This represents the total costs of the wind farm (including construction, maintenance and operation) divided by the total energy produced by the wind farm, leading to the average cost per energy unit over the wind farm's lifetime [62]. This objective can be achieved through a number of sub-objectives, with the most relevant ones being *power maximization*, *load minimization* and *active power control*. *Power maximization* refers to increasing the wind farm's annual energy production which directly translates to an increase in revenues at a specific electricity price. In wind farm flow control applications, this is done by minimizing wake-induced energy losses. *Load minimization* is important because increased turbulence and asymmetry in wind flows increases the turbine's structural loading, leading to shorter turbine lifespan and increased maintenance costs. *Active power control*, amongst other applications, relates to supplying power levels to the electricity grid that meet technical standards and are optimized according to electricity prices. Multi-objective wind farm flow control can be done; however, this study solely focuses on maximizing power [10, 62].

3.2. Wind farm flow control strategies

The performance of wind turbines within a wind farm may be optimized with wind farm flow control strategies. These seek to enhance power production, reduce structural degradation and improve the efficiency with the overall electricity grid network. Since large investments and agreements with many stakeholders are required for the development new farms, the possibility to enhance the performance of existing wind farms remains attractive. Researchers have explored various control techniques.

The first wind farm flow control method proposed is *axial induction control* or *power de-rating* [62]. This is based on adjusting the blade pitch angles and/or the generator torque of the upstream turbines in order to run them on less than their maximum capability (i.e. de-rating). This decreases the power output and thus the momentum deficit of the wake shed by the upstream turbine. As a result, the downstream turbines are exposed to higher incoming velocities and generate a higher power output [53]. This mechanism is shown in Figure 3.3.

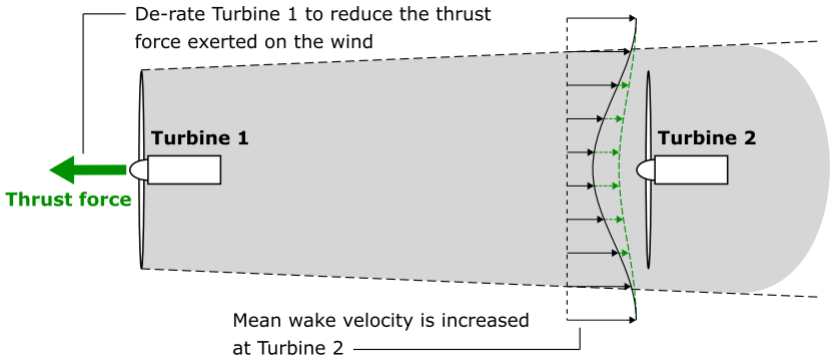

Figure 3.3: Working principle of axial induction control [53]

The number of field experiments for axial induction control remains small with the bulk of research output consisting of low-fidelity simulations and analytical studies [41]. The results of field experiments is inconclusive since many report marginal power gains or power gains that fall within the bounds of statistical uncertainty [1, 11, 57, 100].

On the other hand, *wake steering* - that is also known as *wake redirection* - for power maximization has proven its potential in high-fidelity simulations, wind tunnel tests and field experiments (20, 41). Wake steering is the redirection of the wake shed by the upstream turbines to expose the downstream turbines to a higher incoming flow velocity than the baseline scenario. The goal is to achieve net energy gains compared to the baseline due the downstream turbine's higher energy yield overcompensating for the upstream turbine's reduced energy yield. The wake of the upstream turbine is redirected through the deliberate misalignment of the yaw angle with the wind direction (yaw-based wake steering) or through individual blade pitch control (IPC-based wake steering). In contrast to yaw-based wake steering, interest in IPC-based wake redirection decreased with time. This is because IPC-based wake steering is conventionally used to achieve turbine-level objectives, so IPC-based wind farm controllers would have to meet objectives at both the wind farm level and turbine level [53]. Hence, IPC-based wake steering is not considered in this study. When wake steering is mentioned in the rest of the literature review, it is in reference to yaw-based wake steering only.

When the upstream yaw angle is purposefully misaligned with the incoming wind, a lateral force that deflects the downstream wake is created. This exposes the downstream turbine to a higher incoming flow velocity than the baseline scenario [103]. The secondary steering effect further influences the displacement of the downstream wake. The main working principle of wake steering is shown in Figure 3.4.

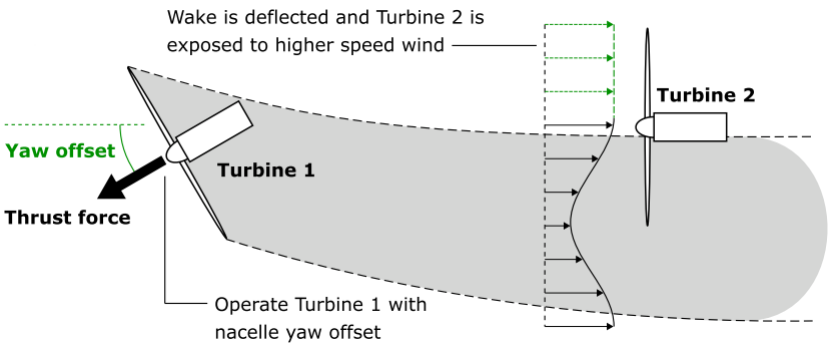

Figure 3.4: Working principle of wake steering [53]

High-fidelity tests mostly show efficiency gains of 5-15% [53]. In addition, studies calculating annual energy production (AEP) gains using realistic wind data show gains of up to 1% which is a significant increase for wind farms [20]. Due to these promising results and significant research output in the past five years [41], Siemens Gamesa released the first commercial wake steering product in 2019 [81]. This was followed by the first full scale commercial implementation of wake steering in 2023 at the Milford I&II wind farms in Utah [106].

Axial induction control and wake steering are wind farm flow control methods categorized according to their physical turbine actuation mechanisms. These control methods may be further divided into *static* and *dynamic* control methods. In static control, the turbine set-points are adapted to meteorological variations such as wind direction and wind speed on the scale of a day. This control method is not responsive to physical effects that occur at time scales faster than the overall wind farm flow, such as wind gusts, turbulence bursts and terrain effects. Dynamic control methods are responsive to the disturbances in flow physics occurring on a smaller time scale, with some even directly influencing wake mixing and turbulence [62]. The previously referenced studies for wake steering and axial induction control were exclusively for the static control methods. With dynamic control concepts the control variables that influence the thrust force on the upstream turbine are changed dynamically in order to accelerate turbulent mixing which in turn leads to faster wake recovery [32, 62]. In an example of a dynamic induction control concept, the thrust force was varied sinusoidally with the goal of increasing turbulent mixing and thus reducing wake losses. However, the variations in thrust force led to power fluctuations that reduces the consistency with which the standard power level was achieved [66]. Although dynamic induction control has been investigated in wind tunnel tests and simulations (eg. [33, 99]), no field experiments on this control method were found. This means that dynamic induction control is at a lower technological readiness level than both static axial induction control and static wake steering. To reduce the power fluctuations, dynamic individual pitch control also known as the helix approach was proposed. This control strategy involves changing the individual blade pitch angles to slowly vary the thrust force and thus the direction of the wake. Hence, turbulent mixing is increased with smaller power fluctuations [32]. LESs showed that the helix approach resulted in higher energy extraction than dynamic induction control and static induction control while decreasing power fluctuations. However, no comparison was made to wake steering, and the approach is still at the proof-of-concept phase [32].

3.3. Controller architecture

In Section 3.2 different wind farm flow control methods were presented. Following a review of the research conducted on these control methods, it was concluded that wake steering has the highest technological readiness level. Wake steering and other wind farm flow control methods are implemented by designing control algorithms on the wind farm level that aim to maximize a specific objective. There are different properties that wind farm controllers can have. As it was explained in Section 3.2, the most widely used controllers for wind farm control are static. In addition to this, the current practice is to use open-loop control for wind farms as it was shown in many field experiments (eg. [11, 21, 27, 83]). Due to the fact that in open loop controllers all uncertainties are propagated forward towards the output, closed-loop control has gained more attention in recent years (eg. [43, 58]). Currently, no practical implementation of closed-loop control has been done [62]. Finally, controllers are model-based or model-free. Model-based controllers

are based on analytical wind farm flow models. This means that they are subject to modelling errors and uncertainties, as the controller is only as good as the accuracy with which it models the flow. The fact that they are simplified models of complex flow physics means that they are straightforward to implement and can handle multi-objective functions. Model-based controllers are often used in wake steering due to their computational efficiency [28, 83]. On the other hand, model-free control aims to handle the limitations of model-based control by treating wind farm flow physics as a ”black box” and optimizing for the ideal control action based on measurement data. Although model-free control aims to eliminate the limitations of model-based control, many optimization algorithms used in model-free control rely on steady-state data for learning. This also means that difficulties with handling time-varying flow conditions occur [22].

The current industry standard for wake steering applications is using steady-state wind farm flow models to generate look-up tables (LUT) for an objective function such as power maximization. The LUTs contain optimal turbine yaw offset angles for all possible wind directions and wind speeds given certain atmospheric conditions and turbine characteristics. These yaw offsets are then fed into each turbine’s yaw controller. An example of a standard wake steering controller is depicted in Figure 3.5.

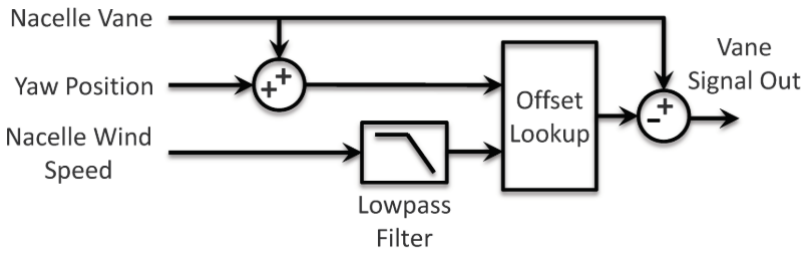

Figure 3.5: Standard wake steering controller whose output vane signal is fed as input to the turbine’s yaw controller. [84]

Since static open-loop model-based controllers have the most practical implementation, the focus of this thesis is on understanding the uncertainties involved in estimating AEP uplift using these wake steering controllers. In order to understand the uncertainties due to the models used in these controllers, the next chapter focuses on wind farm flow models.

4

Wind Farm Flow Modelling

Chapter 3 explained the physics behind wind turbines, wind farms and wind farm control methods. In Chapter 4 the focus is on how to approximate the physics previously explained using simplified mathematical models. Section 4.1 gives the relevant background on wind farm flow models. Then, Section 4.2 presents different types of low-fidelity wind farm flow models and their operating principles. Section 4.3 continues with describing the FLORIS software that implements low-fidelity wake models.

4.1. Overview of wind farm flow models

In order to assess the financial viability of wind farm projects, wind farm developers conduct (energy) yield assessments. This allows developers to predict the annual energy production of a proposed wind farm and to make the optimal design decisions that maximize power [18]. To conduct such an assessment, wake-induced power losses must be quantified. This typically involves the use of wind farm flow models which are simplified mathematical descriptions of the flow. With these mathematical descriptions, it is possible to quantify wake effects with varying degrees of accuracy. Besides energy production estimations, wind farm flow modelling can be used to analyze aerodynamic load variations on turbine blades and power output fluctuations. Hence, wind farm flow models can play an important role in assessing the extent to which wind farm-level objectives are met. Moreover, wind farm flow models are used in the implementation of wake loss mitigation strategies, for example, in the design of model-based wind farm controllers. The main emphasis of this study lies in wind farm flow modelling for wake steering controller design and yield assessment applications.

As the fidelity of a model increases, the accuracy with which it describes flow dynamics increases. However, a high fidelity model also has increased computational complexity. Wind farm flow models can be classified, according to their fidelity, into low fidelity models, medium fidelity models and high fidelity models. *Low fidelity models* estimate the time-averaged flow field characteristics of wind farms for a given wind direction and are usually steady-state [10, 22]. These models have a low computational complexity, although it should be noted that the computational effort increases with the number of wind turbines. Moreover, low fidelity models provide little information on temporal dynamics such as wake meandering effects. Thus, they are less accurate and may have degraded control performance [22]. At the opposite end of the spectrum, *high fidelity models* provide high modelling accuracy as they apply large-eddy simulations to solve three-dimensional Navier-Stokes equations. This means that they are more computationally expensive. An example of a high fidelity model is Simulator for Offshore Wind Farm Applications (SOWFA) developed using computational fluid dynamics tools. *Medium fidelity models* are a compromise between the two extremes. They usually consider more details of flow field dynamics while reducing computational complexity by simplifying Navier-Stokes equations with assumptions that may neglect, amongst other properties, wake asymmetry [22].

With the current trend of building wind farms with an increasing number of wind turbines [88], the computational cost of performing yaw optimizations increases. Due to the high computational cost of yaw optimizations, particularly in large wind farms, wake steering benefit assessments are currently only done with low-fidelity models. A study to higher fidelity models is out of the scope of this thesis.

4.2. Low-fidelity wind farm flow models

Low-fidelity wind farm flow models are simple analytical models that are preferred in wind farm layout optimization and control applications. This is because they have a low computational cost while still capturing the fundamental flow physics unlike empirical models [73]. Sub-models that describe different aspects of wake behaviour are combined in an attempt to give a complete description of flow physics without significantly increasing the computational cost. The complexity of wake aerodynamics and wind farm flow model uncertainties due to factors such as model assumptions still makes validation a challenge. For yield assessment applications specifically, wind farm flow model uncertainties can contribute to power output predictions falling outside of the bounds of statistical uncertainty [70]. This section focuses on some low-fidelity wind farm flow models that are commonly used for yield assessment applications. First, the sub-models that make up wind farm flow models are presented. Then, the combination of sub-models in order to make up the wind farm flow models is explained. The sub-models to be handled in this section are given in Figure 4.1.

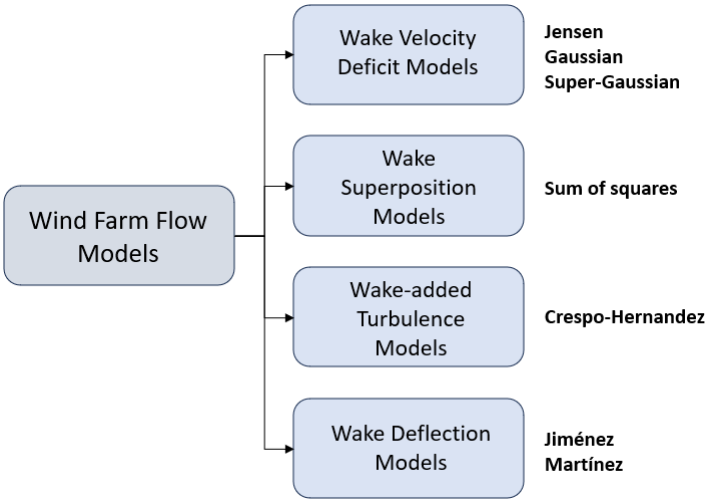

Figure 4.1: An overview of wind farm flow models

Wake velocity deficit models

Wake velocity deficit models describe an individual turbine's wake. In this report the wake velocity deficit models that are most commonly used for yield assessments with the FLORIS tool [69] are explored. Other yield assessment tools such as PyWake may have a different database of wake velocity deficit models available [23]. The oldest wake velocity deficit model is the Jensen model, and it is based on the principle of conservation of mass. It is a so-called top-hat model with a velocity deficit factor that is a function of the downstream distance [47]. This means that the velocity function is uniform inside a cross-section of the wake, with the waked region having a lower velocity than the unwaked region. Wind tunnel tests and high-fidelity simulations show that the Jensen wake model underestimates the velocity deficit at the center of the wake while overestimating it near the edge of the wake [5]. This is attributed to the fact that when observed from a far enough distance downstream the velocity deficit is close to being axisymmetrical having a shape similar to the Gaussian distribution perpendicular to the turbine axis [15]. By applying the principle of mass and momentum conservation and assuming the Gaussian shape for the velocity deficit, better results than the top-hat model were obtained in partial and full wake conditions [5]. However, the Bastankhah model is not accurate in the near wake conditions which is where most wake losses occur. When inter-turbine spacing is small, turbines will generally be in near wake conditions. The super-Gaussian wake model has an approximately top-hat shape in the near wake and a Gaussian shape in the far wake. This shape is more similar to observations from wind tunnel tests. Compared to the Gaussian model, the super-Gaussian model matches better with measurements from wind tunnel tests, particularly in the near wake [9]. Besides the documentations of yield assessment tools, more types of wake velocity deficit models may be found in papers such as [37] and [74].

Wake superposition models

The wake of each turbine is modelled individually, yet in wind farms wakes from multiple wind turbines interact. Thus, the combination of wake velocity deficit models when wakes from multiple turbines overlap is not straightforward. Wake superposition models address the interaction between multiple turbines [80]. One of the most commonly used methods is the sum of squares superposition model. This assumes that the deficit in kinetic energy of the mixed wake is obtained by adding the deficit in kinetic energy of each downstream turbine's wake. The kinetic energy deficit is then used to calculate the velocity of the flow field [52].

Wake-added turbulence models

Turbulence characteristics of wakes influence wake recovery through turbulent mixing. [17] proposed an empirical formula based on results from CFD simulations for the calculation of added turbulence due to turbine operations and ambient turbulent conditions. Thus, when more turbulence is generated due to higher rotor thrust, wake recovery is improved. This added turbulence model has been widely adopted in wind farm flow models [7, 54].

Wake deflection models

Wake deflection models describe the changes in flow due to - amongst other factors - changes in inflow angles. Since this study is focused on wake steering, some models that show the effect of yaw misalignment are specifically studied. One of the earliest adopted models is [48]. This model assumes that the wake has a top-hat shape, and it uses the principle of conservation of momentum. The wake is considered to deflect with a skew angle α that is larger than the turbine's yaw misalignment with the incoming wind. The expression for α is valid for the far wake region which is dominated by ambient turbulent conditions [48]. In high-fidelity simulations it was observed that the wake is not simply deflected using simple geometry. Instead the wake's shape is curled due to counter-rotating vortices being shed simultaneously at the top and bottom of the rotor. These vortices were shown to affect wake steering performance which motivated the creation of the [61] wake deflection model. The wake deflection model developed by [61] solves a simplified version of the Reynolds-averaged Navier-Stokes (RANS) momentum equation and considers the streamwise velocity profile as well as the wake rotation effect and the aforementioned vortices caused by yawing. Ground effects are also accounted for. It does not assume a shape for the wake, and the wake velocity and wake deflection models are derived using the RANS momentum equation.

Wind farm flow models

When the four sub-models are combined, wake steering in wind farms can be characterized. As more wake features are considered, the accuracy with which the wind farm flow is modelled is improved. First, the Jensen wake model is extended with the sum of squares method [52]. This is called the Park wake model. This is the standard model used in many commercial software. However, it does not account for the influence of the yaw angle on the downstream turbine's wake or power production [72]. For wake steering applications, the Park wake model is typically used in conjunction with the Jimenez wake deflection model.

As it is a better description of the flow field, in later wake steering applications [28, 83] the Gaussian velocity deficit model for one wake was further extended to the wind farm level through the use of the sum of squares superposition principle. Since turbulence - amongst other effects - enhances wake recovery, added turbulence is included using the Crespo-Hernandez model [17]. Finally, the Jimenez wake deflection model is included in the Gaussian wind farm flow model [68]. When used to design a wake steering controller in a two-turbine field experiment, an increase in energy gain of 14% has been shown in the downstream turbine [28].

Despite its improvements compared to the Park wake model, the Gaussian wind farm flow model under-predicts the power gains due to wake steering in large wind farms compared to field test and high fidelity analysis [54]. This is because secondary steering effects and the asymmetric nature of wake steering is not fully captured by the Gaussian model. In order to maintain the relatively lower computational cost of the Gaussian wind farm flow model, the Gaussian model is modified by using approximations of the [61] curled wake model. This creates the Gaussian Curl Hybrid (GCH) model [54]. In this model, yaw-added recovery - which is the fact that wake recovers more when the turbine is misaligned with the incoming flow due to turbulence caused by vortices - is included. Moreover, secondary steering effects are included in GCH. With the curl and secondary steering effects included in the model, the predicted power

gain for smaller yaw misalignment angles are substantially higher compared to the former wake model. Annual energy production gains for GCH are shown to be twice as high as the AEP gains for the Gaussian model for large wind farms in high and low turbulence intensity conditions [54].

More recent studies shows that deep array effects are underestimated with GCH, more specifically losses are under-predicted in the rear part of large wind farms and turbine pairs at distances larger than $25D$ [7, 71]. The Cumulative Curl (CC) model [7] and TurbOPark model [71] have been developed to account for these effects. The TurbOPark model has not been validated yet for wake steering applications, so it is out of the scope of the literature survey. On the other hand, CC has been validated in simulations for yawed and non-yawed wind turbine conditions. CC uses the same wake deflection model as GCH, but it enhances the accuracy of its near-wake model by replacing the Gaussian velocity deficit model with the super-Gaussian velocity deficit model in the near wake region [9]. In addition, the velocity deficit model and wake superposition model from GCH is replaced by [6]. This calculates the downstream turbine wake by directly solving an approximation of the equations of conservation of mass and momentum [6]. In this way, deep array effects are considered and more accurate near-wake predictions are made. Therefore, the power and wake estimations are more accurate while the same performance is obtained for smaller wind farms. CC has still not been validated in field experiments with larger wind farms, having been primarily used in simulation studies [7]. The wind farm flow models that were presented can be used in wind farm simulation software in order to understand wake behavior and its effects.

4.3. Modelling the annual energy production uplift from wake steering using FLORIS

Wind farm simulation software uses wind farm flow models in order to perform yield assessments, wind farm and wind turbine siting and structural load analysis amongst other applications. This allows data-backed design decisions to be made during the early wind farm design phase. In addition, novel control technologies such as wake steering can be tested through simulations on different wind farms before full-scale deployment. This has the potential to motivate wind farm developers and OEMs to invest more resources on innovations that may improve energy yield or the lifetime of wind turbine components.

The goal of wake steering yield assessments is to estimate the AEP uplift that can be achieved by wake steering. Confidence in the yield assessment increases as the conditions in the wind farm are modelled accurately since this increases the likelihood of obtaining similar results to field experiments [21]. An example of a wind farm simulation software that can be used for wake steering applications is FLOw Redirection and Induction in Steady-state (FLORIS) [34]. FLORIS has been widely used in field experiments for wake steering controller design, more specifically for finding the optimal yaw angles of wind turbines (eg. [21, 29, 84]). A user-centered visualization of FLORIS for wake steering yield assessments is given in Figure 4.2.

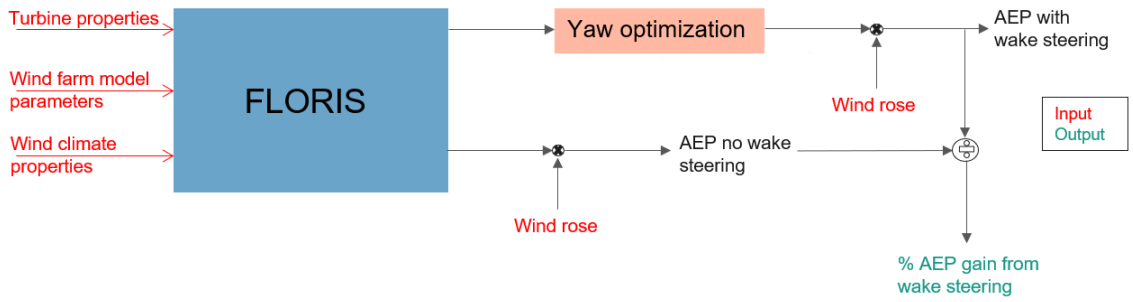

Figure 4.2: Visualization of wake steering yield assessments with FLORIS

In order to start up the software, some input parameters must be selected. Turbine properties are defined by selecting the turbine type and specifying the wind farm layout. Wind farm model parameters are chosen by selecting the four sub-models making up the wind farm flow model. With the wind rose loaded in FLORIS, the yaw angles can be optimized for every wind direction and wind speed possible. However, to decrease the computational cost, the optimization can be done for given wind speed, wind direction and/or turbulence intensity values. Finally, the yaw optimizer method is selected [69]. In most

recent field experiments [65] the serial-refine method has been used for yaw optimization due its reduced computational time [31]. As the focus of the thesis is understanding the impact of the input parameters on the AEP output when wake steering is implemented, further description of the FLORIS algorithm is omitted. For a more detailed view of FLORIS and the model parameters included, please consult the most recent FLORIS documentation [69].

Since FLORIS is a model-based software, the results obtained using it are highly dependent on the accuracy of the wind farm flow model used. Therefore, the choice of the wind farm flow model has a significant impact on the level of model uncertainty introduced to the output. Besides the choice of the model, other sources of uncertainty due to FLORIS have been found in field experiments and uncertainty studies. One source of uncertainty is that FLORIS does not account for differences in power gains during nighttime and daytime conditions that occur due to changes in atmospheric stability and turbulence [29]. This is because FLORIS models the average of the two conditions. Another source of uncertainty is due to the fact that the power curve model in FLORIS is independent of the wind farm flow model. In non-yawed conditions, the C_p is a function of the velocity deficit only. This does not change when more complex wind farm flow models that, for example, include vortex effects are used. In yawed conditions, the power is calculated by multiplying the non-yawed power curve with a correction factor of $cos^{P\rho}(\gamma)$, where $P\rho$ is an empirical parameter value found from wind tunnel tests of yawing turbines. This adjustment to the non-yawed power equation is based on the Jiménez deflection model and is independent of the wind farm flow model selected in FLORIS [34]. Hence, the wind farm flow model and the power curve model can influence the accuracy of the energy production estimation, affecting the validity of the results obtained from wake steering yield assessments.

5

Practical Applications of Wake Steering

Chapter 4 explained the models used to describe the physical properties of wind farms. These models are used in practical wake steering applications. Chapter 5 describes the current state of wake steering technology, highlighting challenges that must be addressed in the future in order to achieve wide-scale adoption of the technology by the industry.

5.1. Wake steering in industry

In Section 3.2 wake steering was presented to be the only wind farm flow control method to date with a commercial application, and it was expected to increase the gains in AEP by up to 1%. In an offshore wind farm with 407 MW capacity - which is the capacity of the Horns Rev 3 wind farm in the North Sea [102] - this translates to an additional annual profit of approximately €500,000 [105]. In addition, the ability to optimize the energy production of the wind farm with wake steering ensures that the targeted energy output is consistently achieved, leading to more stable revenue streams. Projects with lower financial risks are more attractive to investors. These potential financial benefits have led to the creation of Task 44 within the International Energy Agency (IEA) Wind Technology Collaboration Program which is an international cooperation between 24 countries with the goal of advancing wind energy research and development. More specifically, IEA Wind Task 44 - which conducts internationally collaborative research and development projects between academia and industry - has shown significant effort in validating wake steering [45]. Moreover, DNV partnered with National Offshore Wind Research and Development Consortium (NOWRDC), which focuses on the advancement of wind energy technology in the United States, to perform an economic analysis on the effects of wake steering methods on floating offshore wind farms [85]. In 2024 DNV kicked off a joint industry project with offshore wind and transmission developers in order to work on the integration of wind energy into the existing electrical grid network [77].

Industry is continuously exploring wake steering technology because it has shown consistent success in field experiment validations. Results from field campaigns are needed for wind farm flow concepts to achieve a high technology readiness level (TRL) such that commercially viable wake steering products can be produced [62].

5.2. Validation through field experiments

Typically, wind farms are high value assets with multiple stakeholders sharing in the costs, revenues and risks. The potential benefits of new wind farm flow control concepts must be demonstrated alongside the associated risks for the concept to be adopted by industry. These demonstrations first start with a proof-of-concept study using high-fidelity simulations then are followed by validations in wind tunnel experiments. Positive results from these simulations and experiments open the doors to further research. First, field campaigns on a limited number of wind turbines are conducted; these are followed by full-scale field campaigns [62]. Since the focus of this thesis is on practical applications of wake steering using existing controllers, the results of wind tunnel tests and high-fidelity simulations will not be discussed. Instead, the focus is on field experiments with the goal of understanding the current state of wake steering technology.

One of the first field experiments was conducted on one utility-scale wind turbine operating at a fixed misalignment angle with the incoming wind direction to investigate the resulting wake deflection [26]. This

was followed by a two-turbine field test in a commercial offshore wind farm that had 25 Envision turbines that validated the predictions of low-fidelity and high-fidelity simulations - namely FLORIS and SOWFA - with the highest relative increase in power production from wake steering occurring at $7D$ and $8.5D$ turbine spacing [27].

These successful results motivated the scaling up of field tests. An experiment in an operational Canadian wind farm with six utility-scale turbines showed that wake steering increased power production by 7-13% for wind speeds close to the wind farm's average wind speed values and for wind directions that were seen in less than 10% of nocturnal operations and by 28-47% for low wind speeds. Although overall gains in AEP were insignificant, this experiment hints at the dependence of accurate wake steering benefit assessments on wind direction and wind speed as well as the modelling of the power curve [44]. In [28] uncertainties due to the controller's inability to capture changing wind directions persist. As more than 60% of the data is collected in unstable atmospheric conditions, the wake steering controller under-performs. In this case, five closely spaced turbines are tested with the objective of evaluating the effect of two controlled turbines - with one of them placed on a complex terrain and the other on a flat terrain - on one downstream turbine. The wind turbine placed on the flat terrain is at a distance of $5D$ from the downstream turbine, while the one placed on the complex terrain is at a distance of $3D$ from the downstream turbine. Hence, both turbines are influenced by near-wake effects to some extent. Results show an increase of 14% in the downstream turbine's power production for specific range of wind directions and wind speeds. When the upstream turbine's power losses are considered, this power increase reduces to a net gain of 4% over the same wind direction and wind speed range. Additionally, the wake steering controller was designed through the optimization of a FLORIS model which, when the experiment was conducted, did not have the ability to model terrain effects or accurately represent near-wake effects. The same experiment was continued at a later date, incorporating some wind direction uncertainty in the optimization algorithm used to generate the static LUTs. Another important change was using the improved GCH model - that includes complex wake effects due to yaw misalignment - to generate the optimal yaw offset angles [29]. Wake steering reduced wake losses by 6.6%, which was half of the wake loss values predicted by the GCH model used in FLORIS. While for the wind direction regions with the highest gains nearly optimal results were achieved, under-performance was observed in the wind direction regions with lower gains (that are also less studied in high-fidelity simulations). This under-performance may be attributed to losses caused by 'wrong-way steering' (i.e. steering the wake towards the downstream turbine). However, it should be noted that such losses may be better predicted with an improved near-wake model, perhaps leading up to more effective yawing activity. In addition, the FLORIS model uses the average of the daytime and nighttime conditions. Higher energy gains are achieved at nighttime since the atmospheric conditions are more stable and have low turbulence intensity which is more favorable to wake steering [29]. The aforementioned field experiments validated wake steering for a small number of wind turbines. The next step was to demonstrate wake steering on a full-scale wind farm [62]. [21] took this step by demonstrating wake steering in an array of three turbines placed in three consecutive rows in a 43-turbine commercial onshore wind farm. In this experiment, power gains of up to 16% were found for a specific wind direction when the first two turbine rows operated under yaw misalignment. Wake losses at certain wind directions were underestimated by FLORIS and some predicted positive gains were found to have large uncertainty bounds. This was attributed to not only the lack of terrain modelling in FLORIS and to not using GCH, but also to a mismatch between the yaw-power curve of the real turbines and FLORIS. This is because FLORIS assumes a symmetrical yaw-power curve with peak power at $\gamma = 0$ which does not reflect the asymmetrical, flat shape of real yaw-power curves [21].

It can be concluded that power gains calculated by simulation tools are not always accurate. One of the most researched reasons for this is the highly variable nature of wind which the yaw controller cannot immediately react to [78, 84]. This combined with the uncertainty in wind speed creates errors in the calculation of the optimal yaw offset angle [75]. Factors such as measurement inaccuracies and uncertainties in wake model parameters also contribute to power production results with high uncertainty bounds [42, 51]. Therefore, more recent field experiments focus on designing more robust wake steering controllers by including these uncertainties.

5.3. Wake steering under uncertainty

Early wake steering field experiments show the effect of wind speed, wind direction and ambient atmospheric conditions on the success of wake steering. They also reveal insights into the power gain predictions done

by tools such as FLORIS. This is important because energy yield estimation is used for risk management and financial analysis of wind farm projects. Accurate energy yield estimation provides more realistic results, reducing financial risks. Hence, the field of uncertainty quantification is attracting more attention from industry and academia [30]. A common method for uncertainty quantification in wind energy applications involves identifying the sources of uncertainty, modelling them with probabilistic methods, propagating these uncertainties onto the output through simulations and evaluating the impact of the uncertainties on the output (eg. [51, 63, 76]).

In Figure 3.5, it was shown that LUTs are generated as a direct result of the wind direction (which is the sum of the nacelle vane position and yaw position) and the nacelle wind speed. Since wind direction is a direct input parameter, the ideal yaw offset angle is highly sensitive to the wind direction. However, the wind direction is hard to measure and varies over time and in space (in this case, in different places in the wind farm). The wind's unpredictable, time-dependent behaviour is not captured by the static, steady-state yaw controllers used in field experiments. Often, the optimal yaw offset that the wind turbine achieves lags behind the current wind direction. Uncertainty quantification studies consistently show that wind direction variability is one of the most significant uncertain inputs [42, 51, 76]. [84] - using the same experimental design and controller as [28] - showed that, by including probabilistic wind direction and yaw position corrections to the power production estimate, results that matched field experiments more closely were obtained. Additionally, though maximum power gains with uncertain wind direction were lower, the power losses obtained when the turbine deviated from the expected wind direction were also reduced in a simulation study [78]. Variable wind directions were later implemented in a field experiment via yaw controllers that used preview wind direction information. This resulted in increased power gains for perfect preview wind direction information compared to controllers that used static wind direction information for yaw optimization [83, 84]. High-fidelity simulations for wake steering control using preview wind direction information followed, showing that there was academic interest in the subject. For wind direction changes, these simulations predicted increases in average wake steering power gains [79].

Other significant uncertain inputs are yaw misalignment errors and variability in wind speed and turbulence. By taking into account these factors, smaller yaw offset angles and larger power gains compared to the deterministic case were achieved [51, 75, 76]. Smaller yaw offsets decrease the loads on the yaw drives; however, this also means that there is less benefit to performing wake steering. Another important finding was that including variable wind direction and wake model parameters in an open-loop wake steering model (similar to FLORIS) results in a statistically significant higher energy gain only in wind turbines with moderate spacing and operating under low turbulence conditions [42]. This raises the question of whether it is even beneficial to implement wake steering under all atmospheric conditions. Currently, there is an ongoing field campaign that aims to understand physical phenomena that could produce significant sources of uncertainty, including the influence of turbulence on potential energy gains [65]. It should be noted that besides this ongoing field campaign there are no other field experiments that investigate the influence of the other parameters on energy gains. Therefore, additional research on this topic is required.

6

Thesis Contribution

Reflecting on the information presented in the previous chapters, it can be concluded that wake steering is a promising technology but that there is still a long way to industry-wide adoption. One of the main challenges is ensuring that wind farm developers can accurately assess the benefit from wake steering in the early phases of wind farm development. Predicting the energy uplift from wake steering while considering all uncertainties increases confidence in wake steering technology for the early stages of wind farm projects. This scientific gap is explained in Section 6.1. The thesis addresses the scientific gap in Section 6.2. Based on the research questions and the literature review, a tentative research outline is proposed in Section 6.3.

6.1. Research gap

With increasing financial pressure on wind energy viability, both improvement in wind energy innovation and how the innovations are assessed are of vital importance. One such innovation that is quickly maturing to becoming a commercial product is wake steering. However, accounting for the influence of uncertain conditions and models is still a major challenge in the practical application of wake steering. Recent field experiments that considered uncertain wind direction [42] resulted in AEP gain calculations that are within higher uncertainty bounds. When other factors such as yaw misalignment errors are considered, the optimal yaw offset angles are smaller [51]. The question of how much benefit can be obtained from wake steering in real-life applications that are inherently uncertain remain unanswered. By understanding the uncertainties in AEP gain predictions for wake steering, the estimations of AEP gains during the early phases of wind farm project development become more reliable. As a result, the knowledge obtained from such a study can contribute to increasing confidence in wake steering as a potential wake mitigation technique in future wind farms.

6.2. Research questions

This thesis addresses this scientific gap by performing an uncertainty quantification of wake steering in the spirit of [42] and [51]. The **research objective** of the thesis can be formalized as:

Understanding uncertainties in annual energy production gain predictions for wake steering in wind farms through uncertainty propagation

This leads to the following **main research question**:

How do uncertainties affect the predicted annual energy production gains for wake steering?

The wider research question is answered through the **research sub-questions**. Understanding the effect of uncertainties on the predicted AEP gains starts with identifying the possible sources of uncertainty. Since the computational cost increases with the number of turbines and the number of uncertainties considered, focusing on the uncertainties that have the greatest impact on the predicted AEP uplift is the most efficient [76]. This leads to the following research sub-question:

Which input uncertainties have the most significant impact on the predicted annual energy production gains for wake steering?

Recent uncertainty quantification studies modelled uncertainties as stochastic values; however, it is predicted that for some variables deterministic representation may be more suitable [51]. Therefore, the appropriate modelling of uncertainties must still be researched leading to the research sub-question:

How can the uncertainties in input parameters be modelled?

Next, it is important to understand the input parameters that have the most significant impact on wake steering power production since the computational cost increases as the number of uncertainties considered and the wind farm size increase [76]. This problem can be formalized as:

How significant is the impact of input uncertainties on the predicted AEP gain from wake steering?

Both [42] and [51] considered the stochastic input variables as independent. Yet, in reality these variables may depend on each other. At the present moment, there is no research that accounts for the dependency between different input variables which results in the following research sub-question:

How significant is the impact of inter-dependent input uncertainties on the predicted AEP gain from wake steering?

Finally, the benefit gained from wake steering when uncertainties are included must be assessed. This leads to the formalization of the research sub-question:

To what extent is the implementation of wake steering in wind farms beneficial when uncertainties are considered?

By addressing these goals, the thesis aims to validate wake steering technology further for practical engineering applications.

6.3. Research plan

Based on the research questions posed and the literature studied, a high-level plan for the next steps of the research can be made. Note that most likely this plan will change as the research progresses and new information is encountered. The plan may also change if the researcher finds the scope too large for the given resources or finds insignificant results for certain test cases. The research starts with identifying possible sources of input uncertainty in the estimation of AEP uplift for wake steering. These are likely to be chosen based on literature. A sensitivity analysis is performed on a small number of wind turbines with a large number of possible uncertainties. However, instead of modelling all uncertainties as stochastic variables, the researcher expects to also model some uncertainties using a deterministic approach. This is expected to yield the best performance in the most uncertain scenario [51]. With the sensitivity analysis, the most significant uncertainties are identified. Next, uncertainty quantification for the most significant uncertainties is performed on the wind farm level. By reducing the number of uncertainties considered, the computational cost can be kept at manageable levels [76]. The uncertainty quantification can be performed for independent input variable case and the dependent input variable case. By performing the uncertainty quantification for both cases, the impact of inter-dependent input uncertainties on the predicted AEP gain can be determined. The expectation of the researcher based on literature is that wake steering will be beneficial in some operating conditions. Moreover, the researcher expects to obtain smaller yaw offset angles that have larger power gains compared to the deterministic wake steering case [51, 76]. In future works, the uncertainty quantification can be expanded to multiple wind farms, and attempts to create a predictive framework that estimates AEP uplift from wake steering that includes the most significant uncertainties can be made.

Part III

Thesis Methodology and Results

7

Deterministic Analysis

Chapter 6 formalized the research objective as understanding uncertainties in annual energy production gain predictions for wake steering in wind farms through uncertainty propagation. In order to evaluate the uncertainty in the prediction of a wind farm's AEP gain, there must be a baseline AEP gain prediction in which no uncertainties are assumed. This is the deterministic case study representing the conventional wake steering yield assessment as done by wind farm developers. With this deterministic case study, the effect of wake steering on the AEP is quantified. Section 7.1 describes how FLORIS is used to perform the wake steering yield assessment. Next, the wind farms used for the case study are described in Section 7.2. The results from the deterministic wind farm case study are discussed in Section 7.3.

7.1. Methodology

This section offers a detailed description of the method used to predict AEP gains with FLORIS. With this, the user can understand how FLORIS is used to perform wake steering yield assessments. Building this knowledge is important for understanding where input uncertainties occur and how they will be propagated later in the study. The schematic for calculating the deterministic AEP in FLORIS is shown in Figure 7.1. The input variables - such as the wind rose, turbulence intensity and wind farm layout - are shown by arrows pointing towards the schematic, while the output variables - namely the deterministic AEP with no wake steering and the deterministic AEP with wake steering - are emphasized with the red font and arrows pointing out of the schematic.

Within FLORIS, the wake steering assessment can be separated into two parts: yaw optimization and

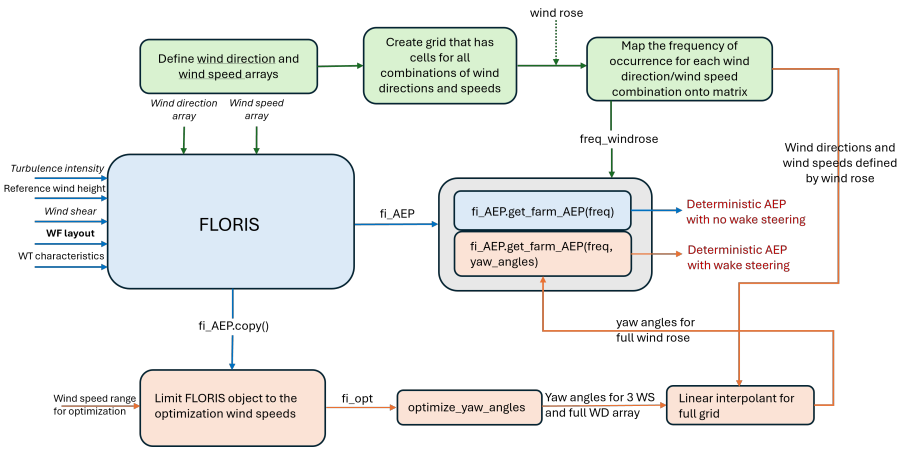

Figure 7.1: Methodology for assessing wake steering yield with FLORIS

annual energy production (AEP) output [69]. The yaw optimization process is depicted in Figure 7.1 with pink boxes, while the flow chart to calculate the annual energy production is depicted with blue boxes. The two calculations are performed separately and independently for the entire uncertainty quantification framework.

The optimum yaw angles over the defined wind direction and wind speed combinations are obtained for a given wind turbine type and wind farm layout. In this case, the Serial-Refine method is used to find the optimal yaw angles that minimize the wake losses of the wind farm. This optimization method reduces computational cost compared to other methods [31] and was used in recent field experiments to identify the optimal yaw angles for wake steering [65]. The wake losses of the wind farm are quantified differently according to the wind farm flow model selected. Therefore, the yaw angle optimization is repeated for different wind farm flow models. Table 7.1 summarizes the specifications of the yaw optimization used in the case study.

Table 7.1: Yaw optimization specifications

Feature	Selection
Optimization method [-]	Serial-Refine [31]
Wind direction array [$^\circ$]	[0,360] with step size of 3°
Wind speed array [m/s]	[1,25] with step size of 1 $[m/s]$

In order to further reduce computational cost, the wind speed array is restricted to three wind speeds. Then, the resulting yaw offset angles for the three wind speeds and full wind direction array are linearly interpolated over the full wind speed array. Thus, the optimal yaw offsets for all combinations of wind direction/wind speed are determined.

The wind direction and wind speed arrays in Table 7.1 are used to create a grid representing all possible combinations of wind direction/wind speed for the defined arrays. Then, SCADA wind direction and wind speed time series data is used to create the wind rose. The wind rose is a representation of the frequency of occurrence of each combination of wind direction/wind speed. This process is illustrated with the green boxes in Figure 7.1. Therefore, the probability of occurrence of each combination of wind direction/wind speed is obtained along with its associated optimal yaw angle.

The deterministic annual energy production output without wake steering is computed by taking the weighted sum of the power for a specific combination of wind direction and speed and the probability of occurrence of that combination of wind direction and wind speed. This weighted sum is multiplied by the number of hours in a year. To calculate the deterministic AEP for wake steering, the power under the yaw offset angle is used for the specific combination of wind direction and speed. For uncertainty quantification, the input variables that were identified as sources of uncertainty are replaced by the random input vector defined in Section 8.2.1. Next, the yaw offset angles are introduced, resulting in the annual energy production with wake steering (optimized AEP). In this way, the effect of the uncertainties in the input variables on the AEP is quantified. This is compared with the AEP without the optimized yaw angles (baseline AEP) to evaluate the AEP uplift due to wake steering. The methodology described in this section is applied to the wind farms described in Section 7.2.

7.2. Case Study Description

This section describes the characteristics of the wind farms used in the case study. With this case study, the effect of wake steering on NoordZeeWind is determined. By the end of the research paper, the accuracy of this deterministic AEP uplift due to wake steering will be quantified. The goal is to develop a method that can potentially be used to quantify the uncertainty in the AEP uplift due to wake steering in different wind farms, thus understanding the extent of the benefit of wake steering.

The case study is conducted on Offshore Windpark Egmond aan Zee (OWEZ) which is located in the North Sea at approximately 10 km off the Dutch shore. This WF has 36 Vestas V90 WTs with a nameplate capacity of 3 MW each. To its south-west, it is neighbored by the Prinses Amalia (PA) Wind Farm. This WF consists of 60 Vestas V80 WTs with a nameplate capacity of 2 MW each. The characteristics of the two turbine types are found in Table 7.2, and the exact locations of the WTs are shown in Figure 7.2.

In Chapter 4 the Gaussian-Curl Hybrid wind farm flow model was identified as the most accurate wind farm flow model that was also validated for wake steering in field experiments. Wind farm flow modeling accuracy was shown to directly impact the AEP uplift estimated by FLORIS. The cumulative curl (CC)

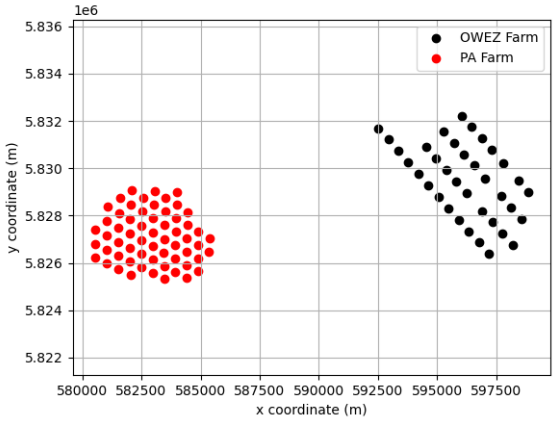

Figure 7.2: Layout of OWEZ and Prinses Amalia Wind Farms

Table 7.2: Characteristics of wind turbines

Feature	Vestas V90	Vestas V80
Nameplate capacity [MW]	3	2
Hub height [m]	70.0	60.0
Rotor diameter [m]	90.0	80.0
Ref. density Cp/Ct [kg/m^3]	1.228	1.225

model was described to be a more accurate WFFM that had not yet been validated in wake steering field experiments. In order to understand the extent to which the wind farm flow model limits the quantification of the AEP uplift due to wake steering, wake steering assessment is performed for both the GCH and CC models.

For the deterministic wake steering assessment, wind direction and wind speed data from the North Sea is collected for the time interval between December 2006 and December 2010. The turbulence intensity in the time series data is constant at 0.06. With this time series data, the wind rose shown in Figure 7.3 is created.

7.3. Results and Discussion

The characteristics described in the previous section are the input parameters for the wake steering assessment in FLORIS. Throughout the case study, the yaw optimization for wake steering is done on OWEZ and the AEP uplift is evaluated for this wind farm. In addition to this, the wake effects of the neighboring wind farm are included in order to provide a more realistic assessment of the WF's annual power output. The same evaluation is repeated for the CC WFFM which models the wind farm's wake more accurately than the GCH WFFM. The results of these evaluations are shown in Table 7.3. In this table, the baseline AEP is equivalent to the deterministic AEP with no wake steering while the optimized AEP is equivalent to the deterministic AEP with wake steering as described in Figure 7.1.

The results for the AEP uplift are verified by calculating the power uplift of the wind farm for one wind speed and a range of wind directions. Due to the orientation of the wind turbines in OWEZ and the wind mostly coming from the south-west direction, it is expected that the greatest power uplift is close to 150°. The break-down of the power uplift per wind direction in Figure 7.4 verifies this.

The comparison between the cases including and excluding the neighboring WF's wake effects shows that the neighboring WF's wake has no significant effect on the AEP uplift. This can be explained by the fact that the WTs are placed 7.5 km apart, which is a distance greater than $80D$. At this distance from the WT, wake mixing has fully occurred. Therefore, the wakes of the WTs from the neighboring WF do not affect the wakes of the WTs from OWEZ. Since the wake effects from the neighbor do not affect the

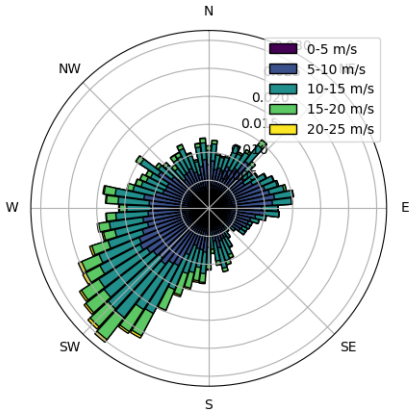

Figure 7.3: Wind Rose for the Deterministic Analysis

Table 7.3: Results of deterministic wake steering yield assessment

WFFM	Baseline AEP [GWh]	Optimized AEP [GWh]	AEP uplift
GCH (with neighbor)	448.428	452.778	+0.97%
GCH (no neighbor)	448.635	452.998	+0.97%
CC (with neighbor)	441.434	446.547	+1.16%
CC (no neighbor)	443.204	448.345	+1.16%

AEP uplift, the uncertainty quantification analysis will only be done on the case studies that ignore the neighboring wind farm. Another interesting conclusion is that the AEP uplift obtained increases when a more accurate WFFM is selected in FLORIS. This shows that in fact the AEP uplift is under-estimated by typical wake steering yield assessments that are conducted using the GCH model. In subsequent chapters, the accuracy of this hypothesis will be tested as uncertainties that mirror the real conditions in a wind farm will be introduced.

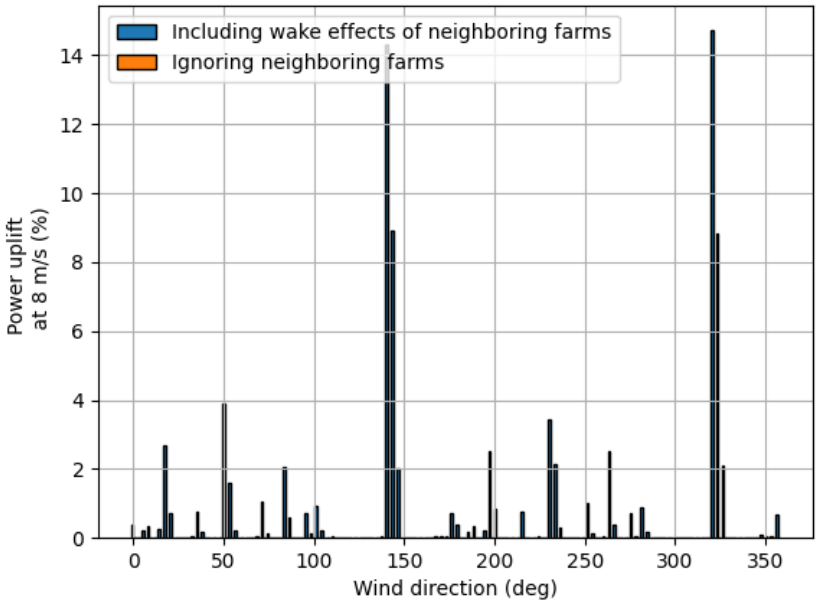

Figure 7.4: Wind Farm Power Uplift at 8 m/s

8

Uncertainty Quantification Methodology

This chapter provides background information on the field of uncertainty quantification and describes the methodology to be followed throughout the research. Section 8.1 gives an overview on the different uncertainty quantification problems in literature and the methods used for conducting the uncertainty quantification analysis. These findings are related to the research objective in order to select the most appropriate uncertainty quantification methods for this study. The application of the methods selected to the research problem is shown in Section 8.2.

8.1. Background on Uncertainty Quantification

Uncertainty quantification involves identifying all sources of uncertainty and error and quantifying their effect on the system in order to, for example, improve the accuracy and dependability of simulations [90, 109]. Due to factors such as the increasing complexity of contemporary systems and advancements in computational power, UQ has been gaining increasing attention across different fields [86]. UQ methods have already been extensively applied in fields such as computational flow dynamics (eg. [67, 104]). Since the wind resource itself is stochastic and heavily dependent on atmospheric conditions, UQ is highly applicable to the wind energy field. For wind farm yield assessments specifically, the following uncertainty quantification problems have been considered [98]:

1. *Forward propagation* that involves analyzing the effect of input uncertainties on the system's output
2. *Model calibration* which deals with adjusting the model parameters in order to obtain more accurate estimations
3. *Optimization and control under uncertainty* that is concerned with obtaining solutions to an optimization problem that are resilient to uncertain conditions while performing well at specific conditions

For this study, the research objective is to understand the uncertainties in annual energy production uplift estimates for wake steering in wind farms via uncertainty propagation. Therefore, this is a pure uncertainty propagation problem. The uncertainty propagation is described in mathematical terms in Equation 8.1

$$P(x|k) \xrightarrow{f} P(y|k) \tag{8.1}$$

The uncertainty propagation is performed on the input parameters that are related to atmospheric stability such as wind shear and turbulence intensity. While in FLORIS these parameters have a single, constant value, in reality these parameters vary in time and are difficult to predict. This means that there is range of possible AEP uplift values that are closer to the real-life AEP uplift due to wake steering. The uncertainty quantification framework involved in performing uncertainty propagation and sensitivity analysis is best illustrated in Figure 8.1.

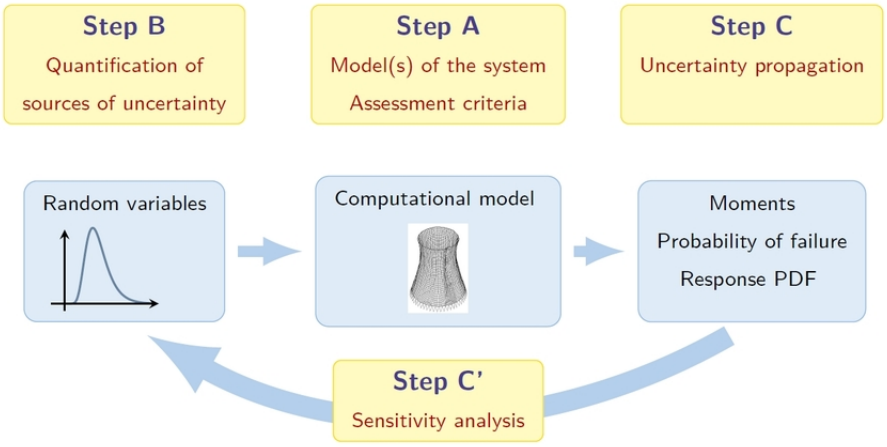

Figure 8.1: Uncertainty quantification framework [89]

The steps shown in the uncertainty propagation framework are briefly described below [89].

- *Step A* relates to defining the model of the physical system and the criteria to assess the physical system. The uncertainties are propagated from the input to the output through the computational model, preferably without introducing additional biases. In this case, the complex wake interactions of the wind farm are modeled with FLORIS software which is a black-box model.
- *Step B*: the sources of uncertainty are quantified by identifying and modeling the uncertain input parameters. In this way, a random vector of input parameters is obtained.
- *Step C*: the uncertainty defined by the random input vector is propagated through the computational model. In this analysis, a response probability distribution function is obtained following the uncertainty propagation.
- *Step C'*: using the relationship between the output and input, the importance of the uncertain input variables are ranked. This is the sensitivity analysis.

The modeling of the sources of uncertainty chosen for creating the uncertainty propagation framework of this study are described in Section 8.2.

There are a wide range of uncertainty propagation techniques available for propagating the uncertainty sources forward. The uncertainty propagation methods most often encountered in wind energy applications at the wind farm level can be listed as [98]:

- Monte Carlo techniques
- Surrogate models

Other uncertainty propagation methods such as First Order Reliability Method (FORM)/Second Order Reliability Method (SORM) are considered to be out of the scope of this study since they are most commonly used for structural reliability studies [98]. For more information on these UQ methods, the interested reader is referred to [89]. Another uncertainty quantification method widely used in wind energy literature is the Bayesian method. This is a probabilistic framework that uses measurement data or high-fidelity data in order to estimate the computational model's parameter uncertainties [98]. Since this a technique used for model calibration, it is out of the scope of an uncertainty propagation study. The reader interested in learning more about Bayesian calibration is referred to [98].

Monte Carlo methods involve generating (quasi-)random samples and running the model for each sample such that the model response to input variables are obtained [89]. With Monte Carlo simulations, the computational model can be assumed to be a 'black box', allowing for the easy implementation of large models and model changes. Therefore, output distributions are produced without imposing another model on top of the computational model [8]. In addition, they do not suffer from the curse of dimensionality. The curse of dimensionality means that the number of samples needed increases exponentially with the number of random variables [98]. The main drawback of the Monte Carlo method is that it may be computationally expensive in experiments with many input parameters or that require many iterations [8].

Surrogate models such as polynomial chaos expansion (PCE) and Kriging decrease the computational cost by approximating the computational model using techniques such as polynomial approximation or the construction of Gaussian processes [98]. Moreover, for example, PCE is sensitive to probability distributions in input parameters and can be efficiently used for uncertainty propagation. However, creating a model approximation introduces a new uncertainty. Although with Kriging an error estimate is obtained, PCE does not provide an estimate for the approximation error [94, 98]. In addition, surrogate models are constructed based on the model response to certain input parameters. Therefore, a change in input parameters would require the construction of a new surrogate model [94].

In this study, the goal is to quantify the uncertainties on the AEP uplift obtained in wake steering assessments on FLORIS. It is preferable that the framework developed can propagate the uncertainties directly and without adding new uncertainties. Moreover, the framework should be adaptable to different wind farms and different distributions of the input parameters. Therefore, the Monte Carlo simulations are the best option for this uncertainty propagation problem unless it is shown that this method is too computationally expensive. Therefore, a convergence study - whose results are in Chapter 9 - is done in order to quantify the number of samples needed for an accurate result with the Monte Carlo technique. If the AEP uplift results converge at a relatively low sample size, then surrogate models are not needed to keep the computational cost manageable.

Another goal of the study is to understand how much each input parameter affects the uncertainty in AEP uplift. This can be achieved with a global sensitivity analysis using Sobol' indices [89]. Sobol' indices decompose the variance of the output into variance contributions of the different input parameters. With Sobol' indices, the significance of the input parameters and the interaction effects of groups of input parameters can be identified [109]. The advantage is that Sobol' indices do not assume that the model is monotonic or linear. In addition, with Sobol' indices the combined influence of the parameters on the uncertainty in the output can be discovered [89]. The total computational cost with MC-based Sobol' indices is $(M + 2) \times N$, where M is the input dimension and N is the sample size [59]. This underlines the importance of conducting a convergence study in order to minimize the computational cost.

8.2. Uncertainty Quantification Method

The uncertainty quantification framework applied to the full wind farm is created with UQLab [60]. UQLab is a framework based in MATLAB that contains a large spectrum of UQ tools, allowing for the easy implementation and creation of algorithms and techniques that solve multidisciplinary UQ problems [60]. This combined with a significant user community makes it the perfect choice for solving the uncertainty propagation problem posed by the research project. In addition, showing that UQLab and FLORIS can be merged paves the way for the possibility of adding extra modules to the uncertainty quantification framework. This gives future researchers a ready-made tool that they can add onto for their uncertainty quantification analysis. For the sake of brevity, the UQ tools used for the thesis and the integration of UQ with FLORIS is described in this section. For more information on the full spectrum of UQLab tools, the reader is referred to the UQLab website [55, 56, 59].

8.2.1. Uncertainty modelling

The input data used to obtain the AEP for the deterministic wake steering yield assessment was described in Chapter 7, while the methodology for wake steering yield assessments in FLORIS was depicted in Figure 7.1. The possible sources of uncertainty in these wake steering assessments are identified as follows:

- Turbulence intensity
- Air density
- Wind shear
- Wind direction
- Wind speed
- Thrust coefficient
- Power coefficient
- Reference wind height

- Hub height
- Rotor diameter
- Wind farm layout

Wind direction and wind speed are related to the chosen wind rose, while the thrust coefficient and power coefficient are related to the wind turbine's thrust curve and power curve. The hub height and the diameter of the rotor are additional parameters related to the characteristics of the wind turbine. The reference wind height is related to the location of the wind farm. Finally, the layout of the wind farm depends on the selected wind farm case study.

The purpose of this study is to simulate the uncertainties encountered in wake steering assessments during early-stage wind farm design. Chapter 1 explained that there were significant uncertainties in the assumed wind rose - due to the difficulty of predicting the wind direction and wind speed - and the thrust coefficient since this is often not given by the wind turbine manufacturer and has to be assumed. The type of wind turbine and the layout of the wind farm are assumed to be already known during the early stage wind farm design phase. Therefore, in this study, possible uncertainties in the reference wind height, hub height, rotor diameter and wind farm layout are not considered. Usually the power curve of the chosen wind turbine is known or readily given by the manufacturer, hence possible uncertainties in the power coefficient are also neglected. Uncertainties are first introduced into the three constant atmospheric input parameters: (1) *air density*, (2) *turbulence intensity* and (3) *wind shear*. These are chosen to verify that the uncertainty quantification framework works properly since they are the easiest to implement within the framework. Additionally, there are numerous studies that quantified the uncertainties in these parameters [51, 76]. Therefore, it is easier to check whether the results obtained following the propagation of uncertainty in these input parameters are accurate. Once the integration of the uncertainty quantification framework is verified with these atmospheric input variables, the uncertainties in wind rose matrix and thrust curve are introduced together with the significant parameters from the initial uncertainty quantification study.

The sources of uncertainty in input variables are modeled as continuous probability density functions in UQLab and are propagated by taking random samples from the PDFs that are the input values for the computational model. The data set used to model the uncertainties in the atmospheric conditions is taken from the measurements at the meteorological mast between July 2005 and December 2010. The turbulence intensity, wind shear and air density variables used in FLORIS represent the annual average ambient atmospheric conditions at OWEZ. With the available data set, the annual average values obtained would be limited to three. This is not sufficient for fitting the data set into a PDF. Therefore, the data set is divided into 12-month intervals starting from July 2005 to December 2009. The annual average turbulence intensity, wind shear and air density (estimated from temperature and pressure measurements) is computed for each 12-month interval. The raw data are shown in histogram form in Figure 8.2.
The probability distribution function that most closely follows the histogram is chosen with the Kolmogorov-Smirnov distance (KS) criterion. According to the KS criterion, the selected PDF has a cumulative distribution that has the lowest maximum distance from the empirical CDF of the data [93]. This is concluded to be the most accurate statistical inference technique available on UQLab since it follows the produced histogram most accurately, avoiding data overfitting and the artificial creation of a peak where the majority of data points accumulate. This results in the Logistic distribution for the turbulence intensity with $\mu = 6.516e-02$ and $s = 1.889e-03$, the Logistic distribution for the wind shear with $\mu = 6.151e-02$ and $s = 2.224e-02$, and the Gumbel distribution for the air density with $\mu = 1.240$ and $\beta = 5.251e-03$. The PDFs are illustrated in Figure 8.3.

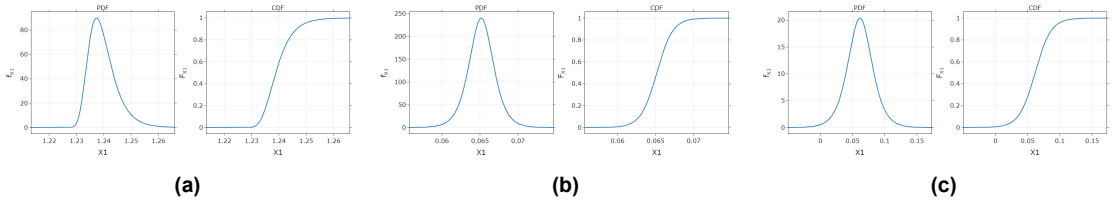

Figure 8.3: Statistical inference with the KS criterion: (**a**) PDF of air density. (**b**) PDF of turbulence intensity. (**c**) PDF of wind shear.

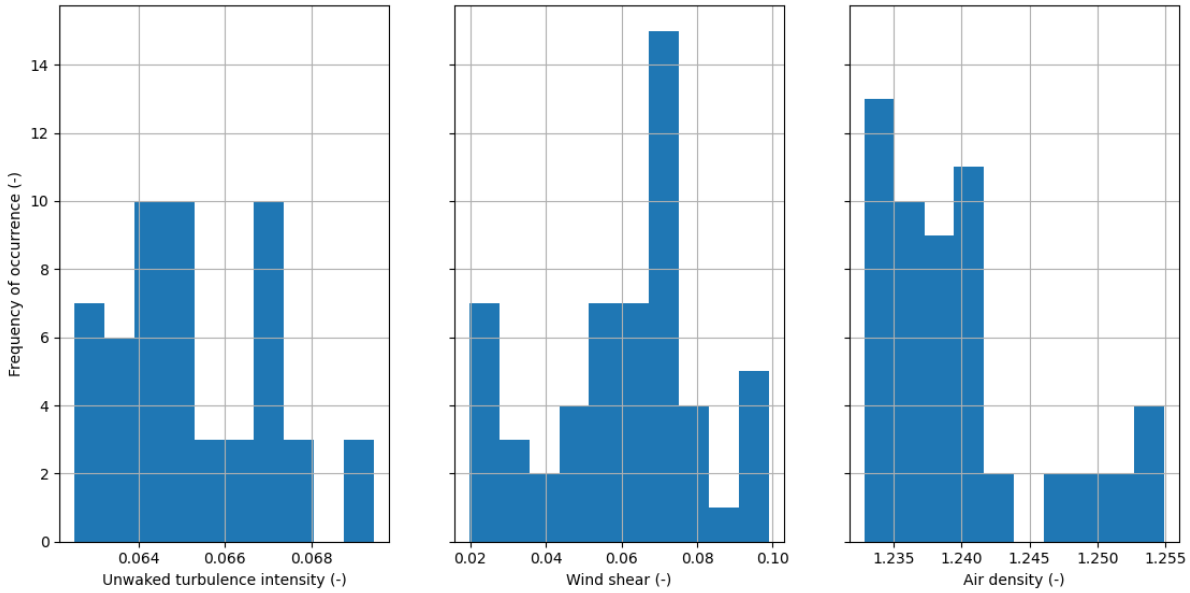

Figure 8.2: Annual Average Turbulence Intensity, Wind Shear and Air Density Distributions

The defined marginal PDFs are assembled into a random input vector with joint PDF $\boldsymbol{X} \sim f_{\mathbf{X}}(\mathbf{x})$ [55]. This input vector is used to propagate the uncertainties and perform the first sensitivity analysis. The significant parameters from the random input vector are identified and transferred to the random input vector for the second uncertainty quantification study. The uncertainties in the chosen wind rose matrix and the chosen thrust curve are added to the input vector together with these significant parameters. The possible wind rose plots are shown in Figure 8.4 and will be referred to by their number in the rest of the report.

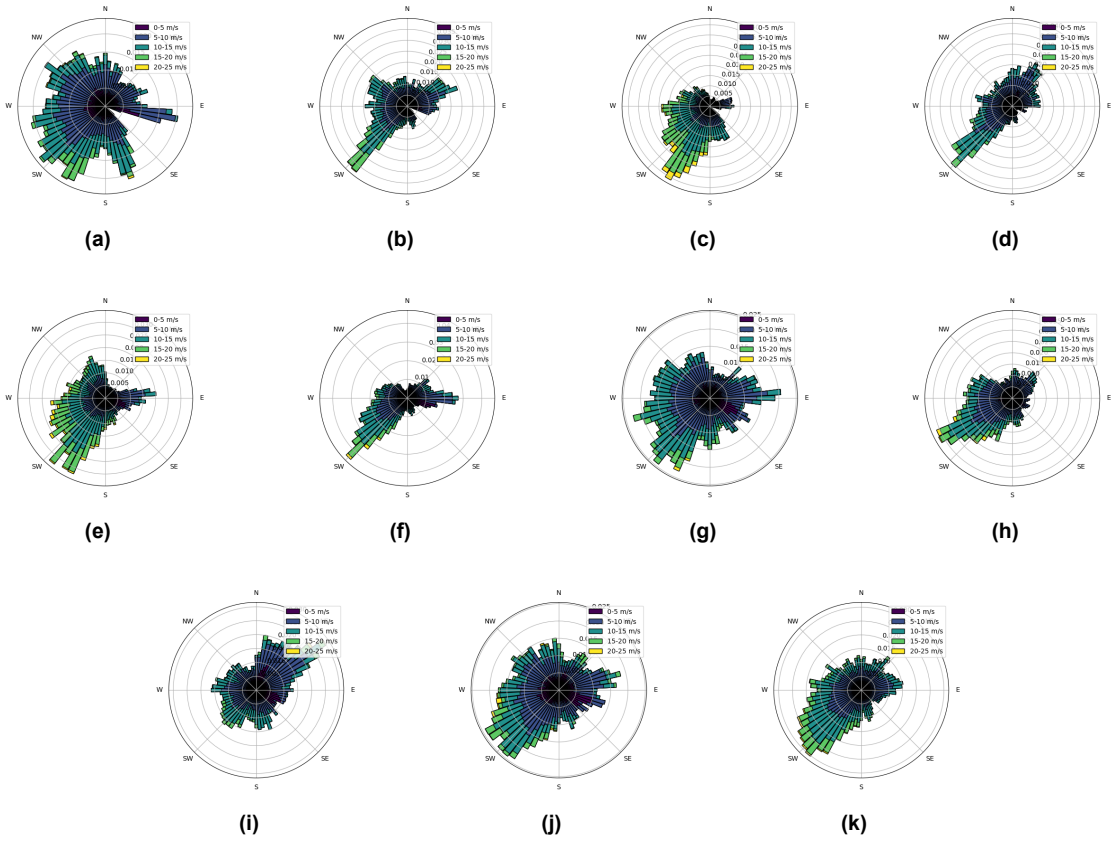

Figure 8.4: Possible wind rose selections: (**a**) Fig.0 (**b**) Fig.1 (**c**) Fig.2 (**d**) Fig.3 (**e**) Fig.4 (**f**) Fig.5 (**g**) Fig.6 (**h**) Fig.7 (**i**) Fig.8 (**j**) Fig.9 (**k**) Fig.10

The uncertainty in the wind rose is propagated by randomly selecting a wind rose from the wind rose data available for NoordzeeWind. This is modeled by creating a uniform distribution with the range [0,10], hence each wind rose has an equal probability of selection. Similarly, nine thrust curves are taken from nine different wind turbines. The thrust curves cannot be shown in this report due to confidentiality. Random samples are generated by modeling the thrust curve selection as a uniform distribution with the range [1,9].

8.2.2. Monte Carlo method

The Monte Carlo method involves generating random samples from the input vector. With Monte Carlo sampling, the samples $\mathcal{U} = \left\{\boldsymbol{u}^{(1)}, \ldots, \boldsymbol{u}^{(N)}\right\}$ are produced in the standard uniform space $\boldsymbol{Z} \sim \mathcal{U}([0,1]^M)$. Then, these samples are transformed back into the samples $\mathcal{X} = \left\{\boldsymbol{x}^{(1)}, \ldots, \boldsymbol{x}^{(N)}\right\} \sim F_{\mathbf{X}}$ for any multivariate distribution $F_{\mathbf{X}}$ with independent marginals F_{X_i} using the inverse probability integral transform (PIT)

$$x_j^{(i)} = F_{X_j}^{-1}\left(u_j^{(i)}\right) \tag{8.2}$$

for all $i = 1, ..., N$ and all $j = 1, ..., M$ [55]. The vector of generated random samples $\boldsymbol{X}$ is inserted into the computational model, in this case FLORIS, which is treated as a black-box

$$\boldsymbol{Y} = \mathcal{M}(\boldsymbol{X}) \tag{8.3}$$

to obtain the vector of model responses $\boldsymbol{Y}$ [56]. This is used to compute the expectation, standard deviation and the confidence intervals [108].

8.2.3. Monte Carlo-based Sobol' indices

The final step is performing a global sensitivity analysis using Sobol' indices. These decompose the total variance of the model response into the sum of the variances of its summands. The variance decomposition

assumes that the input variables are independent [87]. This leads to the definition of the sensitivity measure as [59]:

$$S_{i_1,\ldots,i_s} = \frac{Var(Y(X_{i_1,\ldots,i_s}))}{Var(Y)} \tag{8.4}$$

for a group of variables $X_{i_1,\ldots,i_s}$, where $Var(Y(X_{i_1,\ldots,i_s}))$ denotes the partial variances of the summands and $Var(Y)$ denotes the total variance of the model response Y.

The first-order Sobol' index is the relative contribution of only one input variable X_i on the total variance. The first-order Sobol' indices must be positive. There are also indices with multiple term called higher-order Sobol' indices that account for the effects of the interactions between the input variables that cannot be separated into separated variances. The sum of all Sobol' indices for an input variable X_i is denoted as the total Sobol index S_i^T. The variances described in Equation 8.4 are computed using the mean, variance and partial variance estimators respectively that were derived from the Monte Carlo simulation [59]:

$$\begin{aligned}
\widehat{f_0} &= \frac{1}{N}\sum_{n=1}^{N} f\left(\boldsymbol{x}^{(n)}\right) \\
\widehat{Var(Y)} &= \frac{1}{N}\sum_{n=1}^{N} f^2\left(\boldsymbol{x}^{(n)}\right) - \widehat{f}_0^2 \\
\widehat{Var(Y(x_i))} &= \frac{1}{N}\sum_{n=1}^{N} f\left(x_i^{(n)}, \boldsymbol{x}_{\sim i}^{(n)}\right) f\left(x_i^{(n)}, \boldsymbol{x}_{\sim i}^{\prime(n)}\right) - \widehat{f}_0^2
\end{aligned} \tag{8.5}$$

where $\boldsymbol{x}'$ denotes a realization of $\boldsymbol{X}$ independent of $\boldsymbol{x} = \left\{x_i^{(n)}, \boldsymbol{x}_{\sim i}^{(n)}\right\}^\top$, and the subscript $\boldsymbol{x}_{j,\sim i}$ indicates the j-th realization of $\boldsymbol{x}$ which does not contain the input variable i.

In the next chapter, the uncertainty quantification framework developed is applied on a smaller test case and on the full wind farm.

9

Uncertainty Quantification Results

In this chapter, the results of the uncertainty quantification framework described in Chapter 8 are presented. First, the samples obtained from the input parameters are processed individually through the UQ framework in FLORIS in order to understand the relationship between the input parameters and the AEP uplift in Section 9.1. Next, in Section 9.2 a convergence study is performed on five wind turbines in order to get an estimate of the sample size required for the case study and to understand the sensitivity of the parameters to the number of wind turbines. Finally, the estimated sample size is used to run the UQ framework on the full wind farm in Section 9.3.

9.1. Understanding FLORIS

First, a few samples taken from the probability distribution function of each input data set are individually run through the uncertainty quantification framework. In this way, the effect of each individual parameter on the AEP uplift during wake steering assessments is understood. This is called one-at-a-time (OAT) variation. Both GCH and CC are selected as wind farm flow models on FLORIS in order to understand how the model assumptions influence the output. For this analysis, 16 samples are obtained through UQLab's and Numpy's Mersenne Twister random number generators. This is done in order to understand the differences between UQLab and Numpy, as the code used in UQLab is verified against the one initially built in Numpy.

Air density

In FLORIS air density has a linear relationship with AEP. This is shown in Figure 9.1 and Figure 9.2. As the air density increases, the optimized AEP increases. In general, the AEP uplift increases with air density.

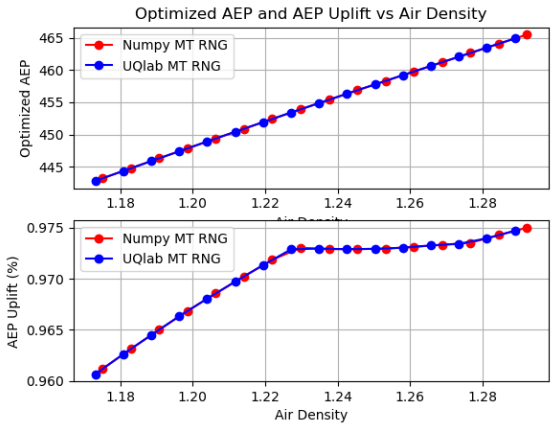

Figure 9.1: Effect of air density for GCH

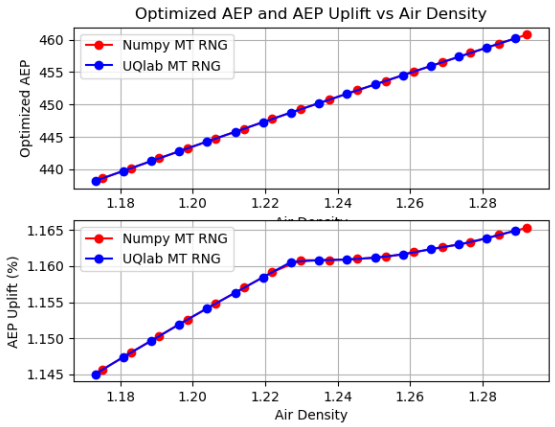

Figure 9.2: Effect of air density for CC

Interestingly, for the GCH model the relationship with air density becomes almost constant between around 1.23 and 1.28 kg/m^3. This is due to the baseline (no wake steering) AEP and optimized AEP (with wake

steering) increasing at almost the same rates and having similar values. Since the typical deterministic air density is 1.225 [kg/m^3] (standard air density at sea level under standard atmospheric conditions) during wake steering assessments, it can be concluded that the benefit from wake steering cannot be increased further with higher air density. This occurs when, for example, the temperature is colder than standard temperature at 15°. However, the benefit from wake steering can decrease significantly with lower air density which can occur at temperatures higher than 15°and/or with more humid air (standard atmospheric conditions assume 0% humidity).

Turbulence intensity

The effect of the turbulence on the velocity deficit is quantified with the wake expansion factor. As the wake expands, the wake recovery is accelerated. At higher turbulence intensities, wake expansion is higher. This means that the power output increases. Moreover, when the thrust coefficient of the WT is higher the TI increases which increases wake recovery and power. Therefore, it is no surprise that the benefit from wake steering, as shown in Figure 9.3 and Figure 9.4, decreases at higher turbulence intensities. As wake recovery occurs more rapidly, wake steering is less effective for improving the AEP. Although the relationship between the turbulence intensity and AEP uplift remains the same for both the

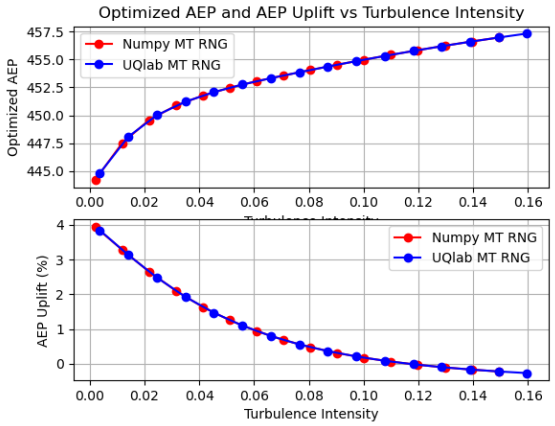

Figure 9.3: Effect of turbulence intensity for GCH

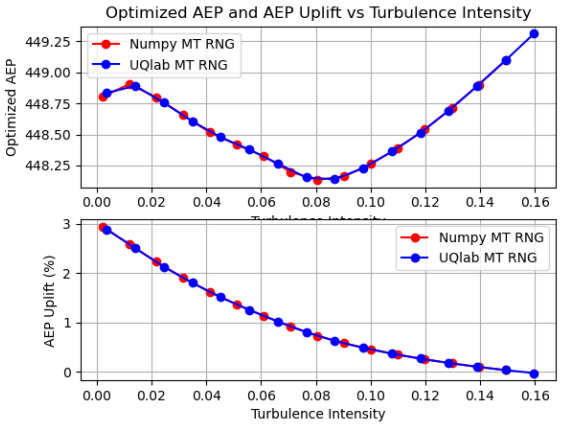

Figure 9.4: Effect of turbulence intensity for CC

GCH and CC, differences are observed in the optimized AEP. In the GCH model, the optimized AEP is a downward-facing parabola with a steeper gradient for the turbulence intensity values up to 0.04. This means that the optimized AEP increases at a greater pace until TI = 0.04, after which the rate of increase in optimized AEP is smaller. GCH models the turbulence with the Crespo Hernandez model. This is based on results from experiments and CFD simulations starting from TI = 0.05 that are fitted onto a straight line [17]. This could explain the change in the optimized AEP's rate of increase. In contrast, the optimized AEP calculated with the CC model decreases until TI = 0.08, after which it increases at almost the same rate. This is because CC models wake recovery in the medium to far-wake regions better, as it uses the super-Gaussian wake model [7]. These differences are not observed with the AEP uplift because the baseline AEP has the same relationship with the turbulence intensity as the optimized AEP.

Wind shear

The wind shear coefficient α is directly related to the velocity gradient with respect to the hub height as shown in Equation 9.1.

$$\frac{dU}{dz} = \frac{\alpha}{z_H} \cdot \left(\frac{z}{z_H}\right)^{\alpha-1} \tag{9.1}$$

The relationship is exponential with the exponent being the wind shear. This means that a higher wind shear coefficient would result in an increased velocity deficit. The power output at the wind turbine is obtained by tripling the velocity deficit at the wind turbine. As the wind shear exponent increases, the velocity deficit and thus the power output decreases faster. The optimized AEP and AEP uplift of both the GCH and CC models in Figure 9.5 and Figure 9.6 follow this shape for positive wind shear values, while

for negative wind shear values the power output increases as α increases. While the relationship of α

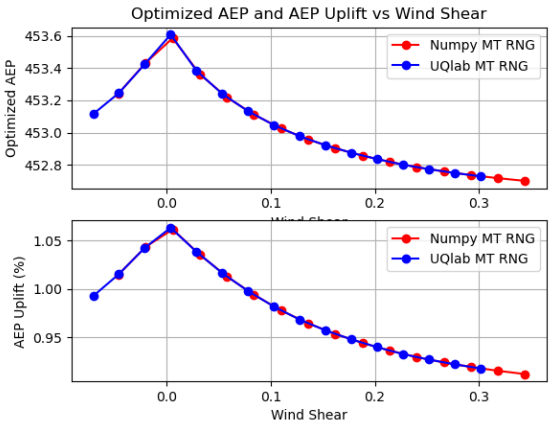

Figure 9.5: Effect of wind shear for GCH

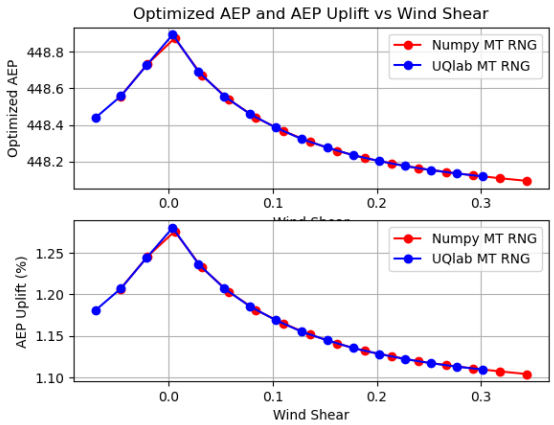

Figure 9.6: Effect of wind shear for CC

with optimized AEP and AEP uplift is the same for both WFFMs, the gradient of the graph is steeper for the CC model which means that changing α produces a greater change in the AEP. Changes in the wind shear could have a more significant effect on the AEP uplift with the CC model due to the vertical velocity gradient being modelled as greater than in the GCH model.

Once the individual effects of the input parameters on the AEP uplift are understood, the convergence study is run to determine the optimum sample size that minimizes computational cost.

9.2. Convergence Study

For the case study with the full wind farm, samples are taken from the input parameters simultaneously. As this increases the computational cost, it is important to find the minimum sample size at which convergence occurs. If the minimum sample size needed for convergence using the Monte Carlo method is low enough, a surrogate model is not needed. In order to reduce the computational cost, the convergence study is conducted on a small sample of equally distanced five Vestas V90-3 MW WTs using the GCH model. It is assumed that the rate of convergence for five WTs is the same as the rate of convergence for the full OWEZ WF with 36 WTs. This assumption is verified later in the section by performing a convergence study for the AEP uplift for increasing numbers of wind turbines. The results of the convergence study on the mean AEP uplift for the five WTs are shown in Figure 9.7. Starting from N = 100, the variation between the maximum and minimum AEP uplift is within 0.65% which indicates a relatively small range of fluctuation. As the sample size increases, the range of fluctuation in AEP uplift decreases further, indicating convergence. Therefore, N = 100 is chosen to be the minimum sample size for calculating the AEP uplift with the MC method. This sample size has a low enough computational cost to not necessitate the use of surrogate models.

Next, the convergence study is repeated for the Sobol indices under the same conditions as the convergence study for the Monte Carlo method. The total Sobol index for a chosen uncertain input parameter - in this case turbulence intensity - is calculated for increasing sample sizes. Figure 9.8 shows the results of the convergence study. Starting from N = 225, the total Sobol index for turbulence intensity fluctuates by 25%. At N = 1228, the rate of fluctuation in the total Sobol index decreases to 12% which indicates that at higher sample sizes convergence occurs. Thus, the Sobol index has a moderate level of sensitivity to sample size. Despite this, the fluctuation rate is not significant enough to change conclusions regarding the importance of input parameters on the AEP uplift. Since computing Sobol indices is more resource-intensive than MC-sampling for uncertainty propagation, there is further motivation to select the lowest sample size that leads to the appropriate conclusions. Therefore, N = 225 is selected to be the minimum sample size required for the computation of Sobol indices.

Finally, the assumption that the minimum sample size for convergence obtained for the five WT can be used for the full OWEZ wind farm is verified. For this, the convergence rate in AEP uplift and first order Sobol indices as a function of the number of wind turbines is computed for N = 225 and N = 400 in

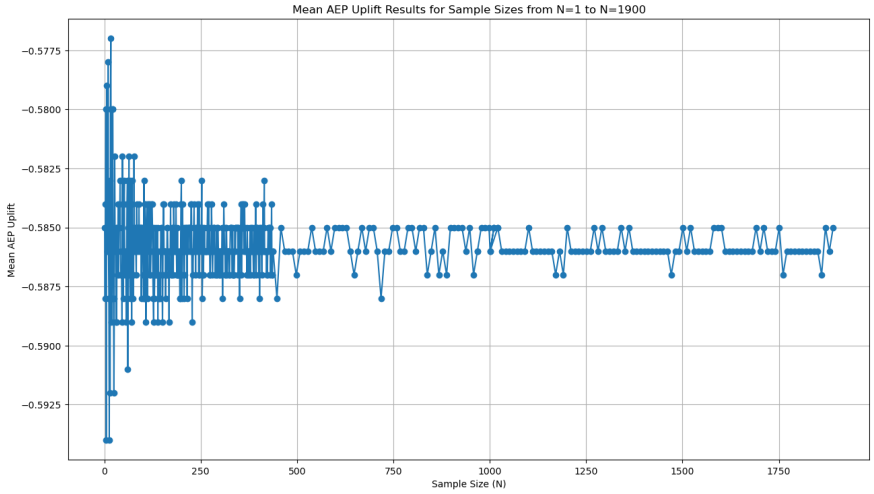

Figure 9.7: Mean AEP Uplift for 5 WTs from N=1 to N=1900

Figure 9.9. The convergence rate for the first order Sobol index of turbulence intensity is almost the same for both sample sizes, while ones for the air density and wind shear are constant for both sample sizes due to the AEP uplift being almost entirely driven by the turbulence intensity. Hence, it is shown that while there are small differences in the first order Sobol indices as the number of samples increases, the difference is negligible enough to not change the conclusions obtained from the study. In addition, a serendipitous finding emerged, revealing that the Sobol indices converge at 20 wind turbines. It is theorized that this is due to the aerodynamic flow becoming fully developed as one goes deeper into the wind farm; therefore, after once a specific limit is reached no changes would be observed in the resulting AEP uplift estimates as parameters are varied [107]. This indicates the possibility of reducing the computational cost further by running the wake steering assessment on fewer wind turbines from the OWEZ wind farm in future research.

To conclude, N = 225 is the sample size chosen for the application of the UQ framework on the case study. To allow for correct analysis of the UQ results, the more conservative sample size is chosen for the AEP uplift and Sobol index calculations.

9.3. Application on Nordzeewind Case Study

Following the conclusions of Chapter 7, Chapter 8 and Section 9.2, the uncertainty quantification framework is applied to the OWEZ wind farm ignoring the neighboring wind farm. The purpose of this case study is to demonstrate how the UQ framework can be used to provide more accurate estimates of AEP uplift by considering uncertainties in the input parameters and by understanding the significance of these uncertainties in the AEP uplift. First, uncertainties in air density, turbulence intensity and wind shear are propagated forward for the GCH and CC WFFMs. The same thrust curve and wind rose as the deterministic analysis is used for this uncertainty quantification study. The first UQ study is performed to verify that the uncertainty quantification framework is implemented correctly. Moreover, the computational cost is reduced further as only the significant parameter(s) found with the Sobol' analysis are used in the second uncertainty quantification study. The purpose of the second uncertainty quantification study is to propagate the uncertainty sources most commonly encountered in yield estimations during early-phase design, namely the wind rose and the thrust curve, as well as the significant parameter(s) found in the first uncertainty quantification study.

First Uncertainty Quantification Study

The resulting AEP uplift distribution for the GCH is shown in Figure 9.10, while the one for the CC model is shown in Figure 9.11. The AEP uplift responses to the PDFs of the input parameters are similar in shape to the Gaussian distribution, with the response of the Gaussian-curl hybrid model having a mean of 0.865% and a standard deviation of 0.055 and the response of the cumulative curl model having a mean

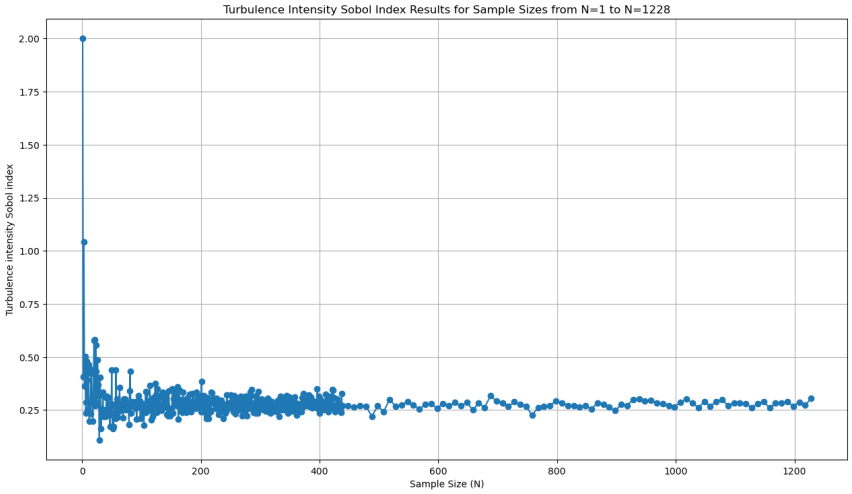

Figure 9.8: Total Sobol Index of Turbulence Intensity for 5 WTs from N=1 to N=1228

of 1.083% and a standard deviation of 0.049. For both models, there is still benefit from wake steering within one standard deviation of the mean. An interesting observation for both models is that there are a small number of outliers for the AEP uplift. These are the AEP uplift values greater than 1% for GCH and greater than 1.2% for CC and the AEP uplift values smaller than 0.7% for GCH and smaller than 0.95% for CC. The smaller AEP uplift values have larger positive wind shear coefficients and turbulence intensity values. This can be explained by the fact that at higher turbulence intensities wake recovery occurs faster, increasing the power output. Therefore, the AEP uplift due to wake steering decreases as the higher AEP is obtained without wake steering. Higher positive wind shear coefficients, on the other hand, result in smaller velocity deficits and power output at the wind turbine level. OAT shows that this translates to smaller optimized AEP and AEP uplift. On the opposite end of the scale, the higher AEP uplift values have smaller positive wind shear coefficients and smaller turbulence intensity values. To evaluate the AEP uplift due to wake steering that most frequently occurs, we look at the 95% confidence interval (C.I.). For the GCH, this is between 0.858% and 0.873% and has a small range of 0.015, while for the CC this is between 1.076% and 1.089% and has the same range of 0.013. It is interesting to note that, although a more accurate wind farm flow model is used, there is a very small change in C.I.. Additionally, for both cases, the most frequently occurring AEP uplift values and the mean AEP uplift are more conservative than the deterministic AEP uplift due to wake steering. It should be noted that the AEP uplift distribution from uncertainty propagation is heavily dependent on the size of the input data chosen. This highlights the importance of further research into the modeling of measurement data. Additionally, it is not possible to draw conclusions about the true AEP uplift from the confidence interval or the probability distribution, as this is not only heavily dependent on the correctness of the study's assumptions but also on repeating the simulations with a variety of input data and the size of the input data [36].

Next, a sensitivity analysis with the Sobol' method is performed to rank the significance of the input variables on the estimated AEP uplift. The first order Sobol indices are presented for the AEP uplift estimates for both the GCH and CC models in Figure 9.12 and Figure 9.13. The first order Sobol indices show the independent contribution of each input parameter's variance to the AEP uplift's variance. Therefore, they must be positive. For both WFFMs, there are negative first order Sobol indices. In Section 10.1 it is proven that this is due to the Sobol indices not fully converging at the chosen sample size. However, both Section 9.2 and Section 10.1 show that as the number of samples increases, there is no significant change in the Sobol indices. As the computational cost increases with more samples, N = 225 remains the optimal number of samples. In Figure 9.12 and Figure 9.13, the main driving parameters of the AEP uplift and optimized AEP differ. Section 9.1 showed that the change in AEP uplift and in optimized AEP can be quite different when parameters are varied one at a time. For both WFFMs the AEP uplift is almost entirely driven by the turbulence intensity. While the wind shear has a greater contribution for the CC model, this is not large enough to significantly influence the AEP uplift estimation.

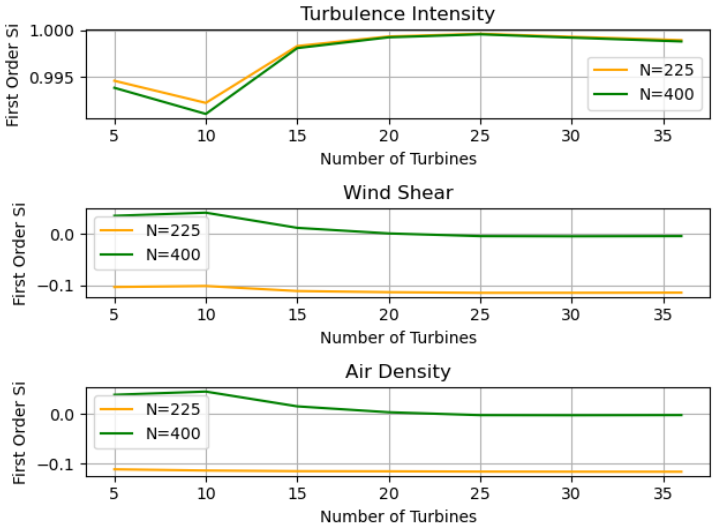

Figure 9.9: Convergence Study of Sobol Indices for Increasing Number of Wind Turbines

The first order Sobol indices do not consider the combined effect that the parameters have on the output. To quantify the combined effect, higher order Sobol indices are necessary. Total Sobol indices are the sum of the first order Sobol indices and the higher order Sobol indices. These are illustrated for the GCH and CC model in Figure 9.14 and Figure 9.15 respectively. The most significant parameter for estimating the AEP uplift is turbulence intensity. The wind shear has a smaller contribution to the AEP uplift (around 10% for the GCH model and around 20% for the CC model), while the air density does not contribute to the AEP uplift. This is consistent with findings in literature demonstrating that significant changes in yaw misalignment angles occur for turbulence intensity, but not for wind shear and air density, following an uncertainty quantification study [51]. On the other hand, the optimized AEP is fully determined by the air density. For both models and both output results, there is nearly no difference between the first order Sobol indices and total Sobol indices of the significant input variables. Therefore, there are no correlations that significantly impact the estimated AEP uplift or optimized AEP. To minimize computational costs, the turbulence intensity is the only parameter that is used in the second uncertainty quantification study.

Second Uncertainty Quantification Study

The uncertainty quantification is performed on the turbulence intensity, the thrust curves and the wind roses. Figure 9.16 and Figure 9.17 show the results of the AEP uplift distributions for the GCH and CC models respectively. The mean AEP uplift for the GCH model is 0.906% with a standard deviation of 0.190, while the mean AEP uplift for the CC model is 1.105% with a standard deviation of 0.228. In both cases, there is benefit from wake steering within one standard deviation of the mean. Compared to the first uncertainty quantification study, the AEP uplift distributions for both cases are less similar to a Gaussian distribution and a wider spread is observed. This can also be inferred from the 95% C.I. for both models. The 95% C.I. for the GCH model is between 0.881% and 0.931% with a range of 0.05, while the 95% C.I. for the CC model is between 1.075% and 1.135% with a range of 0.06. Thus, the range in the 95% C.I. is higher compared to the first UQ study, and the difference in the two WFFMs is more pronounced. In order to understand the reason behind this, the extreme AEP uplift values for both WFFMs are analyzed.

In the GCH model, the smallest AEP uplift is between 0.45% and 0.64%. Fig. 2 and Fig. 4 are the most frequently occurring wind roses with the dominant wind direction coming from the south and south-west and a heavy skew towards the western direction, and wind speeds of 15-20 m/s concentrated on the dominant wind directions. The turbulence intensities are between 6.6% and 7.0%, and - while this AEP uplift range has a mix of different thrust curves - thrust curve 6 appears the most frequently. On the other end of the spectrum, the largest AEP uplift values are between 1.16% and 1.33%. Fig. 8 is the most frequently occurring wind rose with the dominant wind direction coming from the north-east direction. Fig.0 - that has a wider spread across different wind directions - and Fig.3 - whose wind directions are concentrated in the south-west direction - are also frequently observed at this AEP uplift range. Wind speeds in the range

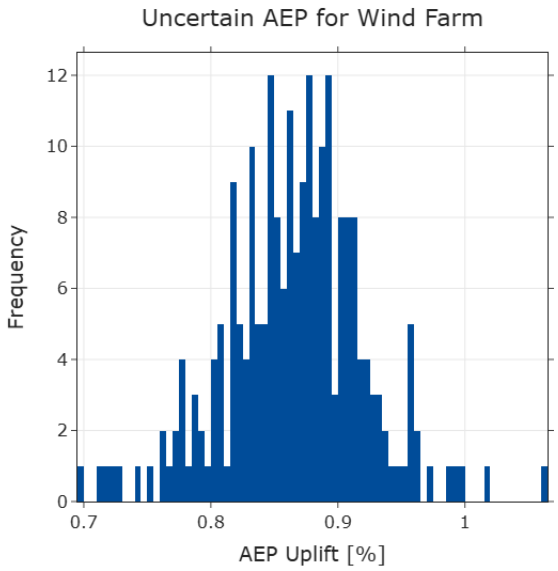

Figure 9.10: AEP Uplift Distribution for GCH

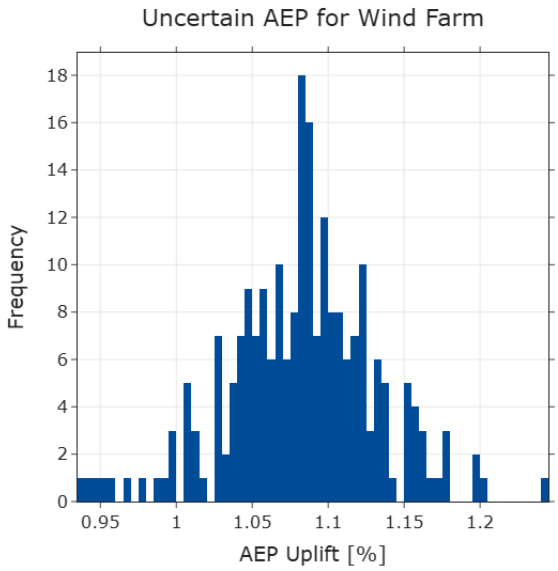

Figure 9.11: AEP Uplift Distribution for CC

5-10 m/s and 15-20 m/s and turbulence intensities between 6.2% and 6.45% occur the most. Thrust curve 1 is also most frequently used. From this analysis, it is already concluded that the thrust curve has a more modest influence on the estimated AEP uplift than the wind speed and wind direction combination. At the 95% C.I., there is no dominant thrust curve, which confirms the previous conclusion. The dominant wind direction is from the south-west direction and the dominant wind speed is between 10-15 m/s with significant 15-20 m/s wind speed components in the same direction. The turbulence intensity varies between 6.4% and 6.8%. This shows the importance of the wind speed contribution and, to a lesser extent of the wind direction, in determining the estimated AEP uplift.

The CC model has slightly smaller turbulence intensities than the GCH, but the range of turbulence intensities is the same for the different AEP uplift levels. Therefore, the influence of the turbulence intensity on the estimated AEP uplift does not show a significant change. At the largest AEP uplift values, which are between 1.16% and 1.33%, fig. 5 replaces fig. 0 as one of the most frequently occurring wind roses. Therefore, the wind roses that result in the highest AEP uplift either have the combination of the dominant wind direction in the north-east and wind speed of 5-10 m/s or the combination of the dominant wind

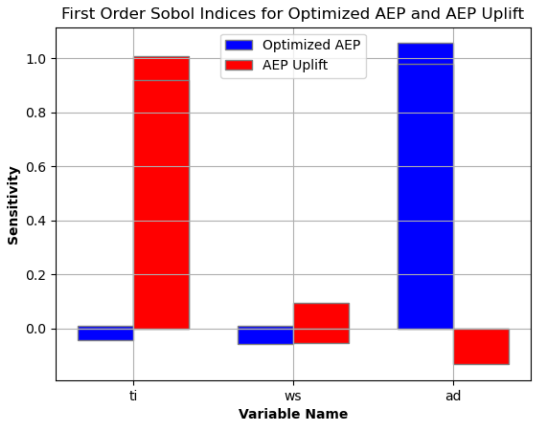

Figure 9.12: First Order Sobol Indices for GCH

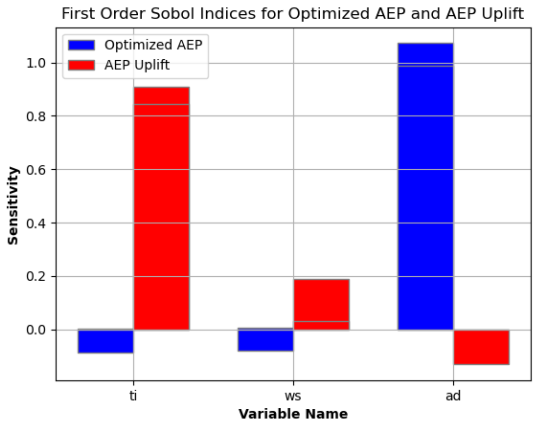

Figure 9.13: First Order Sobol Indices for CC

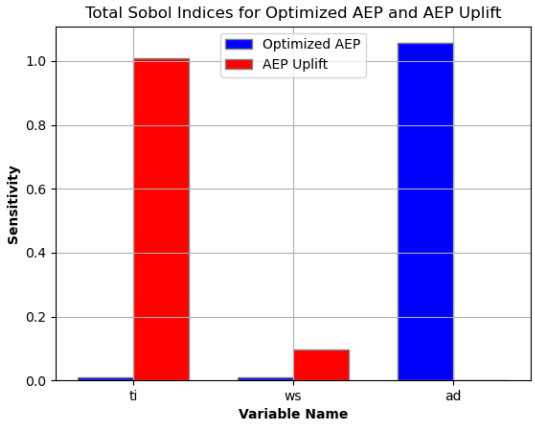

Figure 9.14: Total Sobol Indices for GCH

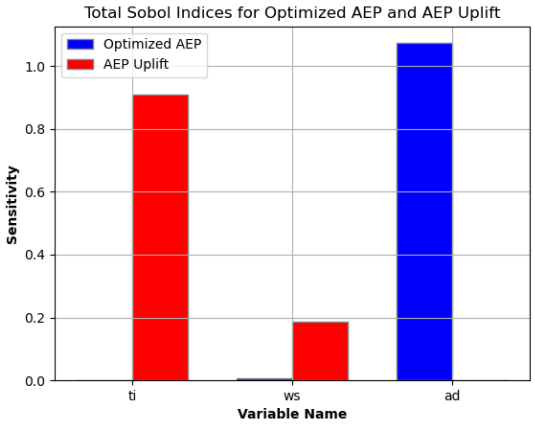

Figure 9.15: Total Sobol Indices for CC

direction in the south-west and the higher wind speeds of 10-15 m/s or 15-20 m/s. It is thus concluded that these combinations benefit the most from wake steering. At the 95% C.I., the GCH model had one dominant wind rose. The 95% C.I. for the CC model has more than one dominant wind rose. Besides the wind direction/wind speed combination that occurs in the GCH, wind roses with the dominant south-west wind direction and a heavier skew towards the western direction combined with wind speeds of 10-15 m/s and some 5-10 m/s components.

To quantify the contribution of individual variances on the total variance, the Sobol' analysis is performed. The results of the Sobol' analysis in terms of the first order Sobol' indices are shown in Figure 9.18 and Figure 9.19. As in the first uncertainty quantification study, the difference between the two models in terms of the ranking of the first order Sobol' indices is insignificant. However, unlike the first uncertainty quantification study, in this case the ranking of the input variables is the same for the optimized AEP and for the AEP uplift. Nevertheless, compared to the optimized AEP, the influence of the wind rose is smaller on the AEP uplift. The thrust curve and turbulence intensity are slightly more prominent for the AEP uplift instead. The first order Sobol' indices only show the independent influence of the input variables on the output. The interactions between variables also contribute to the variance of the output. In order to understand the total influence of the input variables on the output, the interaction effects between the input variables must also be considered. The total Sobol' indices are thus shown in Figure 9.20 and Figure 9.21. The total Sobol' indices of the turbulence intensity and thrust curve for the optimized AEP are zero, and the variance of the optimized AEP is fully defined by the wind rose. The total Sobol' indices for the AEP uplift decrease by the same amount for each of the input variables. This results in the wind rose being the most significant input variable. The thrust curve and turbulence intensity have a relatively insignificant influence on the AEP uplift. The fact that the wind rose has such a large contribution to the total variance of the AEP uplift is attributed to the significant variations in the wind directions of the input wind roses. This is a limitation of the input data available and shows the sensitivity of the output to the selected input range.

9.4. Final Words

This chapter presented the AEP uplift distributions for two wind farm flow models following two uncertainty quantification studies and concluded that the wind rose has the greatest influence the AEP uplift for both wind farm flow models while the selected thrust curve and turbulence intensity have less significant influences. The optimized AEP and AEP uplift were shown not necessarily to have the same significant input variables, with the wind rose being the only parameter that influenced the optimized AEP. Additionally, it was shown that the output's uncertainty bounds are heavily dependent on the uncertainty bounds chosen for the input. This means that correctly choosing and modelling the input data is essential for accurate AEP uplift estimations. Moreover, statistical analysis involving confidence intervals are only relevant if all the assumption are correct. Thus, while the uncertainty quantification framework can be used to estimate the uncertainties in the AEP uplift during early-stage yield assessments in FLORIS, high-fidelity simulations and field experiments are still needed to quantify the extent to which the implementation of wake steering

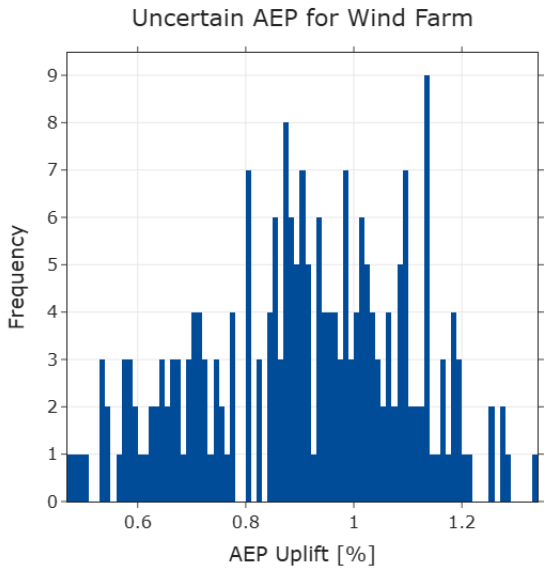

Figure 9.16: AEP Uplift Distribution for GCH

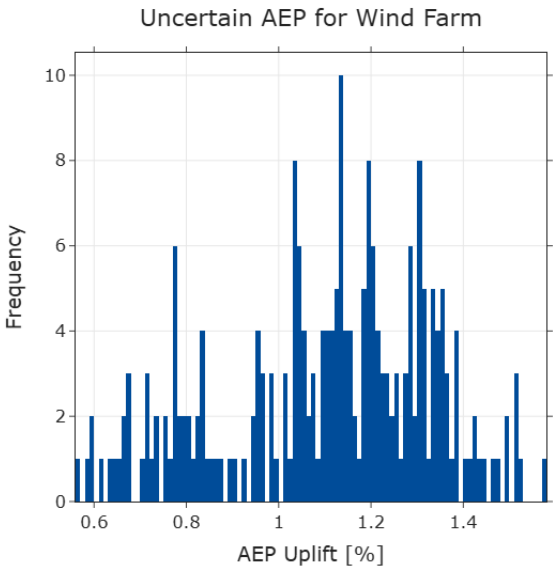

Figure 9.17: AEP Uplift Distribution for CC

in wind farms is beneficial when uncertainties are considered. Lastly, it should be emphasized that it is not possible to reach global conclusions about the AEP uplift distribution from the study conducted since the AEP uplift distribution is bound by the input parameters of the study. Instead, this study proves that the uncertainty quantification framework developed works and that it can be used in further studies involving wake steering for any wind farm flow model available on FLORIS. A wider study that considers wind farms with varying layouts in different locations and with different wind turbine configurations is necessary to start making generalizations about the AEP uplift. Even under these conditions, the input data must be varied and carefully selected, so that biases in input sampling do not lead to misleading conclusions.

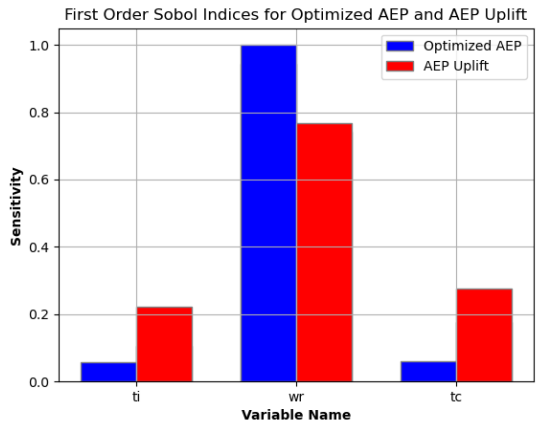

Figure 9.18: First Order Sobol Indices for GCH

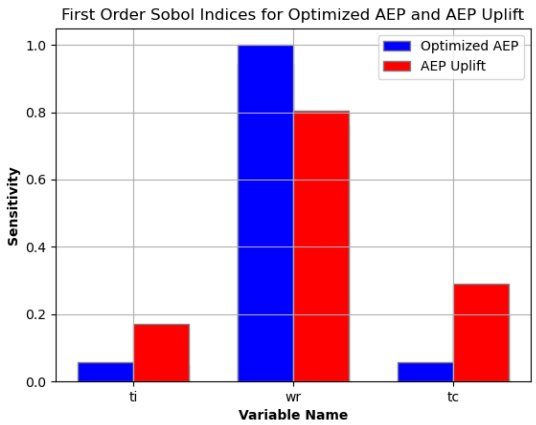

Figure 9.19: First Order Sobol Indices for CC

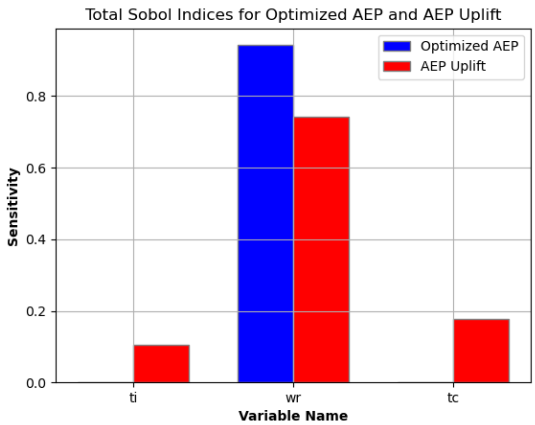

Figure 9.20: Total Sobol' Indices for GCH

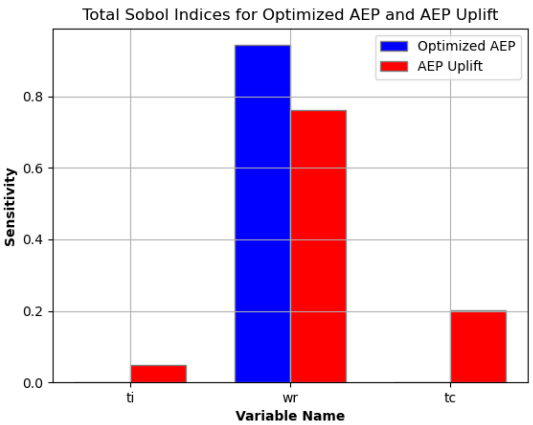

Figure 9.21: Total Sobol' Indices for CC

10

Verification

In Chapter 9 the independent input parameters were first processed through the UQ framework, then a convergence study was conducted followed by the application of the framework to the OWEZ case study. Chapter 10 is concerned with verifying this proposed framework.

10.1. Verification of Uncertainty Quantification Framework

The uncertainty quantification framework is verified by using the individual parameters sampled in Section 9.1. The AEP uplift and optimized AEP resulting from the UQ framework are compared to the same output values generated by a Monte Carlo simulation created using the Numpy library [38]. If the output values obtained with the two methods match, the UQ framework has been successfully integrated with FLORIS. Once the framework is verified, the convergence of the results are verified. If the conclusions drawn from the results obtained with a much greater sample size, the conclusions stemming from the results with the smaller sample size - that aims to minimize computational cost - are valid.

The uncertainty quantification framework on UQLab is built block by block to ensure that the method is understood in depth and that it is verified at each step. In order to verify the FLORIS model implemented in UQLab, the MC method is first implemented directly on the deterministic model. This is done by fitting each input data into its respective probability distribution function, then taking samples using the Monte Carlo method and plotting the histogram of the sampled values. To keep the output reproducible, a random seed is used. The histogram is plotted in order to group the sampled probability values into bins. This is done to increase the computational speed of the AEP calculation. In this case, one-at-a-time variation of the input parameters is done. This leads to a range of AEP and AEP uplift values generated by the uncertain parameter. These ranges are used to create box plots. The expected AEP is calculated by normalizing the cumulative probability of each respective bin and multiplying it by the AEP value obtained for each bin. The box plots obtained are verified in the following way:

- **Verification 1:** Plot a small number of the x-values generated by sampling the probability distribution in order to verify if the effect of the parameter on the AEP within the software matches the expected effect
- **Verification 2:** Create the histogram from the PDFs. Decrease the number of bins and generate the x-values via MC-based sampling. Plot the effect of the input values on the AEP and generate the box plots. The shape of the plots and graphs should match verification 1.
- **Verification 3:** Compare the individual box plots to the figure obtained when all three box plots are plotted. The purpose of this verification is to check if performing the uncertainty quantification individual input parameters creates a bias. The individual box plots should match the figure with all three box plots for there to be no bias.

The results of verification 1 and verification 2 for $N = 16$ was shown in Section 9.1. Following the verification steps for the GCH model at $N = 10000$ results in Figure 10.1 and Figure 10.2. The box plots resulting from the Monte Carlo simulation done by varying the input variables one-at-a-time are similar for both the FLORIS model implemented in UQLab and the simulation done using Numpy. There is only a small difference in output values which is due to the slight difference in the input samples generated by the two random number generators. This difference was also shown in the figures in Section 9.1.

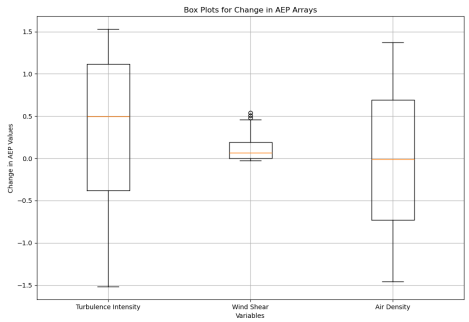

Figure 10.1: Optimized AEP for Numpy

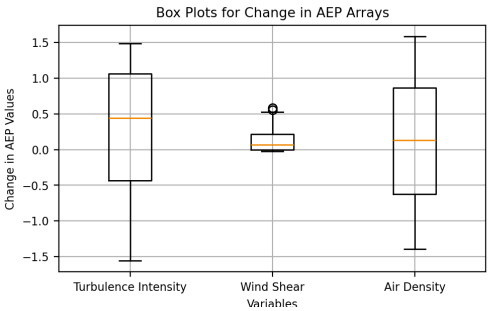

Figure 10.2: Optimized AEP for UQLab

Part IV

Closure

11

Conclusions and Recommendations

This chapter presents the main conclusions and recommendations of the master's thesis. In this thesis a novel uncertainty quantification framework for wake steering assessments for the early design phase of offshore wind farms was introduced in order to answer the following research questions: *How do uncertainties affect the predicted annual energy production gains for wake steering?* and *How significant is the impact of input uncertainties on the predicted AEP gain from wake steering?*. The proposed framework combined uncertainty propagation methods and historical atmospheric data within the wake steering assessment tool FLORIS. From a practical perspective, FLORIS and the uncertainty quantification tool were successfully integrated, creating a prototype that could be used in industrial applications and for further research. With the framework developed, uncertainties on the AEP uplift due to wake steering were quantified, allowing for the refinement of energy yield estimates and thus decreasing financial risks. The framework's effectiveness was demonstrated on the OWEZ wind farm for a given wind rose and two wind farm flow models by quantifying the uncertainties in turbulence intensity, wind shear and air density. The results were then verified and validated with a higher number of samples and on a different wind rose. The knowledge gained was used to quantify the uncertainties in turbulence intensity, the thrust curve and the wind rose for both wind farm flow models. These parameters were the most relevant for the application in the early stage wind farm design phase. Following the case study, the conclusions enumerated in Section 11.1 were made. These led to the recommendations in Section 11.2.

11.1. Conclusions

- **The uncertainty quantification framework effectively propagated input uncertainties for different wind farm flow models and wind rose data, leading to more accurate AEP uplift estimates due to wake steering.** The uncertainty quantification framework was verified against a Monte Carlo simulation created with Python's Numpy library. One-at-a-time variation of the input parameters showed that FLORIS was integrated correctly for uncertainty quantification. Since the AEP uplift and Sobol' indices converged at a sample size with a manageable computational cost, the framework developed was successfully used to propagate uncertainties in atmospheric conditions forward to estimate AEP uplift of a full wind farm. The framework was validated for different wind roses and thrust curves, indicating that it could be used under varying wind conditions and with different wind turbine types. This contributed to the quantification of uncertainties in the estimation of AEP uplift due to wake steering using FLORIS as the wake steering assessment tool of choice.
- **There were significant uncertainties on the AEP uplift due to wake steering; yet, for all cases, the implementation of wake steering was beneficial.** The AEP uplift was estimated for the GCH and CC models. The 95% confidence interval consistently showed positive AEP uplift that was more conservative than the AEP uplift calculated in the deterministic analysis. For the GCH model, this was between 0.86% and 0.87% for the uncertainty quantification of atmospheric conditions and between 0.88% and 0.93% for the uncertainty quantification of the wind rose, thrust curve and turbulence intensity. For the CC model, the AEP uplift was between 1.08% and 1.09% for the uncertainty quantification of the atmospheric conditions and between 1.08% and 1.14% for the uncertainty quantification of the wind rose, thrust curve and turbulence intensity. These AEP uplift estimates were more conservative than the deterministic AEP uplift estimates of 0.97% and 1.16% respectively. However, despite the introduction of input uncertainties, the AEP uplift estimates do not

decrease significantly, showing that wake steering is beneficial. Moreover, the range in AEP uplift estimates for the 95% confidence interval is relatively small. This means that the margin of error in the estimated AEP uplift is most likely relatively low. To conclude, the framework was validated for two wind farm flow models in FLORIS, showing that, even with uncertainties in input variables, wake steering was beneficial.

- **The convergence study showed that the Monte Carlo method could be used for the defined uncertainty propagation problem and substantially reduce the computational cost for further studies.** For the Monte Carlo simulation, the AEP uplift converged to within 0.65% at $N = 100$; while for the Sobol' indices, the total Sobol' indices converged enough at $N = 225$. Furthermore, a convergence study was run on the Sobol' indices, concluding that the first order Sobol' indices converged at 20 wind turbines. This was important for future studies, as it showed that sensitivity analysis could be done on fewer WTs in the wind farm without changing the final results. This was an important contribution because it could significantly reduce the computational cost for future wind farm sensitivity analyses.
- **Finally, the wind rose was shown to be the most important factor in determining the AEP uplift. The thrust curve and turbulence intensity had almost negligible effects on the AEP uplift.** When only the atmospheric conditions were considered, the turbulence intensity was the only significant variable while the wind shear had a smaller, relatively insignificant influence on the AEP uplift and the air density did not influence the AEP uplift. In order to minimize computational costs, the uncertainty in the turbulence intensity was propagated together with the uncertainties in wind rose and thrust curve. The wind rose was the most significant parameter for estimating the AEP uplift. The thrust curve had a smaller, almost insignificant influence while the turbulence intensity had almost no influence. Moreover, for all UQ studies, the correlations between the input parameters were insignificant and had little effect on the uncertainty in the AEP uplift. Therefore, for wake steering assessments in FLORIS, it was concluded that to minimize computational costs the AEP uplift could be estimated by only modelling the wind rose and, to a lesser extent, the thrust curve.

11.2. Recommendations

The functionality of the uncertainty quantification framework developed can be further expanded to broaden its scope and make it usable for its application. In order to reliably use this framework in wake steering assessments, while ensuring that a more refined AEP uplift than the current application is obtained, the following recommendations are made.

- **The UQ framework can be validated further on (1) different input data and (2) different wind farms.** The first involves creating PDFs with different data sets and running the framework through the OWEZ wind farm in order to validate the conclusions of the study, while the second involves repeating the case study on different wind farms in order to broaden the scope of the research. In the latter case, different conclusions to the current study may be obtained due to differences in WF layout and WT spacing. In addition, for the latter, the convergence study must be repeated, as the minimum sample size required may differ for different WF configurations.
- **The validation studies done on different wind farms can be classified and references for the AEP uplift and the uncertainty associated with it can be derived.** Wind farms can be selected and clustered into different groups, for example based on geographic regions. The AEP uplift and uncertainty associated with each cluster can later be used to develop a tool that predicts this output based on certain wind farm characteristics, such as geography or layout.

Besides the further development of the existing UQ framework, further research can be conducted to address certain gaps occurring due to the assumptions of the research.

- **Improve input uncertainty modelling.** The output of any uncertainty propagation study is heavily dependent on the uncertainty bounds defined by the input. Therefore, in order to ensure that the uncertainty in the AEP uplift is modelled accurately, refining the input PDFs is essential. Currently, input modelling is based on processing existing measured data. Instead, focusing on the drivers of these atmospheric conditions could lead to better understanding of the probability of occurrence of certain uncertainties. Furthermore, the probability of occurrence of different atmospheric conditions can be matched with the respective wind farms. A significant portion of this task falls into the purview

of statisticians and climate scientists. This could involve taking a larger data set and modelling the atmospheric conditions while considering any weather conditions that are out of the norm, as well as creating dependent PDFs that consider the interactions and relationships between different parameters of interest. In this way, AEP uplift predictions can be made for future wind farm projects.

- **Account for WT's structural reliability and fatigue life.** The goal of this UQ framework was to quantify the uncertainties in the AEP uplift when wake steering was performed with the sole objective of power maximization. One of the greatest obstacles to adoption by industry of wind farm control technology is the risk of decreasing wind turbine life due to structural stress. Considering the effect of certain input uncertainties on the wind turbine's structural life in conjunction with the AEP uplift could build a better case for the adoption of wake steering technology in the wind farm project in development.

Bibliography

[1] Ahmad, T., Coupiac, O., Petit, A., Guignard, S., Girard, N., Kazemtabrizi, B., and Matthews, P. C. (2018). Field implementation and trial of coordinated control of wind farms. *IEEE Transactions on Sustainable Energy*, 9(3):1169–1176.

[2] Balasubramanian, K., Thanikanti, S. B., Subramaniam, U., N., S., and Sichilalu, S. (2020). A novel review on optimization techniques used in wind farm modelling. *Renewable Energy Focus*, 35:84–96.

[3] Baraniuk, C. (2021). Why giant turbines are pushing the limits of possibility. `https://www.bbc.com/news/business-58704792`. Accessed: 21/03/2024.

[4] Barthelmie, R., Hansen, K., Frandsen, S., Rathmann, O., Schepers, J., Schlez, W., Phillips, J., Rados, K., Zervos, A., Politis, E., and Chaviaropoulos, P. (2009). Modelling and measuring flow and wind turbine wakes in large wind farms offshore. *Wind Energy*, 12(5):431–444.

[5] Bastankhah, M. and Porté-Agel, F. (2014). A new analytical model for wind-turbine wakes. *Renewable Energy*, 70:116–123.

[6] Bastankhah, M., Welch, B. L., Martínez-Tossas, L. A., King, J., and Fleming, P. (2021). Analytical solution for the cumulative wake of wind turbines in wind farms. *Journal of Fluid Mechanics*, 911.

[7] Bay, C. J., Fleming, P., Doekemeijer, B., King, J., Churchfield, M., and Mudafort, R. (2023). Addressing deep array effects and impacts to wake steering with the cumulative-curl wake model. *Wind Energy Science*, 8:401–419.

[8] Benke, K. K., Norng, S., Robinson, N. J., Benke, L. R., and Peterson, T. J. (2018). Error propagation in computer models: analytic approaches, advantages, disadvantages and constraints. *Stochastic Environmental Research and Risk Assessment*, 32:2971–2985.

[9] Blonde, F. and Cathelain, M. (2020). An alternative form of the super-gaussian wind turbine wake model. *Wind Energy Science*, 5:1225–1236.

[10] Boersma, S., Doekemeijer, B. M., Gebraad, P. M., Fleming, P. A., Annoni, J., Scholbrock, A. K., Frederik, J. A., and Wingerden, J. W. V. (2017). A tutorial on control-oriented modeling and control of wind farms. In *Proceedings of the American Control Conference*, pages 1–18. Institute of Electrical and Electronics Engineers Inc.

[11] Bossanyi, E. and Ruisi, R. (2021). Axial induction controller field test at sedini wind farm. *Wind Energy Science*, 6(2):389–408.

[12] Brugger, P., Markfort, C., and Porté-Agel, F. (2022). Field measurements of wake meandering at a utility-scale wind turbine with nacelle-mounted doppler lidars. *Wind Energy Science*, 7(1):185–199.

[13] Burton, T., Jenkins, N., Bossanyi, E., Sharpe, D., and Graham, M. (2021). *Wind Energy Handbook (3rd Edition)*. John Wiley Sons.

[14] Centraal Bureau voor de Statistiek (2023). Wake steering performance evaluated at scale. `https://www.cbs.nl/en-gb/figures/detail/81528ENG#shortTableDescription`. Accessed: 25/04/2024.

[15] Chamorro, L. P. and Porté-Agel, F. (2011). Turbulent flow inside and above awind farm: A wind-tunnel study. *Energies*, 4:1916–1936.

[16] Charhouni, N., Sallaou, M., and Mansouri, K. (2019). Realistic wind farm design layout optimization with different wind turbines types. *International Journal of Energy and Environmental Engineering*, 10:307–318.

[17] Crespo, A. and Hernandez, J. (1996). Turbulence characteristics in wind-turbine wakes. *Journal of Wind Engineering and Industrial Aerodynamics*, 61:71–85.

[18] Deloitte (2022). Establishing the investment case: Wind power. Technical report, Deloitte.

[19] Dighe, V. V., Becker, M., Göçmen, T., Sanderse, B., and van Wingerden, J.-W. (2022). Sensitivity analysis and bayesian calibration of a dynamic wind farm control model: Floridyn. *Journal of Physics: Conference Series*, 2265(2):022062.

[20] Doekemeijer, B. M. (2020). *Closing the loop in model-based wind farm control*. PhD thesis, Delft University of Technology.

[21] Doekemeijer, B. M., Kern, S., Maturu, S., Kanev, S., Salbert, B., Schreiber, J., Campagnolo, F., Bottasso, C. L., Schuler, S., Wilts, F., Neumann, T., Potenza, G., Calabretta, F., Fioretti, F., and Wingerden, J. W. V. (2021). Field experiment for open-loop yaw-based wake steering at a commercial onshore wind farm in italy. *Wind Energy Science*, 6:159–176.

[22] Dong, H., Xie, J., and Zhao, X. (2022). Wind farm control technologies: From classical control to reinforcement learning. *Progress in Energy*, 4.

[23] DTU Wind Energy (2024). Pywake. `https://topfarm.pages.windenergy.dtu.dk/PyWake/index.html`. Accessed: 21/05/2024.

[24] Eurostat (2023). Energy consumption in households. `https://ec.europa.eu/eurostat/statistics-explained/index.php?title=Energy_consumption_in_households#Energy_products_used_in_the_residential_sector`. Accessed: 25/04/2024.

[25] Fleming, P., Annoni, J., Churchfield, M., Martinez-Tossas, L. A., Gruchalla, K., Lawson, M., and Moriarty, P. (2018). A simulation study demonstrating the importance of large-scale trailing vortices in wake steering. *Wind Energy Science*, 3:243–255.

[26] Fleming, P., Annoni, J., Scholbrock, A., Quon, E., Dana, S., Schreck, S., Raach, S., Haizmann, F., and Schlipf, D. (2017a). Full-scale field test of wake steering. In *Journal of Physics: Conference Series*, volume 854. Institute of Physics Publishing. static LUT.

[27] Fleming, P., Annoni, J., Shah, J. J., Wang, L., Ananthan, S., Zhang, Z., Hutchings, K., Wang, P., Chen, W., and Chen, L. (2017b). Field test of wake steering at an offshore wind farm. *Wind Energy Science*, 2:229–239. static LUT.

[28] Fleming, P., King, J., Dykes, K., Simley, E., Roadman, J., Scholbrock, A., Murphy, P., Lundquist, J. K., Moriarty, P., Fleming, K., van Dam, J., Bay, C., Mudafort, R., Lopez, H., Skopek, J., Scott, M., Ryan, B., Guernsey, C., and Brake, D. (2019). Initial results from a field campaign of wake steering applied at a commercial wind farm – part 1. *Wind Energy Science*, 4:273–285.

[29] Fleming, P., King, J., Simley, E., Roadman, J., Scholbrock, A., Murphy, P., Lundquist, J. K., Moriarty, P., Fleming, K., Dam, J. V., Bay, C., Mudafort, R., Jager, D., Skopek, J., Scott, M., Ryan, B., Guernsey, C., and Brake, D. (2020). Continued results from a field campaign of wake steering applied at a commercial wind farm - part 2. *Wind Energy Science*, 5:945–958.

[30] Fleming, P., Simley, E., and Eguinoa, I. (2022a). Iea wind tcp task report 2022. Technical report, International Energy Agency.

[31] Fleming, P. A., Stanley, A. P., Bay, C. J., King, J., Simley, E., Doekemeijer, B. M., and Mudafort, R. (2022b). Serial-refine method for fast wake-steering yaw optimization. In *Journal of Physics: Conference Series*, volume 2265. Institute of Physics.

[32] Frederik, J. A., Doekemeijer, B. M., Mulders, S. P., and van Wingerden, J. W. (2020a). The helix approach: Using dynamic individual pitch control to enhance wake mixing in wind farms. *Wind Energy*, 23:1739–1751.

[33] Frederik, J. A., Weber, R., Cacciola, S., Campagnolo, F., Croce, A., Bottasso, C., and van Wingerden, J.-W. (2020b). Periodic dynamic induction control of wind farms: proving the potential in simulations and wind tunnel experiments. *Wind Energy Science*, 5(1):245–257.

[34] Gebraad, P. M. O., Teeuwisse, F. W., van Wingerden, J. W., Fleming, P. A., Ruben, S. D., Marden, J. R., and Pao, L. Y. (2016). Wind plant power optimization through yaw control using a parametric model for wake effects—a cfd simulation study. *Wind Energy*, 19(1):95–114.

[35] González-Longatt, F., Wall, P., and Terzija, V. (2012). Wake effect in wind farm performance: Steady-state and dynamic behavior. *Renewable Energy*, 39(1):329–338.

[36] Greenland, S., Senn, S., Rothman, K., Carlin, J., Poole, C., Goodman, S., and Altman, D. (2016). Statistical tests, p values, confidence intervals, and power: a guide to misinterpretations. *European Journal of Epidemiology*, 31:337–350.

[37] Göçmen, T., van der Laan, P., Réthoré, P.-E., Diaz, A. P., Larsen, G. C., and Ott, S. (2016). Wind turbine wake models developed at the technical university of denmark: A review. *Renewable and Sustainable Energy Reviews*, 60:752–769.

[38] Harris, C. R., Millman, K. J., van der Walt, S. J., Gommers, R., Virtanen, P., Cournapeau, D., Wieser, E., Taylor, J., Berg, S., Smith, N. J., Kern, R., Picus, M., Hoyer, S., van Kerkwijk, M. H., Brett, M., Haldane, A., del Río, J. F., Wiebe, M., Peterson, P., Gérard-Marchant, P., Sheppard, K., Reddy, T., Weckesser, W., Abbasi, H., Gohlke, C., and Oliphant, T. E. (2020). Array programming with NumPy. *Nature*, 585(7825):357–362.

[39] Hartman, L. (2023). Wind turbines: the bigger, the better. `https://www.energy.gov/eere/articles/wind-turbines-bigger-better`. Accessed: 14/05/2024.

[40] Henley, J. (2023). European countries pledge huge expansion of north sea wind farms. `https://www.theguardian.com/environment/2023/apr/24/european-countries-pledge-huge-expansion-of-north-sea-wind-farms`. Accessed: 01/05/2024.

[41] Houck, D. R. (2022). Review of wake management techniques for wind turbines. *Wind Energy*, 25:195–220.

[42] Howland, M. F. (2021). Wind farm yaw control set-point optimization under model parameter uncertainty. *Journal of Renewable and Sustainable Energy*, 13.

[43] Howland, M. F., Ghate, A. S., Lele, S. K., and Dabiri, J. O. (2020). Optimal closed-loop wake steering – part 1: Conventionally neutral atmospheric boundary layer conditions. *Wind Energy Science*, 5(4):1315–1338.

[44] Howland, M. F., Lele, S. K., and Dabiri, J. O. (2019). Wind farm power optimization through wake steering. *Proceedings of the National Academy of Sciences of the United States of America*, 116:14495–14500. static LUT.

[45] IEA Wind TCP (2024). Iea wind task 44. `https://iea-wind.org/task44/`. Accessed: 24/04/2024.

[46] IRENA (2024). Renewable capacity statistics 2024. Technical report, International Renewable Energy Agency.

[47] Jensen, N. O. (1983). A note on wind generator interaction. Technical report, Risø National Laboratory.

[48] Jiménez, □ Crespo, A., and Migoya, E. (2010). Application of a les technique to characterize the wake deflection of a wind turbine in yaw. *Wind Energy*, 13(6):559–572.

[49] Jung, C. and Schindler, D. (2021). A global wind farm potential index to increase energy yields and accessibility. *Energy*, 231.

[50] Kamran, M. (2023). Chapter 6 - planning and modeling of wind energy systems. In *Fundamentals of Smart Grid Systems*, pages 271–298. Academic Press.

[51] Kanev, S. and Bot, E. (2021). Dynamic robust active wake control. *Wind Energy Science*.

[52] Katic, I., Højstrup, J., and Jensen, N. O. (1987). A simple model for cluster efficiency. In Palz, W. and Sesto, E., editors, *EWEC'86. Proceedings. Vol. 1*, pages 407–410. A. Raguzzi.

[53] Kheirabadi, A. C. and Nagamune, R. (2019). A quantitative review of wind farm control with the objective of wind farm power maximization. *Journal of Wind Engineering and Industrial Aerodynamics*, 192:45–73.

[54] King, J., Fleming, P., King, R., Martínez-Tossas, L. A., Bay, C. J., Mudafort, R., and Simley, E. (2021). Control-oriented model for secondary effects of wake steering. *Wind Energy Science*, 6:701–714.

[55] Lataniotis, C., Torre, E., Marelli, S., and Sudret, B. (2024a). UQLab user manual – The Input module. Technical report, Chair of Risk, Safety and Uncertainty Quantification, ETH Zurich, Switzerland. Report UQLab-V2.1-102.

[56] Lataniotis, C., Zhu, X., Marelli, S., and Sudret, B. (2024b). UQLab user manual – The Model module. Technical report, Chair of Risk, Safety and Uncertainty Quantification, ETH Zurich, Switzerland. Report UQLab-V2.1-103.

[57] Lee, J., Son, E., Hwang, B., and Lee, S. (2013). Blade pitch angle control for aerodynamic performance optimization of a wind farm. *Renewable Energy*, 54:124–130.

[58] Liew, J., Göçmen, T., Lio, W. H., and Larsen, G. C. (2023). Model□free closed□loop wind farm control using reinforcement learning with recursive least squares. *Wind Energy*.

[59] Marelli, S., Lamas, C., Konakli, K., Mylonas, C., Wiederkehr, P., and Sudret, B. (2024). UQLab user manual – Sensitivity analysis . Technical report, Chair of Risk, Safety and Uncertainty Quantification, ETH Zurich,Switzerland. Report UQ[py]Lab - V1.0-106.

[60] Marelli, S. and Sudret, B. (2014). *UQLab: A Framework for Uncertainty Quantification in Matlab*, pages 2554–2563. Vulnerability, Uncertainty, and Risk: Quantification, Mitigation, and Management.

[61] Martínez-Tossas, L. A., Annoni, J., Fleming, P. A., and Churchfield, M. J. (2019). The aerodynamics of the curled wake: A simplified model in view of flow control. *Wind Energy Science*, 4:127–138.

[62] Meyers, J., Bottasso, C., Dykes, K., Fleming, P., Gebraad, P., Giebel, G., Göçmen, T., and Wingerden, J. W. V. (2022). Wind farm flow control: Prospects and challenges. *Wind Energy Science*, 7:2271–2306.

[63] Miller, D. C., Ng, B., Eslick, J., Tong, C., and Chen, Y. (2014). Advanced computational tools for optimization and uncertainty quantification of carbon capture processes. In Eden, M. R., Siirola, J. D., and Towler, G. P., editors, *Proceedings of the 8th International Conference on Foundations of Computer-Aided Process Design*, volume 34 of *Computer Aided Chemical Engineering*, pages 202–211. Elsevier.

[64] Minister of Economic Affairs and Climate Policy (2022). Letter to parliament on offshore wind energy 2030-2050. Technical Report DGKE-E/22174505, Government of the Netherlands.

[65] Moriarty, P., Bodini, N., Cheung, L., Hamilton, N., Herges, T., Kaul, C., Letizia, S., Pekour, M., and Simley, E. (2023). Overview of recent observations and simulations from the american wake experiment (awaken) field campaign. In *Journal of Physics: Conference Series*, volume 2505. Institute of Physics.

[66] Munters, W. and Meyers, J. (2018). Towards practical dynamic induction control of wind farms: analysis of optimally controlled wind-farm boundary layers and sinusoidal induction control of first-row turbines. *Wind Energy Science*, 3(1):409–425.

[67] Najm, H. N. (2009). Uncertainty quantification and polynomial chaos techniques in computational fluid dynamics. *Annual Review of Fluid Mechanics*, 41(Volume 41, 2009):35–52.

[68] Niayifar, A. and Porté-Agel, F. (2015). A new analytical model for wind farm power prediction. In *Journal of Physics: Conference Series*, volume 625. Institute of Physics Publishing.

[69] NREL (2024). Floris wake modeling and wind farm controls software v4.0.1. `https://github.com/NREL/floris`. Accessed: 30/04/2024.

[70] Nygaard, N. G. (2015). Systematic quantification of wake model uncertainty. Technical report, EWEA Offshore.

[71] Nygaard, N. G., Steen, S. T., Poulsen, L., and Pedersen, J. G. (2020). Modelling cluster wakes and wind farm blockage. In *Journal of Physics: Conference Series*, volume 1618. IOP Publishing Ltd.

[72] Park, J. and Law, K. H. (2015). Cooperative wind turbine control for maximizing wind farm power using sequential convex programming. *Energy Conversion and Management*, 101:295–316.

[73] Porté-Agel, F., Bastankhah, M., and Shamsoddin, S. (2020a). Wind-turbine and wind-farm flows: A review. *Boundary-Layer Meteorology*, 174:1–59.

[74] Porté-Agel, F., Bastankhah, M., and Shamsoddin, S. (2020b). Wind-turbine and wind-farm flows: A review. *Boundary-Layer Meteorology*, 174:1–59.

[75] Quick, J., Annoni, J., King, R., Dykes, K., Fleming, P., and Ning, A. (2017). Optimization under uncertainty for wake steering strategies. In *Journal of Physics: Conference Series*, volume 854. Institute of Physics Publishing.

[76] Quick, J., King, J., King, R. N., Hamlington, P. E., and Dykes, K. (2020). Wake steering optimization under uncertainty. *Wind Energy Science*, 5:413–426.

[77] Rolfvondenbaumen, T. (2024). Dnv launches joint industry project to identify barriers to the use of high voltage direct current transmission in the u.s. grid. https://www.dnv.com/news/dnv-launches-joint-industry-project-to-identify-barriers-to-the-use-of-high-voltage-direct-curren Accessed: 03/05/2024.

[78] Rott, A., Doekemeijer, B., Seifert, J. K., Wingerden, J. W. V., and Kühn, M. (2018). Robust active wake control in consideration of wind direction variability and uncertainty. *Wind Energy Science*, 3:869–882.

[79] Sengers, B. A. M., Rott, A., Simley, E., Sinner, M., Steinfeld, G., and Kühn, M. (2023). Increased power gains from wake steering control using preview wind direction information. *Wind Energy Science*, 8:1693–1710.

[80] Shao, Z., Wu, Y., Li, L., Han, S., and Liu, Y. (2019). Multiple wind turbine wakes modeling considering the faster wake recovery in overlapped wakes. *Energies*, 12.

[81] Siemens Gamesa (2019). Siemens gamesa now able to actively dictate wind flow at offshore wind locations. https://www.siemensgamesa.com/en-int/newsroom/2019/11/191126-siemens-gamesa-wake-adapt-en. Accessed: 14/03/2024.

[82] Sijtsma, L. (2023). Financial auctions for offshore wind.

[83] Simley, E., Fleming, P., and King, J. (2020). Design and analysis of a wake steering controller with wind direction variability. *Wind Energy Science*, 5:451–468.

[84] Simley, E., Fleming, P., King, J., and Sinner, M. (2021). Wake steering wind farm control with preview wind direction information. In *2021 American Control Conference (ACC)*, pages 1783–1789.

[85] Slater, N. (2021). Dnv and partners begin uk-us research project to investigate the application of wake steering on floating offshore wind farms. https://www.dnv.com/news/dnv-and-partners-begin-uk-us-research-project-to-investigate-the-application-of-wake-steering-on- Accessed: 24/04/2024.

[86] Smith, R. C. (2013). *Uncertainty Quantification: Theory, Implementation, and Applications*. Society for Industrial and Applied Mathematics, Philadelphia, PA.

[87] Sobol, I. M. (1993). Sensitivity estimates for nonlinear mathematical models. *Mathematical Modelling and Computational Experiments*, 1:407–414.

[88] SSE (2022). Construction begins on the world's largest offshore wind farm. https://www.sse.com/news-and-views/2022/04/construction-begins-on-the-world-s-largest-offshore-wind-farm/. Accessed: 02/05/2024.

[89] Sudret, B. (2007). *Uncertainty propagation and sensitivity analysis in mechanical models - Contributions to structural reliability and stochastic spectral methods*. PhD thesis, Université Blaise Pascal - Clermont II.

[90] Sullivan, T. (2015). *Introduction to Uncertainty Quantification*. Springer.

[91] Sørensen, J. (2011). *4 - Wind turbine wakes and wind farm aerodynamics*, pages 112–131. Woodhead Publishing.

[92] The Economist (2022). Why the oil price is spiking again. https://www.economist.com/finance-and-economics/2022/05/31/why-the-oil-price-is-spiking-again. Accessed: 01/05/2024.

[93] Torre, E., Marelli, S., and Sudret, B. (2019). UQLab user manual – Statistical inference. Technical report, Chair of Risk, Safety and Uncertainty Quantification, ETH Zurich,Switzerland. Report # UQLab-V1.3-114.

[94] Tyson, S., Donovan, D., Thompson, B., Lynch, S., and Tas, M. (2015). Uncertainty modelling with polynomial chaos expansion: Stage 1 – final report. Technical Report 149297, University of Queensland.

[95] UN News (2021). Climate and weather related disasters surge five-fold over 50 years, but early warnings save lives - wmo report. https://news.un.org/en/story/2021/09/1098662. Accessed: 01/05/2024.

[96] University of Bergen (2023). The wake effect: Offshore wind farms can 'steal' wind from one another. https://techxplore.com/news/2023-10-effect-offshore-farms.html. Accessed: 01/05/2024.

[97] van Beek, M., Viré, A., and Andersen, S. (2021). Sensitivity and uncertainty of the floris model applied on the lillgrund wind farm. *Energies*, 14(5):1293.

[98] van den Bos, L. and Sanderse, B. (2017). Uncertainty quantification for wind energy applications - literature review. Technical Report SC-1701, Centrum Wiskunde Informatica.

[99] van der Hoek, D., Frederik, J., Huang, M., Scarano, F., Simao Ferreira, C., and van Wingerden, J.-W. (2022). Experimental analysis of the effect of dynamic induction control on a wind turbine wake. *Wind Energy Science*, 7(3):1305–1320.

[100] van der Hoek, D., Kanev, S., Allin, J., Bieniek, D., and Mittelmeier, N. (2019). Effects of axial induction control on wind farm energy production - a field test. *Renewable Energy*, 140:994–1003.

[101] van der Laan, M. P., Baungaard, M., and Kelly, M. (2022). Brief communication: A clarification of wake recovery mechanisms. *Wind Energy Science*.

[102] Vattenfall (2024). Horns rev 3. https://powerplants.vattenfall.com/horns-rev-3/. Accessed: 24/04/2024.

[103] Wagenaar, J. W., Machielse, L. A., and Schepers, J. G. (2012). Controlling wind in ecn's scaled wind farm.

[104] Wenig, P. J., Kelm, S., and Klein, M. (2023). Cfd uncertainty quantification using stochastic spectral methods—exemplary application to a buoyancy-driven mixing process. *Nuclear Engineering and Design*, 409. Cited by: 5.

[105] Wind Energy Technologies Office (2019). Wake steering performance evaluated at scale. https://www.energy.gov/eere/wind/articles/wake-steering-performance-evaluated-scale. Accessed: 24/04/2024.

[106] Wind Systems (2023). Windesco installs industry-first wake steering. https://www.windsystemsmag.com/windesco-installs-industry-first-wake-steering/. Accessed: 13/03/2024.

[107] Wu, K. L. and Porté-Agel, F. (2017). Flow adjustment inside and around large finite-size wind farms. *Energies*, 10.

[108] Zhang, J. (2021). Modern monte carlo methods for efficient uncertainty quantification and propagation: A survey. *Wiley Interdisciplinary Reviews: Computational Statistics*, 13.

[109] Zhang, J., Yin, J., and Wang, R. (2020). Basic framework and main methods of uncertainty quantification. *Mathematical Problems in Engineering*, 2020(1):6068203.